Goddard
GCNT
111-13-CR
140235
2548

RF Project 761054/711055
Report No. 384

BASELINE ESTIMATION FROM SIMULTANEOUS SATELLITE LASER TRACKING

George C. Dedes
Department of Geodetic Science and Surveying

(NASA-CR-182750) BASELINE ESTIMATION FROM SIMULTANEOUS SATELLITE LASER TRACKING (Ohio State Univ.) 204 p CSCL 22A

N88-22052

Unclas
G3/13 0140235

NATIONAL AERONAUTICS AND SPACE ADMINISTRATION
Goddard Space Flight Center
Greenbelt, Maryland 20771

Grant No. NSG 5-265, Supp. No. 10

October 1987

The Ohio State University Research Foundation
1314 Kinnear Road
Columbus, Ohio 43212

BASELINE ESTIMATION FROM SIMULTANEOUS SATELLITE LASER TRACKING

by

George C. Dedes

Report No. 384

Department of Geodetic Science and Surveying
The Ohio State University
Columbus, Ohio 43210-1247

October, 1987

DEDICATION

To Alexandra
... who never ceases
to wonder...

PREFACE

This project is under the supervision of Professor Ivan I. Mueller, Department of Geodetic Science and Surveying, The Ohio State University. The science advisor is Dr. David E. Smith, and the technical officer is Dr. Gilbert B. Mead, both at Code 601, Crustal Dynamics Project, Space and Earth Sciences Directorate, NASA Goddard Space Flight Center, Greenbelt, Maryland 20771. The work is carried out under NASA Grant No. NSG 5265, OSU Research Foundation Project No. 711055.

This report is an expanded version of a dissertation submitted to the Graduate School of The Ohio State University in partial fulfillment of the requirements for the PhD degree.

ABSTRACT

Simultaneous Range Differences (SRD's) to Lageos are obtained by dividing the observing stations into pairs with quasi-simultaneous observations. For each of those pairs the station with the least number of observations is identified, and at its observing epochs interpolated ranges for the alternate station are generated. The SRD observables are obtained by subtracting the actually observed laser ranges of the station having the least number of observations from the interpolated ranges of the alternate station. On the basis of these observables semidynamic single baseline solutions have been performed. The aim of these solutions is to further develop and implement the SRD method in the real data environment, to assess its accuracy, its advantages and disadvantages as related to the range dynamic mode methods, when the baselines are the only parameters of interest.

Baselines, using simultaneous laser range observations to Lageos, have also been estimated through the purely geometric method. These baselines formed the standards of comparison in the accuracy assessment of the SRD method when compared to that of the range dynamic mode methods. On the basis of this comparison it was concluded that for baselines of regional extent (i.e., up to 3700 km) the SRD method is very effective, efficient and at least as accurate as the range dynamic mode methods, and that on the basis of a simple orbital modeling and a limited orbit adjustment.

The SRD method is insensitive to the inconsistencies affecting the terrestrial reference frame and simultaneous adjustment of the Earth Rotation Parameters (ERP's) is not necessary. Therefore, this method offers an inexpensive alternative for projects designed to study regional plate tectonic motions.

ACKNOWLEDGMENTS

Although it is difficult to acknowledge all those individuals who contributed to the successful completion of this work in the the long journey of studies, acknowledgments are given but by no means is this list meant to be complete.

My deepest appreciation and thanks go to my wife Alexandra for her endless love and her continuing patience, support and encouragement tirelessly shown during the difficult but very fruitful years of my graduate studies. Special thanks and appreciation are due to my parents who, with their tireless guidance and their continual support in my high school and undergraduate years, provided me with courage, faith and love for knowledge making the graduate studies a long and very challenging experience. The support and understanding of my parents-in-law during the last years of my studies is also greatly appreciated.

My gratitude and appreciation are also due to my supervisor and mentor Dr. I.I. Mueller for his expert guidance, constructive criticism, continual encouragement and tireless support during the course of this work and throughout my graduate studies at the Department of Geodetic Science and Surveying. His patience and continual involvement to successfully provide financial support even in very difficult times is greatly appreciated. His well organized and vast personal library, ready at my disposal, was at times of invaluable help and for this I am indeed very thankful.

I wish also to express my thanks to Dr. U. A. Uotila and Dr. C. C. Goad for their constructive criticisms and their valuable suggestions which enhanced the quality of this work. Special thanks are also given to Dr. Walter Mitchell for reading the dissertation, in which form this report was first presented.

The overall guidance of the faculty members provided in the coursework throughout my studies at Ohio State is also greatly appreciated.

I would especially like to thank former student Dr. E.C. Pavlis (now of EG&G Analytical Services) for his valuable suggestions in regard to the successful implementation of GEOSPP software, which he developed during his studies at Ohio State. His continuing support in providing information on Lageos' orbit is also greatly appreciated. The discussions with former student Dr. Brent Archinal (now at the U.S. Naval Observatory) helped to clarify many aspects in regard to the efficient use of the computer facilities which proved to be of great value in the course of this study. Acknowledged are also the valuable suggestions of David Rowlands, a former student of this Department, related to the efficient use of GEODYN programs.

Special thanks are extended to my fellow students past and present, Mike Baker, Lucia Tsaoussi, Nikos Pavlis, Vasilios Despotakis, George Priovolos, Dr. Y. Bock (now of the Massachusetts Institute of Technology) and Dr. H.B. Iz (now of ST Systems Corporation), who, although deeply occupied with their own work, were always ready to listen, discuss and offer valuable advice for my problems.

Thanks are also extended to Dr. D. C. Christodoulidis (now of Jet Propulsion Laboratory, Pasadena) for providing the data sets employed at the initial stage of this study and also to Dr. Steve Klosko at EG&G for furnishing valuable information about the quality, distribution and simultaneity of the laser range observations to Lageos. Dr. Henry Linder at GSFC, with his valuable comments, clarified many aspects related to the contents of the tapes containing the laser range observations to Lageos.

The financial support for this work provided by NASA Research Grant NSG 5265, OSURF Project 711055, is also greatly appreciated. Also acknowledged is the financial support of the American Association of Geodetic Surveying (AAGS)-American Congress on Surveying and Mapping(ACSM) Graduate Fellowship (1984) and the Wild Heerbrugg-ACSM Geodetic Fellowship(1986).

The extensive computer funds necessary for the completion of this work were provided by the Instruction and Research Computer Center (IRCC) of The Ohio State University.

Last but not least I wish to thank Irene Tesfai for her excellent typing and valuable suggestions as well as Karen Wasielewski and Tracy Runyon for the excellent typing of parts of this manuscript.

TABLE OF CONTENTS

PRECEDING PAGE BLANK NOT FILMED

LIST OF TABLES

LIST OF FIGURES

ABBREVIATIONS AND ACRONYMS

AAGS	American Association of Geodetic Surveying
ACSM	American Congress on Surveying and Mapping
AU	Astronomical Unit
BIH	Bureau International de l'Heure
BTS	BIH Terrestrial Reference System
CCR	Cube Corner Reflectors
CCRS	Conventional Celestial Reference System
CDDB	Crustal Dynamics Data Bank
CDIS	Crustal Dynamics Information System
CEP	Celestial Ephemeris Pole
COTES	IAU/IAG Joint Working Group on the Establishment and Maintenance of a Conventional Terrestrial Reference System
CRF	Celestial Reference Frame
CSR	Center for Space Research
CTRS	Conventional Terrestrial Reference System
EG&G	EG&G Washington Analytical Science Center
ERP	Earth Rotation Parameters
FR	Full Rate
GAST	Greenwich Apparent Sidereal Time
GEML2	Goddard Earth Model L2
GEOM	GEOMetric solution
GMST	Greenwich Mean Sidereal Time
GPS	Global Positioning System
GSFC	Goddard Space Flight Center
GTLN	Goddard Laser Tracking Network
IAU	International Astronomical Union
IERS	International Earth Rotation Service
IUGG	International Union of Geodesy and Geophysics
LAGEOS	LAser GEOdynamic Satellite
MCP	MicroChannel Plate
MERIT	Monitor Earth Rotation and Intercompare the Techniques of observation and analysis
MMC	Main MERIT Campaign
NASA	National Aeronautics and Space Administration
OTIU	Optical Time Interval Unit
PC	Personal Computer
PLN	Participating Laser Network
PMT	PhotoMultiplier Tube
PPN	Isotropic Parametrized Post-Newtonian n-body metric
RMS	Root Mean Square
SLR	Satellite Laser Ranging
SR	Simultaneous Ranges
SRD	Simultaneous Range Differences

SSD	SeaSat Decimal format
TAI	International Atomic Time
TDB	Barycentric Dynamical Time
TDT	Terrestrial Dynamical Time
TIU	Time Interval Unit
TLRS	Transportable Laser Ranging System
TRF	Terrestrial Reference Frame
USNO	United States Naval Observatory
UT	Universal Time
UTC	Universal Coordinated Time
UTX	University of Texas
UT1	Universal Time corrected for polar motion
UT1R	UT1 with the effects of zonal earth tides up to 35 days removed
ZIPE	Central Institute for Physics of the Earth at Potsdam

Chapter 1

INTRODUCTION

1.1 BASELINE ESTIMATION IN THE DYNAMIC AND SEMIDYNAMIC ENVIRONMENT

In the dynamic environment accurate baseline estimation requires a highly sophisticated orbital modeling and a baseline-pass geometry leading to near cancellation of the accumulated along-track and cross-track orbital errors caused by the erroneous constraints imposed on a large number of estimable quantities (Rao, 1973), the recovery of which is not possible due to their reduced data sensitivity. In this environment proper implementation of the Terrestrial Reference Frame (TRF) requires simultaneous recovery of the Earth Rotation Parameters (ERP) or utilization of a consistent set of ERPs obtained through a separate step.

Although fulfillment of these requirements makes it possible to effectively recover baselines of global and regional extent, it results in low temporal resolution of baseline recovery.

In the semidynamic environment (Section 2.2), and on the basis of simultaneous observations, only regional baselines can be recovered with an accuracy compatible to that of the observed laser ranges. The maximum regional baseline length effectively recovered in this environment depends on whether the simultaneous observations collected by the baseline end stations are enough to result in a steady state response (Section 4.2.1). This, however, is a function of the satellite altitude, and for the Lageos satellite the effective regional extent may include baselines of up to 3703 km (Section 4.4.2).

In the semidynamic environment a relatively simplified orbital model is required and only the position and the orientation of each of the arcs involved is adjusted to "best" fit the available observations (Section

2.2.6). Adjustment for the ERP parameters is not necessary since proper implementation of the TRF frame is warranted by the use of only simultaneous observations. The relaxing data requirements and the limited orbit adjustment make it possible to increase the resolution of baseline recovery without any loss on the achieved accuracies, and at the same time to substantially decrease the required computations, thereby making it possible to effectively implement the semidynamic methods with limited computer facilities as, for instance, in the personal computer (PC) environment.

The sophistication of the orbital modeling in the semidynamic environment can be further simplified by appropriately transforming the observed laser ranges to bring them "closer" to the estimable quantities being recovered (i.e., baselines). The term "closer" indicates that on the basis of the same orbital model the errors affecting the computed value of the transformed observations, referred to from now on as "observables," are smaller than those affecting the computed value of the observations themselves. By bringing the observations closer to the estimated baselines, the sophistication of the orbital modeling could be further reduced if the performed transformation cancels out the errors caused by the model simplifications.

Transformation of the laser range observations to Simultaneous Range Difference (SRD) observables brings them closer to the estimated baselines (Pavlis, 1982). The potential of using SRD observables to estimate baselines was studied with simulated data by Pavlis (1982). The results of this study were very promising not only with respect to their accuracy but also with respect to their simplicity.

1.2 SCOPE OF THIS INVESTIGATION

For the reasons mentioned in the previous section, it was considered appropriate and worthwhile to pursue the present investigation, the aim of which is to further develop and implement the SRD method (Section 2.2.1) in the real data environment, to assess its accuracy, its advantages and disadvantages as related to range dynamic mode methods, when the baselines are the only parameters of interest.

Since during the MERIT Main Campaign many stations collected simultaneous observations (Section 3.4), it was decided to proceed not only with the development of the SRD method but also with baseline estimation through the geometric method (Section 4.3). These baselines formed the standards of comparison in the accuracy assessment of both the SRD and the range dynamic mode methods (Section 4.5).

In pursuing this study, the geometry does not take part in the physical events, as happens in general relativity, but rather it is used in its deductive form either purely (i.e., geometric methods) or in combination with an inductive form (i.e., dynamic and semidynamic methods), both of which were employed to formulate the spatial-temporal relationships of the observing stations and the observed satellite positions.

In a pure deductive mode the geometric method is entirely based on Euclidean geometry, without any reference to the inductive inference that the satellite moves along the path chosen by its physical environment. The implied Euclidean geometry is revealed, in the arithmetic framework, on the basis of Cartesian coordinates (Section 2.1.1). There exist, however, configurations in which some of the vertices of the resulting figures are free to move along a locus of points, thereby forming configurations that are not unique and are referred to as "critical configurations" (Section 2.1.3).

In the inductive mode, the differential form of a satellite's motion, modeled on the basis of Newton's inductive laws, is expressed through its equations of motion (Section 2.2.5). These equations are integrated, on the basis of the deductive mathematical framework, to reveal the geometric path of the satellite (i.e., orbit), chosen by the satellite's physical environment (Section 2.2.3). Having the geometric path of the satellite, the observing stations are connected with this path through the Euclidean distance formulated in terms of Cartesian coordinates. Since the simplest geometry of the satellite orbit reveals itself in an inertial reference frame, the satellite's equations of motion are expressed with respect to such a frame (Section 2.2.4). However, the estimated Cartesian coordinates of the observing stations are referenced with

respect to an earth-fixed frame (Section 2.2.2).

The deductive and/or inductive formulation described above contains a large number of slow varying quantities which can be considered constant for the time span of the observations and a subset of which constitutes a set of quantities that are estimable only if the necessary units, constants and/or constraints have been properly adopted for their unique determination (Rao, 1973).

There are three types of estimable quantities that can be differentiated from their relation to the physical environment, or the observing environment, or the links of these two environments.

In satellite geodesy the interstation distances (i.e., baselines) are estimable quantities related to the observing environment. The estimable quantities of the physical environment are those related to its cause (i.e., A_{nm} and B_{nm} potential coefficients) and those to its effect (i.e., geometric and dynamic characteristics of the orbit). The estimable quantities molded in the link of the physical and the observing environments are those resulting from the latter as relates to the cause and effect duality of the former (i.e., station geocentric distances, latitudes, and longitude differences).

The baselines are computed from the earth-fixed station coordinates which are recovered through an inversion process, such as least-squares adjustment, on the basis of both the geometric and the SRD methods (Sections 2.1.2 and 2.2.6). The input to this inversion process are the Simultaneous Ranges (SR) and SRD observables. These observables were generated through an interpolation of the observed laser ranges because it is quite unlikely, if not impossible, to record simultaneous observations to a passive satellite (Section 3.6). Because of the peculiarities of the SLR system (Section 3.1), it is very likely that the recorded laser ranges will be affected not only by white noise but also by large blunders (Section 3.2). For this reason and since the SR and SRD observables will be generated via an interpolation, it is important to edit the laser ranges before proceeding with the geometric and the orbit adjustments.

In the geometric method the recovered baselines will only be affected by the errors resulting from an improper or from the not yet reached steady state response (Sections 4.2). The steady state response of the geometric method, on the basis of a minimum least-squares solution, is affected only by the observational errors. Such a response, however, was not possible for longer baselines (Section 4.3.1), and therefore an overconstrained solution was adopted to form the standards of comparison with the anticipation that it is the least erroneous when it is compared either to SRD or to dynamic solutions (Section 4.3.2).

The accuracy of the baselines, recovered via the SRD (Section 4.4) is assessed from the comparison with the baselines obtained via the geometric methods and the range dynamic mode methods (Section 4.5). The response of the SRD method to the simplification of the orbital model has also been investigated (Section 4.6).

Chapter 2

ESTIMATION METHODS

In this chapter an attempt is made to briefly describe the mathematical models and the principles involved in the geometric and dynamic mode methods as they are applied to satellite geodesy. Although the geometric solutions performed in this study are only used as standards of comparison (Sections 4.3 and 4.5), their mathematical formulation is presented first because historically the geometric methods were the first ones to result in accurate differential positioning.

2.1 GEOMETRIC METHODS

Geometric methods are based on the analysis of the relative geometry of the observations without any reference to the physical processes creating the problem under question. On the contrary, some or all of the systematic corrections applied to the observations are computed with the use of physical models.

In the geometric approach of satellite geodesy (Veis, 1960; Mueller, 1964a), the observed satellite positions are treated as auxiliary independent points in space, and they are only used to relate the observations geometrically. This in turn leads to the generation of space networks. These networks manifest not only the relative geometry of the observations, but also any a priori information which is necessary for their realization. Thus each observation relates the position of the observing station with the observed satellite position. The unknown parameter vector includes the Cartesian coordinates of the observing stations together with the Cartesian coordinates of the observed satellite positions at each of the observing epochs. Since the coordinates of the unknown satellite positions constitute an independent set of unknowns,

it is necessary to have a sufficient number of observations at each observing epoch. The number of observations should be sufficient not only to eliminate the unknown satellite coordinates at each of those epochs, but also to solve for the unknown station coordinates.

The process described, however, necessitates the usage of simultaneous (referenced to satellite time) observations without any reference to the fact that the motion of the satellite obeys the physical laws of dynamics. These two distinct features create the advantages and disadvantages of the geometric approach to satellite geodesy.

2.1.1 Mathematical Model

The mapping of the parameter space into the observational space is referred to as observational modeling. The analytical expression responsible for the realization of this mapping is referred to as either the mathematical or the observational model. The mathematical model employed in the geometric approach is that of the Euclidean range from a ground station to an observed satellite position expressed in terms of Cartesian coordinates:

$$F_{ij} = [(u_j-u_i)^2 + (v_j-v_i)^2 + (w_j-w_i)^2]^{\frac{1}{2}} - r_{ij} = 0 \qquad (2\text{-}1)$$

The quantity r_{ij} is the true value of the range observable from the ground station i to the satellite position j (see Section 3.1), while the quantities u_i, v_i, w_i and u_j, v_j, w_j denote the true values of the Cartesian coordinates of station i and satellite position j. These coordinates may be referred to any arbitrarily chosen Cartesian coordinate system since ranges are invariant under any rigid body rotations.

The linearized form of equation (2-1) forms the basis for the generation of the observation equations when four or more stations are observing simultaneously (see Section 2.1.3). With these observation equations the normal equations are derived on the basis of a weighted constrained least squares adjustment (Uotila, 1967; Krakiwsky et al., 1967). The resulting normal equations are reduced by eliminating the unknown satellite coordinates. The reduced normals are then solved to

estimate the stations' Cartesian coordinates which are finally transformed to interstation distances.

Inverting the normals on the basis of the minimum required information (i.e., minimum constraints) leads to baseline errors that depend solely on the errors of the observed ranges and on their geometric strength as well. This is true only when the scale has been properly incorporated into the solution either through the observations and their geometry, or if this is not possible, through some other additional constraints (see Section 4.3).

2.1.2 Normal Equations

The observation equations used to derive the normal equations are obtained from the linearization of equation (2-1). Linearization is achieved with a Taylor series expansion about the approximate values of the station coordinates, the satellite coordinates and the observed ranges as well. The resulting linear equations have the form:

$$A_{ij}\,\hat{X}_{ij} - V_{ij} + L_{ij} = 0 \qquad (2\text{-}2)$$

where

$$A_{ij} = [\, a_{ij} \,\vdots\, -a_{ij}] \qquad (2\text{-}3)$$

$$a_{ij} = \frac{\partial F_{ij}}{\partial (u_j,\ v_j,\ w_j)} \qquad (2\text{-}4)$$

$$\hat{X}_{ij} = \begin{bmatrix} du_j \\ dv_j \\ dw_j \\ du_i \\ dv_i \\ dw_i \end{bmatrix} \qquad (2\text{-}5)$$

V_{ij} = residual vector corresponding to the range observable

L_{ij} = the computed minus the observed range

In cases when the geometric strength of the observations is not good enough to warrant a steady state response, it could still be possible to reach such a response if estimated or observed interstation distances are incorporated into the solution (see Section 4.3). This is accomplished by introducing the interstation distances as fictitious observations into the adjustment. Appropriate weights should be applied to these (fictitious) observations in order to avoid any scale conflicts that might contaminate the solution (Uotila, 1967).

The mathematical model of the interstation distance between stations k and ℓ has the following form

$$G_{k\ell} = [(u_\ell - u_k)^2 + (v_\ell - v_k)^2 + (w_\ell - w_k)^2]^{\frac{1}{2}} - L_{k\ell} = 0 \qquad (2\text{-}6)$$

where $L_{k\ell}$ is the true value of the fictitiously observed range between these two stations. Linearization of equation (2-6) about the approximate station coordinates and the fictitiously observed distance results in

$$C_{k\ell}\ \hat{X}_{k\ell} - V_{k\ell} + D_{k\ell} = 0 \qquad (2\text{-}7)$$

where

$$C_{k\ell} = [\ T_\ell \ \vdots\ -T_\ell\ ] \qquad (2\text{-}8)$$

$$T_\ell = \frac{\partial G_{k\ell}}{\partial(u_\ell,\ v_\ell,\ w_\ell)} \qquad (2\text{-}9)$$

$V_{k\ell}$ = residual of the (fictitiously) observed interstation distance

$D_{k\ell}$ = the computed minus (fictitiously) observed interstation distance

So far the observation equations have been developed on the basis of one range observation and one interstation distance. Considering many range observations and many fictitiously observed interstation distances, equations (2-2) and (2-7) take the following form:

$$A\hat{X} - V + L = 0 \tag{2-10}$$

$$C\hat{X} - V_C + D = 0 \tag{2-11}$$

These equations can be rewritten as

$$\begin{bmatrix} A \\ C \end{bmatrix}\hat{X} + \begin{bmatrix} L \\ D \end{bmatrix} = \begin{bmatrix} V \\ V_C \end{bmatrix} \tag{2-12}$$

and with some obvious substitutions they take the following form:

$$A^*\hat{X} + L^* = V^* \tag{2-13}$$

Equation (2-13) forms a set of observation equations which are used to derive the normal equations on either deterministic or statistical grounds.

Deterministically the principle of least squares requires that the quantity $(V^{*T}P^*V^* + \hat{X}^T P_X \hat{X})$ assumes minimum value, subject to the condition $A^*X - V^* + L^* = 0$. The matrix P_X is the weight matrix associated with the coordinates of the ground stations and of the observed satellite positions, while the weight matrix P^* takes the following form

$$P^* = \begin{bmatrix} P & 0 \\ 0 & P_C \end{bmatrix} \tag{2-14}$$

where P and P_C are the weight matrices associated with the range observables and the (fictitiously) observed interstation distances respectively.

Statistically the maximum likelihood principle requires maximization of the a posteriori conditional density function of the parameter vector $\hat{X}$ given that the observations L^* have been obtained. The resulting estimator $\hat{X}$ is referred to as Bayesian least squares estimator. Both of the above principles lead to the same estimator $\hat{X}$ only if normality is assumed not only for the a priori density function of the estimated

parameter vector $\hat{X}$, but also for the conditional density function of the observational vector L^* given that the parameter vector $\hat{X}$ has been estimated. These assumptions should only hold for the maximum likelihood principle since any least squares estimator is a distribution free estimator. The estimator $\hat{X}$ is obtained from the resulting normal equations (Uotila, 1967; Krakiwsky et al., 1967; Cappellari et al., 1976):

$$\begin{bmatrix} A^T P A + P_X & C^T \\ C & -P_c^{-1} \end{bmatrix} \begin{bmatrix} \hat{X} \\ -k_C \end{bmatrix} + \begin{bmatrix} A^T P L \\ D \end{bmatrix} = 0 \qquad (2\text{-}15)$$

where k_C are the Lagrange multipliers associated with the (fictitiously) observed interstation distances. Elimination of the Lagrange multipliers from equation (2-15) leads to the following form for the estimator $\hat{X}$:

$$\hat{X} = -(A^T P A + C^T P_C C + P_X)^{-1} (A^T P L + C^T P_C D) \qquad (2\text{-}16)$$

Substitution of equations (2-2) through (2-5) and (2-7) through (2-9) into equation (2-16) followed by elimination of all the satellite coordinates leads to the following equations (Krakiwsky et al., 1967):

- The 3×3 diagonal matrix associated with the k^{th} ground station

$$N_{kk} = \left(\sum_j a_{kj}^T P_{kj} a_{kj}\right) - \sum_j \left\{a_{kj}^T P_{kj} a_{kj} \left(\sum_i a_{ij}^T P_{ij} a_{ij}\right)^{-1} \cdot a_{kj}^T P_{kj} a_{kj}\right\} + P_k + \begin{bmatrix} 0 \\ 1 \end{bmatrix} T_k^T P_{k\ell} T_k \qquad (2\text{-}17)$$

- The 3×3 off-diagonal matrix corresponding to the k^{th} and ℓ^{th} ground station

$$N_{k\ell} = -\sum_j \left\{a_{kj}^T P_{kj} a_{kj} \left(\sum_i a_{ij}^T P_{ij} a_{ij}\right)^{-1} a_{\ell j}^T P_{\ell j} a_{\ell j}\right\} + \begin{bmatrix} 0 \\ 1 \end{bmatrix} T_k^T P_{k\ell} T_\ell \qquad (2\text{-}18)$$

- The 3×1 constant vector associated with the k^{th} ground station

$$U_k = -\left(\sum_j a_{kj}^T P_{kj} L_{kj}\right) + \sum_j \left\{a_{kj}^T P_{kj} a_{kj} \left(\sum_i a_{ij}^T P_{ij} a_{ij}\right)^{-1} \cdot \right.$$

$$\left. \sum_i a_{ij}^T P_{ij} L_{ij} \right\} + \begin{bmatrix} 0 \\ 1 \end{bmatrix} T_k^T P_{k\ell} D_{k\ell} \qquad (2\text{-}19)$$

In equations (2-17) and (2-19) the j summation is performed over all the satellite positions observed from station k, while in equation (2-18) the j summation is performed over all the satellite positions observed simultaneously from both stations k and ℓ respectively. The summation i, on the other hand, is performed over all the stations observing the satellite position j simultaneously. In these three equations the number 1 is used only when the interstation distance between the stations k and ℓ is involved in the solution, otherwise the value of 0 is used.

Equations (2-17) through (2-19) form the basis for the estimation of the ground station coordinates by inverting the normals through a procedure accredited to Banachiewich. This procedure is carried out in two steps.

- The first step involves the representation of the normal matrix as a product of right and left triangular matrices with the left triangular matrix having unit diagonal elements.
- The second step involves the computation of the inverse normal matrix on the basis of only the inverted diagonal elements of the right triangular matrix and the off-diagonal elements of the left triangular matrix.

The above procedure is very closely related to the Cholesky algorithm (Uotila, 1967).

2.1.3 Critical Configurations

In the geometric approach of satellite geodesy the observed satellite positions (targets) are treated as auxiliary independent points in space. They are used only to relate the observations geometrically through the resulting range space networks (see Section 2.1). In certain cases the ground stations and/or the targets which form the vertices of this

network are involved in a kind of configuration for which a unique adjustment is impossible although the number of observations is sufficient and the coordinate system well defined. These configurations are referred to as "critical."

With range observations the critical configurations have been extensively studied in the past (Rinner, 1966; Blaha, 1971; Tsimis, 1972, 1973). The critical configurations have been traditionally analyzed according to whether all of the observing stations are either in a plane or generally distributed in space. For both of these cases the resulting singularities are divided into three categories:

1. Singularity A, resulting from the relative geometry of an individual station connected to its observed targets.
2. Singularity B, resulting from the relative geometry of the observing stations only.
3. Singularity C, resulting from the relative geometry of all the observing stations connected to their observed targets when singularity A and singularity B are not present.

2.1.3.1 Critical configurations when all of the observing stations are in a plane. When all of the observing stations are in a plane the singularity problem is analyzed according to the number of stations observing all the targets. This number may be three or more, or less than three. The number three is important since ranges from three stations are needed to eliminate the coordinates of one target, provided that this target is not located on the plane of these three stations (Blaha, 1971).

If the number of ground stations observing all the targets is three or more, singularity A occurs when an individual station—excluding the stations used to define the coordinate system, since for these three stations singularity A cannot occur—is either observing less than three distinct targets or is in the same plane with all of its observed targets. Furthermore, singularity B occurs when all the observing stations but one are lying in a straight line or more generally when all the stations

are lying on a second-order curve. Since at least five stations are needed to determine a second-order curve, singularity B can only be avoided if six or more stations are involved. In the absence of singularities A and B singularity C occurs when the stations making off-plane observations (i.e., observed targets are not in the same plane) are not themselves off-curve stations (i.e., not lying in the same second-order curve). To avoid singularity C at least three off-curve stations should make off-plane observations (Blaha, 1971; Mueller et al., 1975). In the case when all the stations observe all the targets, singularity A loses its importance because it always implies singularity C, since off-plane observations are necessary to avoid singularity C.

When there do not exist three stations observing all the targets, elimination of the coordinates for all the targets using the same three stations cannot be achieved. Thus, in the elimination process one, two or all of these three stations will have to be replaced. This leads to the first, second and third replacement respectively, and therefore to at least four-station events.

We first denote with k the station used in the first replacement. In this replacement singularity A for all the stations but k, or singularity B for all stations would occur as though there were three stations observing all the targets. For station k, however, singularity A occurs if any new stations coming into play are lying either on the x-axis of the local coordinate system (e.g., line formed by two of the three stations used to define the local coordinate system) or in the intersection line (denoted by ℓ) of the plane π (see below) with the plane of the ground stations. The plane π, if it exists, is the plane containing station k together with the satellite positions (denoted by j_k) that were observed by this station (e.g., k) up to the epoch at which the new station(s) started observing. Singularity C, in the absence of singularities A and B, is further analyzed according to whether j_k are off-plane or in-plane targets. If j_k are off-plane targets, singularity C occurs whenever stations making off-plane observations are not themselves off-curve stations. The case when j_k form in-plane targets

is not discussed here because it is very unlikely to encounter in practice. This case, of rather academic interest, is discussed in (Blaha, 1971, page 63).

Next we denote by s' the station used in the second replacement. In this replacement, if there is no other station s'' to start observing for the first time after s' has started, singularity A occurs as though only the first replacement would have taken place. However, with station s'' present, singularity A for station k occurs if, in addition to the above, the station s'' is lying either in the x-axis of the local coordinate system or in the line ℓ. Furthermore, singularity A for station s' occurs if in addition to being in the plane π' (defined below), the station s'' is also lying either in the line defined by the station used as the origin of the local coordinate system and the station k or in the intersection line (denoted by ℓ') of the plane π' with the plane of the ground stations. The plane π', if it exists, is the plane containing the station s' together with the targets (denoted by $j_{s'}$) observed by the station s' up to the epoch at which the station s'' started observing. Singularity B occurs as though three stations observing all the targets exist. If $j_{s'}$ and j_k are off-plane targets, in the absence of singularity A and B, singularity C occurs, when no other stations besides k and s' exist to make off-plane observations. The case when $j_{s'}$ or j_k form in-plane targets is not discussed here because of the unlikelihood of encountering it in practice.

The singularities resulting from three or more replacements are similar to the ones described above. By avoiding singularities A, B and C a nonsingular network can only be formed <u>if at least six stations in at least four station events</u> are involved. This is so because five stations are needed to define a second-order curve and only the sixth station is possible to serve as an off-curve station.

Once a nonsingular network has been realized any extension of it will result in a nonsingular one if for any additional station singularity A is eliminated and if no target is lying in the plane of the ground stations.

2.1.3.2 Critical configurations when the observing stations are generally distributed in space. When the ground stations are in general configuration, singularity B loses its meaning because the effect of ground stations cannot be separated from that of the targets. Consequently, singularity B will not be considered here. However, another type of singularity called "reverse singularity B" is the singularity B if one assumes that the satellite points (targets) observe the ground stations. Therefore, this singularity occurs when all the targets are in a plane in a second-order curve. This in practice could approximately occur when two short passes of about the same altitude have been observed.

Having the observing stations in a general configuration, a nonsingular network can be formed if at least six targets are being co-observed by at least four stations. Accordingly, the analysis of critical configurations proceeds by grouping the ground stations in tetrads ("quads"). With four stations observing all the targets, singularity A occurs only with respect to the fourth station because singularity A never occurs for the three stations that have been used to define the local coordinate system (Blaha, 1971). With respect to the fourth station, singularity A occurs if all the targets are lying on a plane through this station, or if all the targets are on the plane formed by the stations used to define the local coordinate system. Furthermore, in the absence of singularity A, singularity C occurs when all the observing stations and all the targets are lying on a second-order surface.

With more than four stations observing, the singularity problem is analyzed by grouping the observing stations in quads. If the number of stations observing all the targets is three or more, singularity A occurs, as though all the observing stations were lying on a plane (see Section 2.1.3.1). In the absence of singularity A, singularity C occurs either when all the observing stations with their observed targets are located on a second-order surface or when each tetrad of stations together with its observed targets are located on specific second-order critical surfaces. These surfaces intersect each other in one

second-order curve containing the three stations used to eliminate the coordinates of each target and to define the local coordinate system. Furthermore, when all the stations are co-observing, these second-order critical surfaces coincide.

When three stations observing all the targets do not exist, then the concept of station replacement should be utilized in exactly the same way as described in the previous section. Proceeding with this concept it is found that singularity A occurs as though three stations observing all the targets exist. As for singularity C, it is again associated with other specific second-order surfaces in addition to the ones resulting in singularity C when three stations observing all the targets exist.

By avoiding singularities A and C and reverse singularity B a nonsingular network can be formed. What is important to keep in mind is that when the ground stations are generally distributed in space a nonsingular network can be formed if at least six targets are co-observed by at least four stations. In fact four stations and five targets can uniquely define a second-order surface, and the sixth target could make the network nonsingular if it is not located on this surface.

Once a nonsingular network has been realized, an extension of it will result in a nonsingular one if singularity A is eliminated for any additional station and if no targets are on the plane of the three stations defining the Cartesian coordinate system.

2.2 DYNAMIC AND SEMIDYNAMIC MODE METHODS

In contrast to the geometric methods, the observed satellite positions in the dynamic and in the semidynamic methods are not treated as auxiliary independent points in space but rather they are constrained to lie in a space curve (Schwarz, 1969). This curve should resemble within the required degree of accuracy the satellite orbit under question. The satellite orbits, on the other hand, are modeled either empirically or dynamically or by combining both empirical and dynamical modeling.

Empirical modeling of satellite orbits was extensively used in the early years of satellite geodesy since many of the model parameters

entering the equations of motion were not known with the degree of accuracy required for precise geodetic work (Mueller, 1964b). These methods are used today in very special circumstances and only in combination with dynamic modeling (Tapley et al., 1985a).

Dynamic modeling results in three second-order differential equations or six first-order differential equations referred to as equations of motion of the satellite. These differential equations are integrated either analytically (i.e., general perturbation methods) or numerically (i.e., special perturbation methods) to generate the satellite orbits.

In the general perturbation methods, the equations of motion of the satellite are reformulated in terms of a set of orbital elements leading to a set of differential equations which can be integrated analytically. Unfortunately, a closed form analytical solution for the equations of motion of the perturbed two-body problem does not exist. It is possible, however, to obtain approximate analytical solutions either by restricting the complexity of the perturbation model or by truncating high power expansions (Kaula, 1961, 1966; Mueller, 1964b; Goad, 1977; etc.) These solutions are approximate and in many cases cannot be used for precise geodetic work. They are extremely useful, however, in order to gain a keener insight into the effects of various perturbing forces on the satellite orbits.

In the special perturbation methods, the equations of motion of the satellite are integrated numerically (see Section 2.2.3). The main advantage of these methods is that all the perturbing forces can be accommodated to a high degree of accuracy. The special perturbation methods, on the other hand, have proven to be computationally more efficient, if one takes into consideration the high repetition rate of recent geodetic observations (Rizos et al., 1985; Krakiwsky et al., 1985).

A combination of empirical and dynamic modeling is usually employed either when the satellite orbits are integrated continuously over long periods of time (i.e., two months or more) or when unexplained perturbing accelerations are present. In the latter case the dynamic models are supplemented with empirical models for the as yet not fully

understood perturbing accelerations while in the former the empirical models are employed to account for the accumulated along-track, cross-track and radial errors (Tapley et al., 1985a). For instance, the draglike acceleration of Lageos' orbit which causes a decay of the semimajor axis at a rate of 1 mm/d is modeled empirically (see Section 2.2.5).

The dynamic mode methods are further subdivided into semidynamic (short-arc) and dynamic (long-arc) methods. There is no clear distinction between these two terms and their exact meaning depends on the investigator and on the kind of problem being analyzed.

In the present study the estimation of the baselines is performed in the semidynamic mode environment. In this environment the lengths of the arcs employed are relatively short (i.e., mostly up to three days and very rarely up to seven days) (see Section 4.4). A relatively short arc is defined as having a maximum length over which the total modeling error of a simple dynamic model is well below the noise level of the observations (i.e., an order of magnitude or less). Consequently, with this definition one may select a relatively simple dynamic model and then determine the length of the arc, or one may choose the length of the arc and then determine the required sophistication for the dynamic models. With such a procedure the systematic errors caused by model imperfections cannot accumulate up to a level that may corrupt the semidynamic mode solution. The relatively short arcs, however, are not stable in the sense that their position and orientation in space depends primarily on the geometry of the observations. This instability may also cause ill-conditioning of the normal equations (see Section 4.4). Furthermore, relatively short arcs cannot be well tracked to bring tracking sites of a global extent into a consistent satellite reference frame. This implies that it is not possible to use semidynamic mode methods for absolute position determination. Instead these methods can be effectively used for baseline determinations (Latimer et al., 1977; Christodoulidis et al., 1981; Pavlis, 1982; Section 4.4). Baseline estimates are even more accurate if the observables are insensitive to the position, orientation, and the shape of the trajectory as is the case, for

instance, with the Simultaneous Range Difference observables (see Section 4.4; Pavlis, 1982). With range observables, which are sensitive not only to the position and orientation of the trajectory in space but also to its shape, it is still possible to obtain accurate baselines if a local support tracking network is available (Christodoulidis et al., 1981).

2.2.1 Simultaneous Range-Difference Semidynamic Mode Method

On the basis of the discussion presented in the previous section and keeping in mind that our aim is to achieve highly accurate differential positioning, wc have chosen to use in this investigation the semidynamic (short-arc) method formulated in the context of special perturbations (see Section 2.2.3). Furthermore, the laser range observations have been transformed to Simultaneous Range-Differences (SRDs), and although differencing is a noise generating operation it is anticipated that these observables are less affected by the biases in the orbit, the reference frame and the observations themselves (Pavlis, 1982).

Using laser range observations to Lageos it is impossible to obtain strictly simultaneous observations not only because Lageos is a passive satellite but also because there will always exist synchronization errors among the various observing stations. Therefore Simultaneous Range Differences can only be obtained through an interpolation (see Chapter 3). More specifically, the observing stations are divided into pairs of simultaneously observing stations. For each pair the station with the most observations is interpolated to generate ranges at the observed epochs of the alternate station. Finally the interstation distances for each of the pairs involved are estimated by processing the generated SRDs through a least squares adjustment formulated in the context of the special perturbation methods as applied in the semidynamic mode environment.

2.2.2 Mathematical Modeling

The mathematical model for the Simultaneous Range Difference (SRD) observable $\delta_{\rho j}$ is obtained by subtracting the Euclidean ranges from station 2 and station 1 to the simultaneously observed satellite position j

$$\delta_{\rho j} = \left\{\left(\bar{S}_j - \bar{X}_2\right)^T\left(\bar{S}_j - \bar{X}_2\right)\right\}^{1/2} - \left\{\left(\bar{S}_j - \bar{X}_1\right)^T\left(\bar{S}_j - \bar{X}_1\right)\right\}^{1/2} \qquad (2\text{-}20)$$

where the vectors $\bar{S}_j = (u_j, v_j, w_j)^T$, $\bar{X}_1 = (u_1, v_1, w_1)^T$ and $\bar{X}_2 = (u_2, v_2, w_2)^T$ denote the Cartesian coordinates of the satellite position j, ground station 1 and ground station 2 respectively. Since the SRDs are invariant under any rigid body rotation the above vectors could be expressed in any arbitrarily chosen Cartesian coordinate system. In the present study, the vectors $\bar{S}_j$, $\bar{X}_1$ and $\bar{X}_2$ at epoch j are expressed in a Cartesian coordinate system whose origin is conveniently chosen to coincide with the center of mass of the earth, and its orientation is aligned to that of the true-of-date system (Mueller, 1969).

The adjusted parameters, in any estimation procedure involving a dynamic process, are transformed to a reference frame in which they can be considered constant for a certain period of time. This period should be long enough to allow for collection of a sufficient number of observations needed for a reliable recovery of the adjusted parameters. For this reason the ground station coordinates are transformed to a terrestrial reference frame (TRF) while the coordinates of the satellite at epoch j are transformed to a celestial reference frame (CRF) with the help of the following formulas (see Section 2.2.4)

$$\bar{S}_j = NP\bar{R}_j \;;\; \bar{X}_i = S^T\bar{Y}_i \;, \quad i = 1, 2 \qquad (2\text{-}21)$$

The quantities S, N and P designate the earth rotation, the nutation and precession matrices respectively, while the vectors $\bar{R}_j$, $\bar{Y}_1$ and $\bar{Y}_2$ denote the inertial position vector of the satellite at the epoch j and the earth-fixed position vectors of stations 1 and 2 respectively. The inertial and earth-fixed frames correspond to the CRF and TRF frames respectively as they are described in Section (2.2.4). Substituting equation (2-21) into (2-20) one obtains

$$\delta_{\rho j} = \left(D_{j_2}{}^T D_{j_2}\right)^{1/2} - \left(D_{j_1}{}^T D_{j_1}\right)^{1/2} = |D_{j_2}| - |D_{j_1}| \qquad (2\text{-}22)$$

where

$$D_{j_2} = NP\bar{R}_j - S^T\bar{Y}_2 \text{ and } D_{j_1} = NP\bar{R}_j - S^T\bar{Y}_1 \qquad (2\text{-}23)$$

The satellite position vector $\bar{R}_j$ is a function of an initial state vector and a large number of parameters affecting the motion of the satellite (i.e., potential coefficients, reflectivity, etc.). The choice of the model parameters to be estimated depends on the data coverage and distribution which in turn dictates the adopted lengths for continuous integration of the satellite orbit (see Section 2.2.1). In the present study, the shape of each of the satellite arcs involved is assumed known and only its position and orientation in space is adjusted to "best" fit the available data (see Section 4.4). Thus, the only adjusted parameters inherent to the satellite position vector $\bar{R}_j$ are the components of the initial state vector of the corresponding arc.

In the derivation of the observation equations, on the basis of the equation (2-20), one needs the satellite position vectors at each of the observing epochs together with their partial derivatives with respect to the corresponding initial state vector. The former is obtained by integrating the equations of motion of the satellite while the latter is obtained by integrating the variational equations of state (see Section 2.2.3). The partial derivatives with respect to earth-fixed station coordinates, also needed in the derivation of the observation equations, are easily obtained by differentiating equation (2-20) (see also Pavlis, 1982). The resulting observation equations are used to obtain the normal equations through a weighted least-squares adjustment (see Section 2.2.6). The normal equations are subsequently solved to estimate the initial state vectors for each of the arcs involved together with the earth-fixed coordinates which are finally transformed to interstation distances.

In the present study the initial state vectors are treated as "nuisance" parameters, and therefore one is not concerned with how well each of those initial state vectors has been recovered as long as the a posteriori variance of unit weight is close to unity. In fact, the reason for using SRDs instead of ranges is to reduce the need for accurate knowledge of the satellite orbits and yet to increase the potential for

baseline estimation with an accuracy compatible to or even better than that of the observations. This is possible because SRDs have the potential to reduce the effects of biases caused not only by the orbital model and the reference frames but also by eliminating uncorrectable systematic errors affecting the laser range observations (Pavlis, 1982).

2.2.3 Orbit Determination with the Method of Special Perturbations

Dynamic and semidynamic methods, based on special perturbations, require integration of the satellite's equations of motion. The degree of sophistication in formulating these equations depends on the integration length and the required accuracy.

Following the MERIT standards the relativistic perturbations are ignored from the equations of motion (Melbourne et al., 1983). Accordingly, ephemeris time (t) constitutes the independent variable in the equations of motion. Up to 1983, ephemeris time was used as an independent variable in the planetary equations of motion and therefore in the construction of all the almanacs. Since January 0^h 1984, ephemeris time has been replaced by Terrestrial Dynamical Time (TDT) and Barycentric Dynamical Time (TDB) (The Astronomical Almanac, 1984). This was a necessity since data collected in interplanetary missions are routinely processed in the context of the relativity theory (Moyer, 1971). In this context TDT time corresponds to proper time (i.e., time measured by the observer's clock) while TDB corresponds to coordinate time (i.e., time measured at the barycenter of a motionless solar system in the absence of all gravitational fields).

At each observing epoch j, the ephemeris time (t_j) is computed from the Universal Coordinated Time (UTC_j) with the help of the following formula

$$t_j = 32^s.184 + [TAI - UTC]_j + UTC_j = TDT \text{ (after 1984)} \qquad (2\text{-}24)$$

where

t_j = ephemeris time at the epoch j

$[TAI - UTC]_j$ = no. of leap seconds at the epoch j (The Astronomical Almanac, p. B5)

UTC_j = Universal Coordinated Time at the epoch j.

Using the ephemeris time (t) as an independent variable, the Lageos equations of motion take the following form (Cappellari et al., 1976; Pavlis, 1982):

$$\ddot{\bar{R}} = \ddot{\bar{R}}_{PM} + \ddot{\bar{R}}_{NS} + \ddot{\bar{R}}_{TD} + \ddot{\bar{R}}_{SR} + \ddot{\bar{R}}_{AT} \qquad (2\text{-}25)$$

Each of these accelerations is expressed relative to the center of mass of the earth. More specifically

$\ddot{\bar{R}} = \frac{d^2}{dt^2}\left(u_j, v_j, w_j\right)^T$ = total quasi-inertial Lageos acceleration at the epoch j

$\ddot{\bar{R}}_{PM}$ = gravitational acceleration due to point masses

$\ddot{\bar{R}}_{NS}$ = gravitational acceleration due to nonsphericity of the gravitational potential

$\ddot{\bar{R}}_{TD}$ = acceleration due to solid earth tidal effects

$\ddot{\bar{R}}_{SR}$ = acceleration due to solar radiation pressure

$\ddot{\bar{R}}_{AT}$ = Lageos empirical drag-like acceleration

The acceleration vector $\ddot{\bar{R}}$ is a function of an initial state vector and a large number of parameters affecting the motion of the satellite. These parameters pertain to the gravitational potential, to solar radiation pressure, etc. As it was described in the previous section, the only adjusted orbital parameters considered in this study are the initial state vectors of all the arcs involved. With these orbital parameters the variational equations assume a very simple form (Pavlis, 1982):

$$\ddot{Y}(t) = A(t) \cdot Y(t) \qquad (2\text{-}26)$$

with initial conditions

$$Y_o \equiv [\ I \mid 0\ ]_{3\times 6} \tag{2-27}$$

where

$$Y(t) = \left[\frac{\partial \bar{R}(t)}{\partial(\bar{R}(t_o),\ \dot{\bar{R}}(t_o))} \right]_{3\times 6} \tag{2-28}$$

and

$$A(t) = \left[\frac{\partial \ddot{\bar{R}}}{\partial \bar{R}(t)} \right]_{3\times 3} \tag{2-29}$$

The matrix Y(t) is referred to as the state transition matrix and is used to map the variations of the initial state into variations of the current state.

Equations (2-25) and (2-26) can be integrated either by one-step or by multi-step methods. In each integration step, the multistep methods require fewer derivative evaluations than the one-step methods of compatible accuracy. Fewer computations, on the other hand, not only reduce the round-off errors but also require less computing time. Furthermore, since these methods possess a larger number of parasitic solutions they are more susceptible to instability problems.

The multistep algorithm used in our study employs a self starting, variable step, variable order predictor-corrector mode of operation. This mode selects the order automatically while the stepsize is subject to accuracy requirements and numerical stability. Keeping the stepsize constant, the predictor-corrector is reduced to an Adams-Bashforth predictor of order q and to an Adams-Moulton corrector of order q + 1. With this algorithm the second-order differential equations are integrated directly without reducing them to a first-order system, because a second-order set exhibits better numerical stability characteristics. The described algorithm was developed and implemented in computer coded form by Krogh (1969a, 1969b, 1973a, 1973b, 1974).

2.2.4 Reference Frames and Systems

Reference frames constitute realizations of reference systems. The reference frames are used to describe the spatial relationships and the temporal variations of objects on the Earth (i.e., terrestrial frames) and in space including the Earth (i.e., celestial frames) (Kovalesky and Mueller, 1981). A reference system consists of an underlying principle and all those elements (e.g., physical environment, theories and constants) that are necessary to accomplish its realization. The elements of a system, depending on the application and the accuracy requirements, are selectively chosen and therefore the term "conventional system" is often used to designate the selection process that is usually involved in any realization of a reference system.

In this context the IAU/IUGG MERIT and COTES Joint Working Group recommended the following concepts in regard to reference systems and frames (Wilkins and Mueller, 1986):

> The Conventional Terrestrial Reference System (CTRS) be defined by a set of designated reference stations, theories and constants [necessary elements], chosen so that there is no net rotation or translation between the reference frame and the surface of the earth [underlying principle]. The frame is to be realized by a set of positions and motions of the designated reference stations.
>
> The Conventional Celestial Reference System (CCRS) be defined by a set of designated extragalactic radio sources, theories and constants [necessary elements], chosen so there is no net rotation between the reference frame and the set of the radio sources [underlying principle]. The frame is to be defined by the positions and motions of the designated radio sources. The origin of the frame is to be the barycentre of the solar system.

The above concepts are to be incorporated in the operation of the new International Earth Rotation Service (IERS). This service is scheduled to start operating as of January 0^h, 1988 (Mueller and Wilkins, 1986).

In the Newtonian framework, the reference frame implied by a CCRS can be considered as being an ideal inertial frame in the sense that the time is homogeneous and the space described by this frame is homogeneous and isotropic (Landau et al., 1960). In the general

relativistic framework, on the other hand, the reference frame realizing a CCRS is aimed to describe the curved space time for which a global inertial reference frame does not exist (Moritz, 1979; Fukushima, 1986)! This is the reason why, in the above recommendations, the term "inertial" has been dropped and the term "celestial" has been used instead.

For precise geodetic work, these seemingly conceptual differences manifest themselves when 10^{-8} or 10^{-9} accuracies are sought. Therefore, when working at such accuracy levels, care should be taken to account for relativistic effects either by using Newtonian formalism with small corrections (Moritz, 1979) or by formulating the problem entirely in the general relativistic framework (Fukushima, 1986). In the present study, in accordance with the MERIT standards and since the obtained accuracies hardly reach the 10^{-8} level, we have used the Newtonian formalism to formulate the equations of motion of the satellite.

The status today in terms of reference systems and frames is confusing because the user community employs a variety of different celestial systems (i.e., extragalactic radio source systems, stellar systems, dynamical systems, etc.) and a variety of different terrestrial systems as well (i.e., BIH terrestrial reference system, CSR terrestrial reference systems, etc.). Investigations, however, are currently underway with the objective of linking all of the available terrestrial systems into a unified terrestrial system referred to as "BIH Terrestrial Reference System" (BTS) (Boucher and Altamimi, 1985, 1986). Linking different celestial systems, through their frames, into an ideal celestial frame is not an easy task not only because of lack of collocations but also because daily polar motion resolution is necessary (Mueller, 1985). This kind of resolution is not achievable by the satellite related systems due mainly to the deficiencies in nutation theory (Himwich and Harder, 1986) and to inadequate observational coverage.

The choice of ideal terrestrial and celestial frames is not important in baseline estimation. It is important, however, to consistently link the involved terrestrial and celestial reference frames, by choosing the

appropriate set of transformation parameters. Effective choice of the transformation parameters would only assure a reliable recovery of the relative geometry of the observations since these parameters cannot be effectively recovered in a semidynamic mode environment. The relative geometry of the observations manifests the way the satellite arcs are related to the observing stations. Reliable recovery of the relative geometry, on the other hand, results in accurate baseline estimation simply because baselines are estimable quantities. Estimable quantities are molded by the geometric and dynamic characteristics creating the problem under question.

In the present study, the Terrestrial Reference Frame (TRF) is implied by the gravity field used to integrate the equations of motion and by the adopted polar motion series. The origin of the TRF frame, relative to the center of mass of the earth, is defined by the potential coefficients C_{10}, C_{11} and S_{11}, while its orientation is primarily defined by the potential coefficients C_{21} and S_{21} as well as C_{22} and S_{22}. More specifically, the coefficients C_{21} and S_{21} define the orientation of the third axis, while C_{22} and S_{22} define the orientation of the first axis. The orientation of the first axis, however, is weakly defined because the Earth's equatorial moments are nearly equal (i.e., $C_{22} \doteq S_{22}$).

The modified GEML2 gravity field, proposed by the MERIT standards, has been replaced in this study by the PGS1680 gravity field (Christodoulidis et al., 1985). This violation of the MERIT standards was necessary to make the gravity field consistent with the adopted BIH polar motion series. The modified GEML2 gravity field has all its coefficients but S_{21} and C_{21} equal to the coefficients of the GEML2 gravity field (Lerch et al., 1985). C_{21} and S_{21} have been modified to be consistent with the mean BIH polar motion values, computed over a complete wobble cycle which lasts from 6.5 to 7 years (Melbourne et al., 1983). Modifying only the C_{21} and S_{21} has caused inconsistencies as to what frame the coefficients of the modified GEML2 field refer. As a result, the PGS1680 gravity field was developed in order to avoid these inconsistencies and the resulting confusion as well. In the development of this field the coefficients S_{21} and C_{21} were constrained to the BIH

implied values while the remaining coefficients were free adjusting (Christodoulidis et al., 1985).

The coefficients C_{10}, C_{11} and S_{11} of the PGS1680 gravity field are zero thereby imposing the origin of the TRF frame to coincide with the center of mass of the earth. The computed UT1 time, on the other hand, is assumed to be consistent with the x axis of the implied TRF frame (see Section 4.3).

The Celestial Reference Frame (CRF) employed for the integration of the equations of motion, is realized from the implied TRF frame through the following transformation (Mueller, 1969):

$$(\overline{CRF}) = (SNP)^T(\overline{TRF}) \qquad (2\text{-}30)$$

with

$$S = R_2\ (-x_p)\ R_1\ (-y_p)\ R_3\ (GAST) \qquad (2\text{-}31)$$

where according to the MERIT standards the following quantities have been used.

P Precession matrix based on the IAU (1976) system of astronomical constants (Lieske, 1979)

N Nutation matrix based on the 1980 IAU theory of nutation (Wahr, 1981a). This matrix implies a pole whose nearly diurnal space-fixed and earth-fixed motions vanish. This pole is referred to as the Celestial Ephemeris Pole (CEP) (Mueller, 1981; Moritz and Mueller, 1987)

$$GAST \doteq GMST\ (0^hUT1) + f(UT1) + EQ.E \qquad (2\text{-}32)$$

$$GMST(0^hUT1) = 6^h\ 41^m\ 50\overset{s}{.}54841 + 8640184\overset{s}{.}812866\ Tu + 0\overset{s}{.}093104\ Tu^2 - 6\overset{s}{.}2 \times 10^{-6}\ Tu^3 \qquad (2\text{-}33)$$

where

f = conversion factor from Universal time to sidereal time
= $1.002737909350795 + 5.9006\times10^{-11}\ Tu - 5.9\times10^{-15}\ Tu^2$

Tu = Julian centuries elapsed from J2000.0

$UT1$ = $UTC(USNO) + (UT1 - UT1R) + [UT1R - UTC(BIH)] + [UTC(BIH) - UTC(USNO)]$ (2-34)

UTC(USNO) = USNO Universal Coordinated time (time scale used to time tag the observations of the GLTN stations)

UT1 - UT1R = Tidal variations of UT1 caused by zonal tides with periods up to 35 days (BIH Annual Report 1981 onwards, Table B1)

UT1R - UTC(BIH) = Variations of the regularized UT1 (i.e., UT1R) from the UTC(BIH) (BIH Annual Reports, Table 8)

UTC(BIH) - UTC(USNO) =Variations of UTC(USNO) in relation to UTC(BIH)

$$EQ.E = \Delta\psi \cdot \cos(\bar{\varepsilon} + \Delta\varepsilon) \qquad (2\text{-}35)$$

$\Delta\psi$ = Nutation in longitude computed from the 1980 IAU nutation theory

$\bar{\varepsilon}$ = Mean obliquity of the ecliptic

$$= 23^\circ\ 26'\ 21\overset{''}{.}448 - 46\overset{''}{.}8150Tu - 0\overset{''}{.}00059Tu^2 + 0\overset{''}{.}001813Tu^3 \qquad (2\text{-}36)$$

$\Delta\varepsilon$ = Nutation in obliquity computed from the 1980 IAU nutation theory

The CEP pole positions x_p and y_p in equation (2-31) have been taken from the smoothed values of Circular D (BIH Annual Report, 1983, 1984, Table 7). These pole positions are referenced to the 1979 BIH system during the first period of the MERIT Main Campaign (Sept. 1983 - Dec. 1983), while during the remaining period of the campaign (Jan. 1984 - Dec. 1984) they are referenced to the BIH Terrestrial System (BTS). Our study in not affected by this transition because in shifting from the 1979 BIH system to the BTS system a nonrotation constraint was applied to assure the continuity of the BIH system (Boucher and Feissel, 1984).

2.2.5 Orbital Model

The set of elements necessary to determine a satellite orbit constitutes the orbital model of the satellite. Thus, an orbital model consists of all those elements that are essential to formulate and integrate the

equations of motion (i.e., perturbations to be considered and associated assumptions, initial conditions, etc.).

The Lageos state vectors required in the evaluation of the observation equations (Section 2.2.6) are obtained by numerically integrating the equations of motion (2-25). In this equation the inertial accelerations are expressed relative to the geocenter. The components, however, of Lageos' inertial acceleration caused by the nonsphericity of the earth are evaluated in the TRF frame and subsequently are transformed into the corresponding CRF frame, while the components of the remaining inertial accelerations are directly expressed in the corresponding CRF frame. The two-step procedure used to evaluate the Lageos inertial acceleration caused by the nonsphericity of the earth is necessary because the gravity potential coefficients are conveniently expressed in a TRF frame. Expressing these coefficients directly in a CRF frame would make them time dependent and therefore a potential source of unnecessary complications.

The aim of the present study is not to estimate the Lageos orbit with the highest accuracy but rather to model it as simply as possible and yet be able to recover the baselines with an accuracy compatible to or even better than that of the observations. With this in mind the MERIT standards have been violated whenever the proposed model is complicated and cumbersome to incorporate into the solution. In such cases a simpler model has been adopted. It turns out, however, that in some cases the employed orbital model could be further simplified without affecting the accuracy of the recovered baselines (Section 4.6).

2.2.5.1 Point mass gravitational acceleration. The point mass Lageos gravitational acceleration based on the effects of the three major perturbing bodies (Earth (E), Moon (M) and Sun (S)) and expressed relative to the geocenter takes the following form (Cappellari et al., 1976; Pavlis, 1982)

$$\ddot{\bar{R}}_{PM} = GM_E\left(-\frac{\bar{r}_L^E}{|\bar{r}_L^E|^3} - \frac{M_M}{M_E}\frac{\bar{r}_L^M}{|\bar{r}_L^M|^3} - \frac{M_S}{M_E}\frac{\bar{r}_L^S}{|\bar{r}_L^S|^3} + \frac{M_M}{M_E}\frac{\bar{r}_E^M}{|\bar{r}_E^M|^3} + \frac{M_S}{M_E}\frac{\bar{r}_E^S}{|\bar{r}_E^S|^3}\right) \quad (2\text{-}37)$$

where

$\bar{r}_L^E$, $\bar{r}_L^M$, $\bar{r}_L^S$ =: Lageos position vectors relative to the center of mass of the Earth, the Moon and the Sun respectively

$\bar{r}_E^M$, $\bar{r}_E^S$ =: Earth position vectors relative to the center of mass of the Moon and the Sun respectively

$\frac{M_M}{M_E}$, $\frac{M_S}{M_E}$ =: ratios of lunar and solar masses to the mass of the Earth

GM_E =: geocentric gravitational constant

For the evaluation of equation (2-37), one needs the Lageos geocentric position vector as well as the geocentric position vectors of the Moon and the Sun respectively. The Lageos geocentric position vectors are obtained from the numerical integration of the equations of motion while the heliocentric position vector of the Earth and the geocentric position vector of the Moon are calculated from the information supplied by the DE/LE200 lunar planetary ephemeris (Standish, 1981). This ephemeris is disseminated in terms of Chebychev coefficients. These coefficients can only be used to calculate the geocentric positions of the Moon and the barycentric positions of remaining planets and the Sun. With this information, however, one can very easily calculate the position of any desired planet with respect to any of the remaining planets and to the sun as well.

The reference frame implied from the computed coordinates of the planets has been accurately adjusted to the dynamical equinox J2000.0 (ibid.) The Chebychev coefficients of the DE/LE200 lunar planetary ephemeris are based on the planetary coordinates estimated through the numerical integration process involved in the adjustment of interplanetary observations collected over a long period of time (ibid.). In this adjustment, the planetary equations of motion were formulated on the basis of the isotropic, parametrized post-Newtonian (PPN) n-body metric (Moyer, 1971). The independent variable in the PPN metric is the Barycentric Dynamical Time (i.e., coordinate time), and therefore this time scale should be used as an entry to the DE/LE200 ephemeris.

The TDB time at any epoch j is computed from the ephemeris time of the same epoch via the following formula

$$TDB_j = t_j + \Delta T \qquad (2\text{-}38)$$

where

TDB_j = Barycentric Dynamical Time at the epoch j

t_j = ephemeris time at epoch j, obtained from equation (2-24)

In the PPN framework the ephemeris time coincides numerically but not conceptually with the Terrestrial Dynamical Time (i.e., proper time). Thus, TDB time at any epoch is obtained by adding to the ephemeris time of the same epoch a small correction ΔT. This correction accounts for the general relativistic effects involved in the transformation of proper time (i.e., TDT time) to coordinate time (i.e., TDB time). An approximate value for the correction ΔT is given by the following formula (Astronomical Almanac, 1984)

$$\Delta T = 0^{s}001658 \sin(g) + 0.000014 \sin(2g) \qquad (2\text{-}39)$$

where

$$g = 357^{\circ}53 + 35999.05\ Tu \qquad (2\text{-}40)$$

In both of these equations (2-39 and 2-40), higher-order terms have been neglected, g designates the mean anomaly of the Earth in its orbit, and Tu designates the Julian centuries elapsed since J2000.0.

To complete the evaluation of equation (2-37), one still needs the ratios of the lunar and solar masses to the mass of the earth as well as the geocentric gravitational constant. For the mass ratios, we have used the values recommended by the MERIT standards, but for the geocentric gravitational constant the value estimated simultaneously with the potential coefficients of the PGS1680 gravity field has been used:

$$GM_E = 3.986004359 \times 10^{14}\ m^3/s^2 \qquad (2\text{-}41)$$

The scale in the range dynamic mode methods is implied not only by the adopted value of the geocentric gravitational constant through the modified Kepler's third law but also through the speed of light used to convert time measurements to range measurements. Thus, the adopted value of the geocentric gravitational constant should also be consistent with the speed of light implicit in the range observations. In the present study we have used the speed of light proposed by the MERIT standards (i.e., c = 299,792,458 m/s) (Lerch et al., 1985; Christodoulidis et al., 1985).

The associated partial derivatives of equation (2-37) contributing to the variational equations of state (i.e., to matrix Y(t), equation (2-28)) are given in (Cappellari et al., 1976, eq. 4-21; Pavlis 1982, eq. 13).

2.2.5.2 Gravitational acceleration due to nonsphericity of the gravitational potential. The inertial acceleration induced on the satellite by the nonsphericity of the earth is obtained via the gradient of the perturbing potential. The perturbing potential is a scalar function describing the nonspherical part of the geopotential in terms of an infinite spherical harmonic series (Heiskanen and Moritz, 1967):

$$V_{NS}(r,\phi,\lambda) = \frac{GM_E}{r}\left[\sum_{n=2}^{\infty}\left(\frac{a_E}{r}\right)^n \sum_{m=0}^{n}[C_{nm}\cos(m\lambda) + S_{nm}\sin(m\lambda)]P_{nm}(\sin\phi)\right] \quad (2\text{-}42)$$

The zero-degree harmonic has been modeled in equation (2-37) and therefore is not included in the above equation. The first-degree harmonics are also not included because the origin of the PGS1680 implied (TRF) coincides with the the center of mass of the earth (see Section 2.2.4). With the gradient of the perturbing potential the components of Lageos' inertial acceleration, caused by the nonsphericity of the earth, are expressed in the PGS1680 implied (TRF) frame. Incorporation of this acceleration into the equations of motion (2-25) requires transformation of its components from the (TRF) frame into the corresponding (CRF) frame via the transformation equation (2-30)

$$\ddot{\bar{R}}_{NS} = (SNP)^T \ddot{\bar{r}} \qquad (2\text{-}43)$$

where

$$\ddot{\bar{r}} = \left[\frac{\partial V_{NS}}{\partial x} , \frac{\partial V_{NS}}{\partial y} , \frac{\partial V_{NS}}{\partial z}\right] \qquad (2\text{-}44)$$

is the gradient of the perturbing potential function V_{NS} (equation 2-42). The expressions for the partial derivatives of the perturbing potential function V_{NS} are given in (Cappellari et al., 1976). The radius (a_E) of the reference sphere, also needed in the evaluation of the perturbing potential, is the same with the radius employed in the estimation of the PGS1680 gravity field (i.e., a_E = 6378144.11 m). For our study we have truncated this field at degree and order 12 because perturbations caused by higher harmonics over a two-week period contaminate the computed SRD observables with errors having magnitude well below the noise level of the SRD quasi-observables (see Section 4.6). Furthermore, a nonvariant nature of the coefficients C_{21} and S_{21} has been adopted, although it is well known that these two coefficients are largely affected by the forced diurnal motion of the figure axis caused by the nonrigidity of the earth (Moritz and Mueller, 1987).

The associated partial derivatives of equation (2-42) contributing to the variational equations of state are given in (Cappellari et al., 1976, eq. 4-54; Pavlis, 1982, eq. 21).

2.2.5.3 Lageos tidal inertial acceleration. According to the MERIT standards, the tidally induced variations in the earth's external potential should be incorporated in the orbital model as variations in the geopotential coefficients (Melbourne et al., 1983; Eanes et al., 1983). In order to save computing time a two-step procedure is proposed to carry out the implementation of these variations (ibid). In the first step the variations of the geopotential coefficients are computed on the basis of a nominal frequency independent Love number k_n, while in the second step these variations are corrected to account for the frequency dependent nature of the nominal Love number k_n.

The frequency dependent variations of the Love number k_n have been estimated for an elliptical, rotating, elastic fluid outer core and solid inner core, oceanless earth (Wahr, 1981b). Although the proposed two-step procedure is computationally more effective than any one-step procedure, it is not appropriate for our investigation because one still needs to evaluate many trigonometric functions at each of the observing epochs (Melbourne et al., 1983). This however, not only would make the orbital model more complicated but also it would make the SRD method computationally less efficient. Therefore, it was decided to compute the tidally induced space potential by assuming a solid earth (i.e., oceans not included) which exhibits the same elastic response over all possible orders within a certain degree (Diamante et al., 1972; Pavlis, 1982). With such an earth model the tidally induced potential on the surface of the earth takes the following form (Diamante et al., 1972; Goad, 1977; Pavlis, 1982):

$$U_{T_D} = \sum_{n=2}^{\infty} k_n \, U_{T_n}(a_E) \tag{2-45}$$

where k_n is the nominal Love number of degree n and $U_{T_n}(a_E)$ is the n^{th} surface harmonic of the tidal potential. Solving the Dirichlet problem the tidally induced space potential is obtained:

$$U_{T_D} = \sum_{n=2}^{\infty} \left(\frac{a_E}{|\bar{R}|}\right)^{n+1} k_n \, U_{T_n}(a_E) \tag{2-46}$$

where $|\bar{R}|$ is the norm of the Lageos position vector expressed relative to the center of mass of the earth. To the first order, terms with $n > 2$ in equation (2-46) can be neglected (Diamante et al., 1972), and therefore this equation takes the following form

$$U_{T_D} = \frac{a_E^3}{|\bar{R}|^3} k_2 \, U_{T_2}(a_E) \tag{2-47}$$

where

$$U_{T_2}(a_E) = \frac{GM_b}{2|\bar{R}_b|^3} \cdot a_E^2 \left[3\left(\frac{\bar{R}_b}{|\bar{R}_b|} \cdot \frac{\bar{R}}{|\bar{R}|}\right)^2 - 1 \right] \qquad (2\text{-}48)$$

The quantity k_2 denotes the second-degree Love number while M_b denotes either the lunar or the solar mass, or for that matter the mass of any planet that is considered to be a disturbing body. In this study the Moon and the Sun have been considered as the only disturbing bodies. The vectors $\bar{R}$ and $\bar{R}_b$ designate the geocentric position vectors of the satellite and the disturbing body respectively. The components of these vectors are expressed in the corresponding (CRF) frame. In this frame the tidally induced acceleration on Lageos takes the following form (Diamante et al., 1972; Pavlis, 1982):

$$\ddot{\bar{R}}_{TD} = \frac{3}{2} k_2 \frac{GM_b}{|\bar{R}_b|^3} \cdot \frac{a_E^5}{|\bar{R}|^4} \left[(1 - 5(\bar{u}_b \cdot \bar{u})^2)\bar{u} + 2(\bar{u}_b \cdot \bar{u})\bar{u}_b \right] \qquad (2\text{-}49)$$

where

$$\bar{u}_b = \frac{\bar{R}_b}{|\bar{R}_b|} \quad \text{and} \quad \bar{u} = \frac{\bar{R}}{|\bar{R}|} \qquad (2\text{-}50)$$

To account for a phase lag produced by the earth's dissipative forces, the vector $\bar{R}_b$ in equation (2-50) has been replaced by another vector $\bar{R}_b^*$. This vector is obtained from the vector $\bar{R}_b$ via the following transformation

$$\bar{R}_b^* = R_3(-\delta_L)\bar{R}_b \qquad (2\text{-}51)$$

where δ_L (=0°.35) is the phase lag. The R_3 rotation is performed about the third axis of the corresponding CRF frame (see Section 2.2.4). In equations (2-47) and (2-49) the value 0.29 was adopted for the second-degree Love number k_2. This value is different from that proposed by the MERIT standards (k_2 = 0.30). This deviation, although not of much importance, is justified since the tidal corrections applied in the estimation of the PGS1680 gravity field were based on the altered value of k_2 (i.e., k_2 = 0.29). The permanent tidal deformation affecting

the potential coefficient C_{20} is inherently present in equation (2-49). Consistent incorporation of this equation in the equations of motion requires that the permanent tidal deformation is not included in the PGS1680 C_{20} value. This, however, seems to be the case for the PGS1680 gravity field (Melbourne et al., 1983; Christodoulidis et al., 1985). Furthermore, the ocean tidal perturbations are not included in the orbital model of Lageos not only because they are small (i.e., one order of magnitude smaller than the solid earth tidal effects (Section 4.6)) but also because their evaluation would increase the bulk of the computations considerably.

The contribution of the tidally induced acceleration to the variational equations of state is given in (Pavlis, 1982, eq. 30). In that equation the vector $\bar{R}_b$ should be replaced by the vector $\bar{R}_b^*$ from equation (2-51).

2.2.5.4 Lageos solar radiation pressure acceleration. The acceleration induced on Lageos due to photon momentum transfer is referred to as solar radiation pressure acceleration, and it is given by the following formula (El'Yasberg, 1967; Cappellari et al., 1976; Pavlis, 1982).

$$\ddot{\bar{R}}_{SR} = \gamma \cdot \frac{S}{C} \left(\frac{Au}{|\bar{R}_S - \bar{R}|} \right)^2 \cdot C_R \cdot \frac{A}{M} \cdot \frac{\bar{R} - \bar{R}_S}{|\bar{R}_S - \bar{R}|} \qquad (2\text{-}52)$$

The eclipse factor γ assumes the values zero, one, or any other value in between depending on whether the satellite is in complete shadow (umbra), in sunlight, or in partial shadow (penumbra) respectively. In our study the eclipse factor γ is determined by a simple cylindrical model (Cappellari et al., 1976; Pavlis, 1982). This model is easy to incorporate into the equations of motion, but it does not differentiate between umbra and penumbra regions. A full model for the earth's shadow, as proposed by the MERIT standards, would increase the bulk of computations thereby complicating the solution. It is rather doubtful

that this complication would make any difference. The mean solar flux S is the amount of photon energy flow through a unit surface per unit time at a distance of one astronomical unit (AU) (i.e., AU = 1.4959787066 $\times 10^{11}$ meters) (Melbourne et al., 1983). The ratio (S/C) is the photon momentum transfer to a unit surface per unit time at a distance of one astronomical unit. The value (4.5605×10^{-6} N/M^2) was used in our study for the ratio (S/C) as proposed by the MERIT standards. The position vectors $\bar{R}$ and $\bar{R}_S$ in equation (2-52) designate the geocentric position vectors of Lageos and the Sun respectively. The reflectivity coefficient (C_R) depends not only on the mechanism of light reflection but also on the thermal emission distribution of the satellite surface. The monthly values for the reflectivity coefficient (C_R) are shown in Table 1 for the entire MERIT campaign. These values have been estimated together with other parameters in the adjustment of the MERIT laser range data performed by the GEODYN II programs (Pavlis, 1986, private communication). In the present study we have used the reflectivity coefficient values listed in Table 1 instead of using the value proposed by the MERIT standards.

Table 1 Lageos Along-Track Acceleration and Its Reflectivity Coefficients

	Magnitude of Lageos Along-Track Acceleration $\times 10^{-12}$ m/s^2	Lageos Reflectivity Coefficients
Sep. 1983	-2.909	1.141
Oct. "	-3.549	1.136
Nov. "	-3.893	1.135
Dec. "	-3.825	1.133
Jan. 1984	-4.343	1.136
Feb. "	-4.319	1.134
Mar. "	-4.065	1.109
Apr. "	-3.550	1.057
May "	-3.189	1.096
Jun. "	-3.393	1.139
Jul. "	-3.928	1.132
Aug. "	-2.946	1.126
Sep. "	-2.301	1.126
Oct. "	-2.524	1.126

This deviation of the MERIT standards, although plausible, will not affect the accuracy of the estimated baselines. The effective area (A) of the surface normal to the incident light is given, for a spherical satellite like Lageos, from (El'Yasberg, 1967)

$$A = \pi R_S^2 \qquad (2\text{-}53)$$

where R_S is Lageos' radius (i.e., R_S = 0.30 m) (Melbourne et al., 1983). Finally, the Lageos mass (M) of 407 kg has been used in the evaluation of equation (2-52).

The associated partial derivatives of the solar radiation pressure acceleration contributing to the variational equations of state are given in (Cappellari et al., 1976, eq. 4-161 and 4-162; Pavlis, 1982, eq. 25 and 26).

According to the MERIT standards the inertial acceleration induced on the satellite due to the diffused reradiated light from the earth (earth albedo) is not included in the orbital model of the Lageos satellite.

2.2.5.5 Lageos along-track empirical acceleration. Ever since the launch of the Lageos satellite it has been observed that its semimajor axis decreases at a rate of 1 mm/day. This has been traced to an unexpected and still physically unmodelled along-track acceleration acting on the Lageos satellite. Attempts to explain the origin of this mysterious acceleration have either totally or partially failed. These attempts are based on a variety of possible causes ranging from assuming helium concentrations at satellite altitudes (Rubincam, 1980) to considering the solar eclipses (Rubincam et al., 1985). Although all of these attempts have partially failed, it is quite clear that this acceleration is the result of a combined effect caused by the asymmetries of the earth's albedo and by the charged particles traveling in the vicinity of Lageos (Smith et al., 1985; Alfonso et al., 1985). Since the physical process producing this acceleration is unknown, its modeling has been accomplished with an empirical model. This model

assumes a "drag-like" force acting against the satellite motion (Pavlis, 1982):

$$\ddot{\bar{R}}_{AT} = - \alpha \frac{\dot{\bar{R}}}{|\dot{\bar{R}}|} \tag{2-54}$$

where α is the magnitude of the along-track acceleration. The monthly magnitudes of this acceleration are also listed in Table 1 for the entire MERIT campaign. These values have been estimated with the GEODYN II program (Pavlis, 1982, private communication).

Contributions to the variational equations of state due to this acceleration are neglected because of their small magnitudes.

2.2.6 Normal Equations

The observation equations for the SRD quasi-observables are readily obtained through a Taylor series expansion of equation (2-22). In this expansion only the zero- and first-order terms are retained while all of the remaining higher-order terms are neglected. The expansion is performed about the approximate earth-fixed station coordinates and the celestial initial state vector of the corresponding arc:

$$V_j = A_j \bar{X}_j + L_j \tag{2-55}$$

where

$$(A_j)_{1\times 12} = \left[B_j \vdots C_j \right]_{1\times 12} \tag{2-56}$$

$$(B_j)_{1\times 6} = \left[\frac{\partial \delta\rho_j}{\partial(\bar{Y}_1, \bar{Y}_2)} \right]_{1\times 6} \tag{2-57}$$

$$(C_j)_{1\times 6} = \left[\frac{\partial \delta\rho_j}{\partial \bar{R}_j} \right]_{1\times 3} \cdot \left[\frac{\partial \bar{R}_j}{\partial(\bar{R}_o, \dot{\bar{R}}_o)} \right]_{3\times 6} = (S_j)_{1\times 3} \cdot [Y_j(t)]_{3\times 6} \tag{2-58}$$

$$\bar{X}_j = (d\bar{Y}_1 \ , \ d\bar{Y}_2 \ , \ d\bar{R}_o \ , \ d\dot{\bar{R}}_o)^T_{1x12} \qquad (2\text{-}59)$$

L_j = the computed minus the generated SRD quasi-observable

V_j = residual corresponding to the j^{th} SRD observable

The matrices $(B_j)_{1x6}$ and $(S_j)_{1x3}$ are readily obtained by differentiating equation (2-22), while the state transition matrix $[Y_j(t)]_{3x6}$ is obtained in the numerical integration process of the variational equations of state. The celestial satellite coordinates at the epoch j needed to evaluate the vectors $(B_j)_{1x6}$ and $(S_j)_{1x3}$ as well as the scalar L_j are obtained from the numerical integration of Lageos' equations of motion (see Sections 2.2.3 through 2.2.5). The adjusted parameter vector $\bar{X}_j$ contains corrections to the earth-fixed approximate coordinates of stations 1 and 2 (i.e., $d\bar{Y}_1$ and $d\bar{Y}_2$) and to the corresponding celestial initial state vector (i.e., $d\bar{R}_o$ and $d\dot{\bar{R}}_o$). Extension of equations (2-55)-(2-59) to include all the available SRD observables and all the observed satellite arcs leads to the following equations

$$\bar{V} = A^*\hat{\bar{X}} + \bar{L} \qquad (2\text{-}60)$$

where

$$A^* = [\ B^* \ \vdots \ C^*\ ] \qquad (2\text{-}61)$$

$$B^* = \left[\frac{\partial \delta \bar{\rho}}{\partial \bar{Y}}\right]_{nx3k} \qquad (2\text{-}62)$$

$$C^* = \left[\frac{\partial \delta \bar{\rho}}{\partial \bar{R}}\right]_{nx3\ell} \cdot \left[\frac{\partial \bar{R}}{\partial (I_{\bar{R}_o}, I_{\dot{\bar{R}}_o})}\right]_{3\ell x6m} = (S)_{nx3\ell} \cdot [Y^*(t)]_{3\ell x6m} \qquad (2\text{-}63)$$

$$\hat{\bar{X}} = \left[d\bar{Y} \ , \ d\left(I_{\bar{R}_o}, I_{\dot{\bar{R}}_o}\right)\right] \qquad (2\text{-}64)$$

$\bar{L}$ = vector containing the computed minus the SRD quasi-observables

$\bar{V}$ = residual vector

Vector $\bar{\delta\rho}$ contains all the available SRD observables, vector $\bar{Y}$ the Cartesian coordinates of all the observing stations, vector $\bar{Z}$ the Cartesian coordinates of the observed satellite positions, and vectors $I_{\bar{R}_0}$, $I_{\dot{\bar{R}}_0}$ the initial state vectors of all the arcs involved. The adjusted parameter vector $\hat{\bar{X}}$ contains the corrections to the approximate earth-fixed coordinates of the observing stations (i.e., $d\bar{Y}$) together with the corrections to the initial state vectors of the observed satellite arcs (i.e., $d(I_{\bar{R}_0}, I_{\dot{\bar{R}}_0})$). The integers ℓ and n denote the number of the observed satellite positions and the number of observations, while the integers k and m denote the number of the observing stations and the number of the observed satellite arcs respectively.

A close examination of equations (2-62) and (2-63) reveals that the submatrices $(B^*_{n\times 3k})$ and $(S_{n\times 3\ell})$ would be exactly the same even if the satellite positions were treated as auxiliary independent points in space (i.e., geometric approach). The constraints imposed on the observed satellite positions to lie in the corresponding satellite arcs are applied through the state transition matrix $(Y^*(t)_{3\ell\times 6m})$.

Singularity A (see Section 2.1.3) affects the dynamic and geometric solutions in exactly the same way because the submatrix B^* in equation (2-61) is the same for both the geometric and the dynamic approach. With SRD observables singularity A occurs not only from the resulting geometry of one station and its observed targets (see Section 2.1.3) but also from the geometry of two coobserving stations and their observed targets. Singularity B or singularity C cannot exist in a dynamic solution because the structure of the matrix $(S_{n\times 3\ell})$ is altered by its multiplication with the state transition matrix $(Y^*(t)_{3\ell\times 6m})$. The alteration of the matrix $(S_{n\times 3\ell})$ not only differentiates the dynamic from the geometric approach but also furnishes the dynamic approach with better stability characteristics (see Sections 4.2 and 4.4).

Taking into consideration that the state transition matrix is different from epoch to epoch, one can readily prove that in the absence of

singularity A the design matrix A^* (apart from the ill-defined origin of longitudes) is nonsingular if the adjusted parameter vector consists only of corrections to the approximate station coordinates and to the initial state vectors. This is not surprising because the TRF frame, with an ill-defined origin of longitudes, is implied by the PGS1680 gravity field while the CRF frame is subsequently realized via the transformation equation (2-30). Including polar motion and/or variations of UT1 in the adjusted parameter vector results in an extremely ill-conditioned design matrix A^* because polar motion and station coordinate are nearly inseparable, while variations in UT1 and in the satellite node are inseparable parameters as well (Van Gelder, 1978; Pavlis, 1982).

In the present study, polar motion and the variations in UT1 are not included in the adjusted parameter vector. Thus, after resolving the problem of the ill-defined origin of longitudes (see Section 4.4) we proceed with the formation and the solution of the normal equations. Using the same arguments as in Section 2.1.2 and the observation equations (2-60), the normal equations take the following form (Uotila, 1987)

$$(A^{*T}PA^* + P_X)\hat{\bar{X}} + A^{*T}P\bar{L} = 0 \qquad (2\text{-}65)$$

where P and P_X are the weight matrices associated with the SRD observables and the adjusted parameter vector respectively. Since the weight matrix P is diagonal the normals are formed sequentially through the following formula

$$A^{*T}PA^* + P_X = \sum_{j=1}^{n} \frac{A_j^T A_j}{\sigma_j^2} + P_X \qquad (2\text{-}66)$$

where A_j (i.e., equation (2-56)) is the j^{th} row of the design matrix A^*, n is the total number of the SRD observables and σ_j^2 is the variance for the j^{th} SRD observable. These variances are computed via the following formula

$$\sigma_j^2 = \sigma_{j_1}^2 + \sigma_{j_2}^2 \qquad (j = 1, \ldots, n) \qquad (2\text{-}67)$$

where $\sigma_{j_1}^2$ and $\sigma_{j_2}^2$ are the variances of the actually observed and the interpolated ranges respectively. The inversion of the normal equation matrix (2-66) was obtained with the Cholesky algorithm (Uotila, 1967).

Chapter 3

GENERATION OF THE OBSERVABLES

This chapter starts with a description of the SLR system in an attempt to identify and understand the systematic errors affecting the laser ranges. It continues with a description of the data set employed in this investigation and finally ends with the generation of the simultaneous range and SRD observables. These two observables constitute the input to the geometric and SRD methods respectively.

3.1 SATELLITE LASER RANGING

A satellite laser ranging system consists of three basic components:

(i) the ground segment,

(ii) the atmospheric channel, and

(iii) the spaceborne segment.

The ground segment consists of a global network of fixed and highly mobile satellite laser ranging stations forming a network configured to allow measurements of the plate tectonic motions (Coates et al., 1985). Tectonic plate motions are essential in understanding the geodynamic processes necessary for earthquake and volcano erruption predictions. Each of the stations in the network is equipped with the necessary hardware to produce, emit, receive and measure the round-trip flight time of very short laser pulses to a retroreflector equipped artificial satellite such as LAGEOS.

The atmospheric channel is the optical path followed by a laser pulse in its round trip from the station to the satellite.

The spaceborne segment consists of approximately 14 retroreflector equipped satellites (Degnan, 1985). For geodesy and geodynamics Lageos

is an example of such a satellite in orbit high enough not to be influenced by the difficult to model high frequency variations of the gravity field and the atmospheric drag but yet at low enough altitude to assure good signal returns to the tracking stations. Therefore, the propagation of the orbital errors in the estimated geodetic parameters is substantially reduced. This error reduction is very important because variations in certain geodetic parameters such as baselines, polar motion, and length of day are routinely used in understanding the mechanisms driving geodynamic processes.

In the operational environment, depending on the technology employed and the models used, each component of the satellite laser ranging system will contribute in part to the total error affecting the inferred geometric range. The next section contains, for each component of the SLR system, a brief discussion of its operational principles, the error sources, their status during the MERIT Main Campaign and the future possibility of either reducing or eliminating them.

3.2 SATELLITE LASER RANGING SYSTEM, ITS COMPONENTS AND THEIR CONTRIBUTION TO THE TOTAL ERROR BUDGET

3.2.1 Hardware of the Ground Segment

For each satellite ranging system, the hardware of the ground segment consists of the laser transmitter, the laser receiver, their transmittimg and receiving optics, the timing subsystem and the computer.

The ***laser transmitter*** in most of the modern laser systems consists of a mode-locked Nd:YAG laser oscillator followed by one or more Nd:YAG laser amplifiers. The name Nd:YAG is derived from the crystal used in the light amplification by stimulated emission of radiation (i.e., lasing process) which is a YAG crystal (Yttrium aluminum garnet : $Y_3Al_5O_2$) "doped" with Neodymium (Johnson et al., 1978). Since the mode-locked Nd:YAG lasers operate in a single spatial mode they are not affected by "wavefront-distortion" errors (Degnan, 1985). The biases introduced by

the mode-locked transmitters are of the order of subcentimeter level. The crystals used in the lasing process, for the stations participating in the MERIT Main Campaign, are reported in the SLR coordinator's report and its updates (Schutz, 1983b).

The ***laser receiver*** is designed to measure the round-trip flight time of the laser pulse to a retroreflector equipped satellite. This time interval is multiplied by the speed of light and divided by two to infer the optical range from the station to the satellite. The basic elements of a laser receiver are the photomultiplier, the discriminator and the time interval unit.

The ***photomultiplier*** is a device used to detect the incoming laser pulse. Its principle of operation is based on the photoelectric effect (Halliday et al., 1962; Drain, 1980). Most of the SLR systems participating in the MERIT Main Campaign made use of the conventional type photomultipliers referred to as dynode-chain photomultipliers (Degnan, 1985). The time it takes for the photoelectrons to propagate from the photocathode to the anode via the dynodes is called transit time. If the transit time were constant it could be completely accounted for through either calibration or common channel procedures (ibid). Variations in the transit time, referred to as transit time jitter, influence the inferred ranges by as much as 15 cm (ibid). This error is mainly caused by the motion of the satellite image within the photocathode when the instrument tracks the satellite. However, successful focusing of the satellite image onto the photocathode reduces this error to the 1 cm level. Other factors such as the impulse response of the PMT's, the amplitude of the input signals and the background radiation also contribute to this error. These problems are currently being solved with the replacement of the conventional PMT's with the so-called microchannel plate photomultiplier tubes (MCP/PMT) recently introduced on the market. These photomultipliers are characterized by well-defined photoelectron path lengths with much shorter transit times, and greatly reduced sensitivity in the image position effects, the strength of the input signal and the background radiation. When using the MCP/PMT photomultipliers, the resulting

errors in the inferred range appear to be below the 5 mm level (ibid).

The purpose of a ***discriminator*** is to define on the photomultiplier's output waveform a timing point and subsequently to generate a rectangular logic pulse that starts or stops the time interval unit. The output waveform has a quasi-Gaussian form with a randomly varying amplitude. This amplitude variation introduces, in the determination of the timing point, a time bias which is highly repeatable and can be estimated if the amplitude of the input pulse is measured and recorded along with each observation. In practice the amplitude-dependent time bias is determined experimentally and is compensated for by incorporating a hardwired circuitry into the discriminator. The degree of success in implementing this circuitry is determined experimentally and is shown in the time walk characteristic of the discriminator. The time walk characteristic is a curve obtained by plotting the signal amplitude dependent time biases versus the input signal amplitudes. The time walk characteristic shows the time bias introduced by amplitude variations, while its RMS deviation from the zero horizontal line characterizes the efficiency of the discriminator (ibid). For the discrimators used during the MERIT Main Campaign, this RMS deviation reached the value of 1.5 cm, while for discrimators currently appearing on the market this value has been reduced to the 0.2 cm level. The latter discriminators are currently being tested for implementation in the continuously upgraded SLR systems.

The purpose of the ***Time Interval Unit (TIU)*** is to measure the round-trip flight time of the laser pulse. The rectangular logic pulse generated by the start discriminator activates the time interval counter while the corresponding logic pulse from the stop discriminator commands the counter to stop. The basic component of the TIU is an oscillator which determines the stability and accuracy of the TIU. The oscillators used by the SLR stations which participated in the MERIT Main Campaign were either cesium beam type or rubidium type (Schutz, 1983b). To achieve maximum accuracy, the measurement of the round-trip flight time is split up in three parts (i.e., $T = T1 + T12 - T2$), where T1 is the time elapsed from the starting epoch to the first following

positive crossover of the oscillator, T2 is the time elapsed from the ending epoch to the next following positive crossover, and T12 is the time interval between the aforementioned positive crossovers. T12 is obtained by multiplying the number of intervening positive crossovers (N12) by the period (T0) of the master oscillator (i.e., T12 = N12 x T0). The fractional times T1 and T2 are accurately measured either by charging and discharging a capacitor with constant but different currents or by using a second oscillator which is slightly off from the master oscillator. Common biases introduced in measuring T1 and T2 are canceled out because the times T1 and T2 are subtracted in the computation of the round trip flight time (i.e., T). Residual errors at the cm level are still present. These errors can be reduced at the mm level with the use of streak-cameras employed in the Optical Time Interval Unit (OTIU) currently being investigated for implementation in the new two-color laser receivers (Abshire et al, 1985).

The ***transmitting optics*** are used to align the laser pulse towards the satellite being tracked, while the ***receiving optics*** are used to receive and focus the reflected laser pulse onto the cathode of the photomultiplier. Unsuccessful focusing introduces the image position effects previously mentioned. A substantially reduced single dual-purpose telescope performs both of the above functions, thanks to the technological advances in the field of signal detectors, photomultipliers and discriminators. These advances introduced a substantial reduction in the station design which in turn triggered the construction of the highly transportable laser ranging systems TLRS-1 (Silverberg, 1982; Shelus, 1983), TLRS-2 (Transportable Laser Ranging System No. 2), etc. These systems are extremely valuable in the study of geophysical processes because of their ability to make observations of limited time in remote areas, in a hostile environment.

The ***time receiver*** is either a LORAN-C or a GPS receiver and is used to time-tag each observation in the Universal Coordinated Time (UTC) scale. The synchronization accuracy with a LORAN-C receiver is of the order of 1 μs, while with a GPS receiver this accuracy is of the order of 50 ns. Synchronization errors affect the inferred optical range

by about 4 mm/μs. The laser stations used in this study belong either to the Goddard Laser Tracking Network (GLTN) or to the Participating Laser Network (PLN) (Shawe et al., 1985), and their observations are time-tagged with the UTC scale kept by USNO. According to the MERIT standards and for reasons explained in Chapter 2, the UTC(USNO) has been transformed to UTC(BIH).

The *computer* is used as an auxiliary equipment to control satellite tracking operations, to assist the operator with such functions as data quality and quantity assessment, maintenance, testing procedures, etc.

3.2.2 Atmospheric Channel

As the laser pulse propagates through the atmospheric channel it experiences a continuously varying refractive index. This variation depends primarily on the variations of the local pressure with only a weak dependence on the local temperature and local humidity (Degnan, 1985; Abshire, 1985). A varying refractive index, on the other hand, bends the laser pulse according to Snell's law and also decreases the group velocity of the laser pulse as it travels through lower pressure layers at higher altitudes. The error due to bending of the laser pulse is relatively small and reaches a maximum value of 3-4 cm at 10 degrees elevation while the error due to the decrease of the group velocity is very large, reaching the value of about 13 m at the same elevation (Abshire, 1985). A great number of formulas have been developed to correct the inferred optical length of the laser pulses (i.e., the inferred laser ranges) for atmospheric refraction effects. In the present study and according to the MERIT standards, the Marini and Murray formula has been used to correct for these effects (Marini and Murray, 1973). This formula is based on the assumption of a spherically symmetric atmospheric refraction and it uses only the pressure, temperature and relative humidity taken at the ranging site. This formula is in error at the 4-6 cm level as the satellite reaches an elevation angle of 20 degrees (ibid). Today, use of two-color laser ranging systems equipped with streak-camera receivers promises an atmospheric refraction correction with an accuracy down to the mm level, thanks to the weak

dependency of the group refractivity on the water vapor at optical wavelengths (Abshire, 1985).

3.2.3 Space Segment

Although the space segment of the SLR system consists of several satellites, the LAser GEOdynamics Satellite (LAGEOS) is devoted exclusively to geodynamic and geodetic applications (Moritz and Mueller, 1987). Lageos is a passive sphere with a 59.988 cm diameter orbiting the earth at an altitude of about 5900 km. Its mass-to-area ratio of 1.44×10^3 kg/m^2 effectively minimizes the solar radiation pressure and atmospheric drag perturbations. The high altitude of Lageos' orbit not only reduces the effects of the poorly modeled high frequency variations of the gravity field but also warranties good simultaneous tracking of continental extent. The altitude of the orbit, however, is low enough to assure the geometric strength necessary for successful implementation of simultaneous laser satellite tracking methods. Consequently, only laser range observations to Lageos were facilitated in order to investigate the effectiveness of the SRD and geometric methods in baseline determinations.

The surface of the Lageos satellite is speckled with 422 solid-cube-corner reflectors (CCR's) made of fused silica and four made of germanium (Cohen et al., 1985). When the direction of the incoming laser beam relative to the normal of each individual CCR reaches the value of 25 degrees, reflection ceases to take place (Degnan, 1985). As a result, 10 to 15 CCR's contribute to the laser pulse detected at the receiver. Therefore, it is difficult to locate for each returning pulse its reflection point which constitutes the ending point of the inferred optical laser range. The location of the reflection point is needed to compute the correction necessary to transform the ending point of the optical laser range to the center of mass of the satellite. This correction is referred to as center of mass correction, and its value has been determined experimentally for different pulse widths prior to the Lageos launch. The standard deviation in estimating this correction is about 2 mm. In the current investigation the value of 24 cm has been

adopted for the center of mass correction. This value is supplied on each data record in the tape containing the observations (see Section 3.4). Furthermore, the interference of the individual CCR returns, at the receiver's level, may introduce a random error in the inferred laser range the standard deviation of which reaches the value of 1.15 cm (Fitzmaurice et al., 1977). This error is referred to as the coherent fading effect.

3.2.4 Instrument Origin

Effective use of laser range observations necessitates a clear identification of the starting and ending points of the inferred ranges. As already mentioned, the ending point is identified with the center of mass of the satellite. This is a natural choice because the equations of motion of the satellite are conveniently expressed relative to this point. The starting point is identified with a fixed reference point within the laser instrument and is referred to as instrument origin. The instrument origin usually coincides with the intersection of the telescope's azimuth and elevation axes, but other points within the laser instrument may be used as well. Realization of the instrument origin is achieved either through calibration or through the common channel receiver approach (Abshire et al., 1984; Degnan, 1985). During the MERIT Main Campaign, calibration procedures were employed to identify the instrument origin through the estimation of the system delay (Schutz, 1983a). The system delay is measured by making repeated observations to a calibration target of known distance, usually before and after each satellite pass. With this information, the system delay introduced by the instrument's electronics can be readily estimated. The distance to the calibration target is measured with a geodimeter located very close to the laser ranging instrument. Additional surveys, therefore, are necessary to determine the position of the geodimeter relative to the instrument's origin. In this process, errors of the order of 2 cm may be introduced. In order to reduce these errors, some laser instruments are equipped with fiberoptics allowing for self-calibration (Silverberg, 1982). The common channel-receiver

approach, on the other hand, eliminates the need for calibration since the electronic system delay, except for a calibratable signal-amplitude effect, cancels itself out (Abshire et al., 1984; Degnan, 1985). This approach is currently being tested for implementation in the laser ranging systems.

From the above discussion it is obvious that on the basis of the technology employed and the models used, one could come up with a standard deviation depicting the accuracy of the laser range observations recorded by a certain station. This approach, however, would not take into consideration errors resulting from improper calibration, from operator errors or from any other errors not being accounted for. Bearing this in mind, it was considered appropriate to estimate, for every station used in the present study, a standard deviation that would reflect the station's overall performance during the MERIT Main Campaign. Such an estimate can be obtained by taking an average value of the monthly precision estimates determined for every station and for the entire MERIT Main Campaign by the University of Texas (Analysis of Lageos Laser Range Data, Sept. 1983-Oct. 1984). For the stations involved in our study, these estimates are shown in Table 2 along with the station ID's and the kind of laser instruments with which they were equipped during the MERIT Main Campaign.

Table 2. Station Location, Laser Instruments and Precision Estimates.

NAME	ID	LOCATION	LASER INSTRUMENT	OBSERVATIONAL PRECISION (m)
QUINC2	7109	Quincy, CA	MOBLAS-8	0.028
MNPEAK	7110	Mount Laguna, CA	MOBLAS-4	0.033
MAZTLN	7122	Mazatlan, Mexico	MOBLAS-6	0.12/0.05*
GRF105	7105	Greenbelt, MD	MOBLAS-7	0.034
PLATVL	7112	Platteville, CO	MOBLAS-2	0.125
MCDON	7086	McDonald Obs., Ft. Davis, TX	MLRS	0.084
TL0126	7265	Barstow, CA	TLRS-1	0.080
OTAY	7062	Otay Mt., San Diego, CA	TLRS-2	0.060
QUINC3	7886	Quincy, CA	TLRS-1	0.070
MONPK2	7220	Mt. Laguna, CA	TLRS-1	0.060
HOLLAS	7210	Lure Obs., Maui, HI	HOLLAS	0.042
HUAHIN	7121	Huahine, Society Is., Pol.	MOBLAS-1	0.094
ARELAS	7907	Arequipa, Peru	ARE_{fixed}	0.145

*before and after upgrading.

3.3 SYSTEMATIC CORRECTIONS OF THE OBSERVATIONS EXTERNAL TO THE SLR SYSTEM

Effective application of the least-squares adjustment assumes constant adjusted parameters over at least the time span of the observations. Thus, baseline estimation from station coordinates requires corrected station coordinates for their temporal variations. Besides shocks and regional deformations, the temporal variations of station coordinates are caused either by tectonic plate motions or by earth tides. The regional deformations are ignored because either they are unknown or their effects are very small. For instance, the ocean loading effects for the stations used in this investigation are very small (Melbourne et al., 1983). Since the time span of the observations covers about one year, the plate tectonic motions have also been ignored. Thus we have considered only the temporal variations of station coordinates caused by the earth tides. The tidal corrections are accounted for by correcting either the observations or the station coordinates. In the present study the traditional way of correcting the station coordinates has been

adopted. This correction has been conveniently formulated through the station displacement vector caused by the tidal deformation (ibid.). This formulation is based on the same elastic response of a solid earth over all orders within a certain degree, and if only the second degree is considered it takes the following form:

$$\Delta\hat{r} = \sum_{j=2}^{3} \left(\frac{GM_j r^4}{GM_E R_j^{*3}}\right)\left\{[3\ell_2(\hat{R}_j^{*}\cdot\hat{r})]\hat{R}_j + \left[\, 3\left(\frac{h_2}{2} - \ell_2\right)(\hat{R}_j^{*}\cdot\hat{r})^2 - \frac{h_2}{2}\right]\hat{r}\right\} \quad (3\text{-}1)$$

where

$$\hat{R}_j^{*} = R_3(-\delta_L)\cdot\hat{R}_j \quad (3\text{-}2)$$

δ_L = phase lag caused by the earth's dissipative forces

GM_j = gravitational parameter of the attracting body. In the present study only the moon (j = 2) and the sun (j = 3) have been considered

GM_E = geocentric gravitational constant

$\hat{R}_j, R_j$ = unit vector and the magnitude of the geocentric vector of the moon (j = 2) and the sun (j = 3) respectively

$\hat{r}, r$ = unit vector and the magnitude of the stations' geocentric vector

h_2 = nominal second-degree Love number

ℓ_2 = nominal second-degree Shida number

$\hat{R}_j^{*}, R_j^{*}$ = unit vector and the magnitude for the geocentric vector of of the moon (j = 2) and the sun (j = 3) in the absence of dissipative forces

The way the tidal displacements have been incorporated in our study differs in two aspects from what was suggested by the MERIT standards. The phase lag caused by the dissipative forces has been modelled in equation (3-2), while the second-degree Love and Shida numbers have been assumed to be frequency independent. The latter assumption results in a maximum error of 1.3 cm in the stations' height (ibid.). This assumption is well justified not only because the resulting error is well below the noise level of the observations but also because

it reduces the bulk of the computations considerably.

3.4 DESCRIPTION OF THE DATA SET UTILIZED IN THIS INVESTIGATION

Both the SRD and the geometric methods require strict simultaneity. Although baseline estimations based on exclusively simultaneous observations are largely insensitive to the orbital errors (Christodoulidis et al., 1981) and to reference frame model errors (Pavlis and Mueller, 1983), no specific campaign was ever devoted to coordinate simultaneous tracking. This, together with the inability of the SLR systems to track a satellite through a cloudy atmosphere, makes it even more difficult to achieve extensive simultaneous laser tracking.

Fortunately enough, as early as 1978 the IAU Symposium No. 82 on "Time and the Earth's Rotation" recommended setting up a working group to organize a program of international collaboration to Monitor the Earth's Rotation and Intercompare the Techniques of observation and analysis (MERIT). The proposed techniques of observation included laser ranging and radio interferometry (Wilkins, 1980). As early as 1980 (August-October) the MERIT Short Campaign was undertaken to test and develop the organizational arrangements that would be required for a realistic coordination and successful implementation of the MERIT Main Campaign which very successfully took place during the 14-month period of September 1, 1983, to October 31, 1984.

The MERIT Working Group in collaboration with the Conventional Terrestrial Reference System (COTES) Working Group, decided to extend the objectives of the MERIT Main Campaign in order to include the preparation of a catalog with a precise and consistent set of station coordinates (Wilkins et al., 1986). Consistency of the station coordinates is achieved by accurately linking together the reference frames realized by each of the techniques involved. This is accomplished either through collocations or by estimating for each technique the diurnal differences of the earth rotation parameters. Towards achieving this goal, it was decided to have an intensive campaign, during which, in addition to other requirements, all the MERIT stations were asked to

observe as frequently as possible and in full capacity (ibid). The SLR technique, one of the techniques tested during the MERIT Main Campaign, reached its full potential. It would never have reached this potential if it weren't for the NASA Crustal Dynamics Project whose SLR network after several years of buildup approached during the MERIT Main Campaign its full capacity (Coates et al., 1985). It was this peak in the operation of the SLR system that resulted in an extensive SLR simultaneous tracking which in turn sparked the initiation of the present study. Consequently, the SLR observations collected during the MERIT Main Campaign were used in this study and herein this data set is referred to as the MERIT Main Campaign (MMC) data set.

According to the SLR organizational arrangements for project MERIT, each of the observing stations was obligated to submit its Full Rate (FR) observations to the Crustal Dynamics Information System (CDIS) located at Goddard Space Flight Center (GSFC). The FR observations would have to be submitted within three months after their collection (Schutz, 1983b). The MERIT FR data format is a character oriented format referred to as Seasat Decimal Format (SSD) (ibid.).

The MMC data set is available to any investigator from the Crustal Dynamics Data Bank (CDDB). This data set was sent to us upon request in nine-track magnetic tapes. Each record in the tape is stored in SSD format and contains the observed range, the epoch of the observation and a number of indicators pertaining to the corrections that have been applied and to those that have yet to be applied (i.e., atmospheric refraction corrections, center of mass corrections, etc.). The observed ranges stored in those records are corrected for system delay, signal amplitude dependent effects and any other effects pertaining to the laser instrument (see Section 3.2). The center of mass correction has a negative sign, and therefore it should be applied to the computed range. Each record also contains the atmospheric refraction correction computed with the Marini and Murray formula together with the pressure, temperature and relative humidity recorded at the observing site. The meteorological data is included for the analysts who might prefer to compute the atmospheric refraction correction with a different formula

than that of Marini and Murray. The Marini and Murray formulation was suggested for use with the MMC data set as an extension of the MERIT standards (ibid.).

At the time when this study was initiated the MMC data set was not available. Thus, at the initial stage of this work, we employed the Lageos laser ranges recorded during the last three months of the year 1979 by stations 7114 (Owens Valley) and 7115 (Goldstone) located in California. The initial stage of this work was primarily devoted to the development and testing of the software necessary to edit the laser range observations and to generate the simultaneous range and SRD observables which constitute the input to the geometric and SRD methods respectively. Baseline estimation, however, was based solely on the MMC data set (see Chapter 4).

The MMC data set is not a unique data set because for each month there have been several releases issued due to data problems or to missing data (Section 3.6.3). Table 3 shows the monthly releases of the MMC data set used in our study. These releases, besides having erroneous observations, also contain data records with unacceptable characters such as asterisks, plus and minus signs, etc. These records should not have been there since the received data set was supposed to have been preprocessed by the Bendix Field Engineering Corporation (Schutz, 1985). Editing this data set was a tedious process and a considerable amount of time was spent for this purpose.

Table 3.

Monthly MERIT Releases

Month	Release	Final Release
Sep. 1983	C	yes
Oct. 1983	B	no
Nov. 1983	E	yes
Dec. 1983	E	yes
Jan. 1984	E	yes
Feb. 1984	C	no
Mar. 1984	C	no
Apr. 1984	D	no
May 1984	D	no
Jun. 1984	B	no
Jul. 1984	B	no
Aug. 1984	C	no
Sep. 1984	B	no
Oct. 1984	C	yes

3.5 DATA EDITING

The brief description of the error sources affecting the SLR systems (see Section 3.2) reveals that erroneous timing of the returned laser pulse is possible, especially when the observations are made during daylight time with a single photon detection laser instrument (i.e., TLRS 1, 2, 3 or 4) (Shawe et al., 1985). Erroneous timing is even worse for the laser instruments equipped with single stop Time Interval Units (TIU). With single stop TIU's it is not possible to detect the returned laser pulse if a noise pulse with an energy level exceeding the stop discriminator threshold enters the receiver prior to the returned laser pulse. Multistop TIU's, on the other hand, have the potential to reduce erroneous detection substantially since they are designed to detect more than one returning pulse for each of the emitted pulses. The multistop TIU's available on the market today have time resolution at the nanosecond level. Such low resolution makes them inadequate for use with centimeter-level accuracy laser instruments. Erroneous laser range observations may also result from operator errors, inadequate maintenance and from any other sources affecting the proper operation of the laser instrument.

The erroneous observations should be detected and rejected before the generation of the Simultaneous Range (SR) and the Simultaneous Range Difference (SRD) observables. In common practice, editing of the erroneous observations is incorporated in the final adjustment of the observations when station coordinates and baselines are estimated. In the present study, however, the editing of the laser ranges should precede the final adjustment simply because the SR and SRD observables are obtained through an interpolation of the laser ranges, and therefore, the presence of erroneous ranges will affect the entire set of the generated SR and SRD observables. Thus, effective generation of the SR and the SRD observables requires early editing of the observed laser ranges.

3.5.1 Data Snooping Procedure

Any kind of editing procedure requires a functional representation of the observed ranges. The estimation of the parameters involved in this representation allows the prediction of the observed ranges and therefore the estimation of the errors associated with each of those ranges. The difference of the estimated error vector (i.e., residual vector) from the true error vector accounts for the projection of the true error vector into the model space generated by the column space of A (see equation 3-12). This is the component of the true error that is lost in the estimation process, and therefore it cannot be recovered. Based on the statistical properties of the estimated component of the true error (i.e., residual), statistical tests may be derived to allow for the detection and rejection of erroneous observations.

This section proceeds with the development of the statistical formulation necessary for the derivation and implementation of those tests. The next section contains a description and elaboration on how the base functions employed in the functional representation of the laser ranges should be chosen to effectively edit the laser range observations.

Let's consider the linear adjustment model employed in the functional representation of the observed laser ranges (Uotila, 1986)

$$-e = AX - L_b \tag{3-3}$$

where

e = true error vector of the observations
L_b = vector of the observed laser ranges
X = true parameter vector
A = design matrix of the experiment

The minimum variance unbiased estimate of the parameter vector X has the following form (ibid.)

$$\hat{X} = (A^T P A)^{-1} A^T P L_b \tag{3-4}$$

The true errors, under the null hypothesis, have a multivariate normal distribution with 0 mean and Σ_e variance-covariance matrix

$$e \sim N(0, \Sigma_e) \tag{3-5}$$

where

$$\Sigma_e = \sigma_0^2 P^{-1} = \text{variance-covariance matrix of the observations} \tag{3-6}$$

P = weight matrix of the observations
σ_0^2 = the a priori variance of unit weight

The unbiased estimate of the a priori variance of unit weight takes the following form (ibid.)

$$\hat{\sigma}_0^2 = \frac{1}{(n - u)} (A\hat{X} - L_b)^T P (A\hat{X} - L_b) \tag{3-7}$$

where

$n - u$ = degrees of freedom of the adjustment

The projection of the true error vector e into the orthogonal space complement to the model space constitutes the estimated error (i.e., residual) vector

$$V = A\hat{X} - L_b = [A(A^T P A)^{-1} A^T P - I] L_b \tag{3-8}$$

Substitution, in this equation, of the weight matrix P with the identity matrix leads to the following equation

$$V = [A(A^TA)^{-1}A^T - I]L_b \tag{3-9}$$

This substitution is well justified because the editing of the observations is carried out on a station-by-station basis and for each of the stations involved the variance-covariance matrix of their observations is assumed to have a diagonal form and equal diagonal elements. Thus, the weight matrix P, apart from a constant factor, is equal to the identity matrix.

Since the true error vector e has zero mean, equation (3-3) takes the following form

$$L_b = e + E(L_b) = e + AX \tag{3-10}$$

where the symbol E denotes the expected value. Substitution of equation (3-10) into (3-9) leads to the following equation

$$V = Me \tag{3-11}$$

where

$$M = [A(A^TA)^{-1}A^T - I] \tag{3-12}$$

The matrix M is a symmetric idempotent matrix with rank (n - u), and since MA = 0 it represents the orthogonal complement operator of the model space (i.e., projects any vector into the orthogonal complement of the model space) (Pope, 1976).

With the help of equation (3-11) and the law of covariance propagation, the variance-covariance matrix of the residuals takes the following form

$$\Sigma_V = M\sigma_0^2 \tag{3-13}$$

$$\hat{\Sigma}_V = M\hat{\sigma}_0^2 \tag{3-14}$$

The first factor of the matrix M (eq. 3-12) depends on the design matrix A or, in other words, on the chosen experiment. From an estimation point of view the experiment (i.e., design matrix) should be chosen to minimize the projection of the true observational error into the orthogonal complement of the model space (i.e., to minimize the effect of the true observational error on the predicted ranges). From an editing point of view in which we are interested, the M matrix should be nearly diagonal. This is preferred because each individual residual (v_i) will be primarily affected by the corresponding true error e_i. This makes it easier to identify erroneous observations with one-dimensional residual testing (see next section).

Using an independent set of analytic base functions for the functional representation of the laser ranges results in a severe limitation in regard to the choice of the model space. This limitation arises because any analytic base function can be approximated by a partial sum of monomials up to degree k. Thus, the space spanned by the monomials (1, t, . . . , t^k) closely resembles the model space spanned by any independent set of base functions. The basis, however, selected to span the model space will determine the conditioning of the normal matrix (i.e., A^TA) and the distribution of the approximation errors in the interval of approximation. Choosing Chebychev polynomials as base functions results not only in a well-conditioned normal equations matrix but also in an even distribution of the residuals over the interval of approximation (see next section).

Having a functional representation for the observed laser ranges we can proceed with the editing of those ranges using one-dimensional statistical testing of the residuals. This is accomplished with the one-dimensional data-snooping procedure originated by Baarda (1968). In this procedure, under the null hypothesis the true observational errors have a multivariate normal distribution with zero mean and Σ_e variance-covariance matrix (equation 3-5). Thus, under the null hypothesis H_o the residuals have a multivariate normal distribution

$$V \sim N(0, \Sigma_V) \qquad (3\text{-}15)$$

with zero mean and Σ_V variance-covariance matrix (equation (3-13)). This leads to a normal marginal distribution for each individual residual with zero mean and variance $\sigma_{v_i}^2$

$$v_i \sim n(0,\sigma_{\hat{V}_i}^2) \qquad (i = 1, \ldots, n) \tag{3-16}$$

Thus, the original null hypothesis H_o is now replaced by a sequence of null hypotheses H_{o_i} $(i = 1, \ldots, n)$:

$$H_o : v_i \sim n(0, \sigma_{\hat{V}_i}^2) \qquad (i = 1, \ldots, n) \tag{3-17}$$

where

v_i = the residual of the i^{th} observation

$$\sigma v_i = \sigma_o \sqrt{m_{ii}} \tag{3-18}$$

σ_o^2 = a priori variance of unit weight

m_{ii} = diagonal elements of the matrix M (equation 3-12)

Under the sequence of the hypothesis H_{o_i} $(i = 1, \ldots, n)$ the statistic $W_i = v_i/\sigma_{v_i}$ has a standard normal distribution

$$W_i \sim n(0, 1) \qquad (i = 1, \ldots, n)$$

The capital letter N in the above equations denotes multivariate normal distribution while the small letter n denotes one-dimensional normal distribution.

The theoretical value σ_o in equation (3-18) is unknown and therefore the estimated $\hat{\sigma}_o$ (i.e., a posteriori variance of unit weight) is used to evaluate the W_i statistic. This new $(\hat{W}_i)$ statistic, under the sequence of null hypotheses H_{o_i} $(i = 1, \ldots n)$, and as the degree of freedom becomes larger and larger tends to have a student's t distribution (Pope, 1976)

$$\hat{W}_i = \frac{v_i}{\hat{\sigma}_{v_i}} \sim t_{n-u,\ \alpha_o} \tag{3-19}$$

where

$$\hat{\sigma}_{v_i} = \hat{\sigma}_o \sqrt{m_{ii}} \tag{3-20}$$

α_o = Type I error = P (rejecting H_o | when H_o is true)

$n - u$ =: degrees of freedom

$\hat{\sigma}_o^2$ =: a posteriori variance of unit weight (equation (3-7))

The critical region C of a statistical test based on the $\hat{W}_i$ statistic takes the following form

$$C = \left\{ \hat{W}_i : |\hat{W}_i| > t_{n-u,\ \alpha_o} \right\} \tag{3-21}$$

while the Type I error becomes

$$\alpha_o = P\left[\frac{|v_i|}{\hat{\sigma}_{v_i}} > t_{n-u,\ \alpha_o} \right]$$

Therefore, the data-snooping procedure is carried out in the following steps:

1. Choose a probability level ($\alpha_o = 0.005$)
2. Take from a student t table the critical value (c) for rejection (e.g., $c = t_{n-u,\ \alpha_o}$, with $n - u \geq 200 \approx 2.84$)
3. Compute the individual statistic $\hat{W}_i$
4. Reject each observation L_{b_i} leading to $\hat{W}_i > c$

If the observations are correlated a slightly different data snooping is required (Pope, 1976). The data-snooping procedure has been effectively applied in photogrammetry (Gruen, 1979), in deformation analysis (FIG Deformational Analysis Working Group, Heck 1982) and in the present study to edit laser range observations.

3.5.2 Effectiveness of the Data Snooping Procedure in Editing the Laser Range Observations

Implementation of the data-snooping procedure requires a functional representation of the observed laser ranges. Before proceeding with the choice of the base functions, we should try to single out those properties of the base functions that would make the data-snooping procedure more effective. To accomplish this, we should realize that the data-snooping procedure is based on a sequence of one-dimensional tests carried out for each residual individually. These one-dimensional tests would be effective if the residuals are uncorrelated and evenly distributed over the interval of approximation. It is not possible to obtain uncorrelated residuals with the linear adjustment model (3-3); if this were possible it would imply that rank (M) = n, which is a contradiction since rank (M) = n - u (see equation (3-12)). Thus we can only look for base functions yielding residuals with reduced correlations. This, however, is not possible because a set of k independent analytic base functions can be uniquely mapped into the linear space spanned by the monomials up to degree k (i.e., 1, t, . . . , t^k). Thus we are left only with the choice of base functions that yield an even distribution of the residuals over the interval of approximation and presumably a well-conditioned normal equations matrix.

To understand how an uneven distribution of the residuals may result, we choose the monomials to represent the observed laser ranges in the interval $[t_B, t_E]$. Since any such arbitrary interval can be transformed to the interval [-1, 1] by the change of variables,

$$\tau = \frac{2t - t_E - t_B}{t_E - t_B} \qquad \begin{matrix} t_B \leq t \leq t_E \\ -1 \leq \tau \leq 1 \end{matrix} \tag{3-22}$$

it is sufficient to examine the behavior of the monomials $(1, \tau, \tau^2, \ldots \tau^k)$ in the interval [-1, 1]. In this interval each monomial assumes the same maximum absolute magnitude 1 at $\tau = \pm 1$ and the same absolute minimum magnitude 0 at $\tau = 0$. If the observed ranges would be approximated with the polynomial

$$R_a(\tau) = \hat{X}^T \cdot \bar{T} \tag{3-23}$$

where

$$\bar{T} = (1, \tau, \tau^2, \ldots \tau^k)^T \tag{3-24}$$

$\hat{X}$ = estimated monomial coefficient vector (equation (3-3))

the errors in the parameter vector $\hat{X}$ will produce small residuals for small τ (i.e., τ near zero) and large residuals for τ close to 1 or close to -1. Such uneven distribution will apparently place limits on the effectiveness of the data-snooping procedure. In addition to this, use of monomials as base functions gives rise to numerical problems associated with the inversion of a nearly-singular normal matrix when k is moderately large (Carnahan et al., 1969; Pavlis, 1982). These numerical problems further deteriorate the effectiveness of the data-snooping procedure. Thus, the monomials cannot be effectively used with the data-snooping procedure.

To avoid uneven distribution of the residuals it seems reasonable to look for functions having evenly distributed extreme values of equal magnitude in the interval [-1, 1]. The Chebychev polynomials appear to be good candidates since their $\cos(n\theta)$ origin fulfills the above requirements. These polynomials are defined with the following equations

$$T_n(\tau) = \cos(n\theta) \; ; \quad n = 0, 1, \ldots k \tag{3-25}$$

where

$$\theta = \cos^{-1}(\tau) \tag{3-26}$$

From this definition, one readily obtains

$$T_0(\tau) = 1 \tag{3-27}$$

$$T_1(\tau) = \tau \tag{3-28}$$

and

$$T_n(\tau) = 2\tau \cdot T_{n-1}(\tau) - T_{n-2}(\tau) \qquad (3\text{-}29)$$

The n real roots of the polynomial $T_n(\tau)$ occur in the interval [-1, 1] at the points

$$\tau_i = \cos\left[\frac{(2i - 1)\pi}{2n}\right] ; \quad i = 1, \ldots k \qquad (3\text{-}30)$$

Using equations (3-25) through (3-29) it is a matter of simple exercise to prove that the extreme values of Chebychev polynomials have the same absolute magnitude of (1) and are evenly distributed in the interval [-1, 1]. In this interval the Chebychev polynomials are orthogonal with respect to a weighted integral operator with weight function $w(\tau)$:

$$w(\tau) = 1 / \sqrt{1 - \tau^2} \qquad (3\text{-}31)$$

We desire, however, that these functions be orthogonal with respect to summation as well. Fortunately, this is true but only if the summation is carried out over a specific set of points in the interval [-1, 1] (Pavlis, 1982)

$$\sum_{\ell=0}^{m} T_i(\tau_\ell)\, T_j(\tau_\ell) = \begin{cases} 0 & i \neq j \\ \dfrac{m + 1}{2} & i = j \neq 0 \\ m + 1 & i = j = 0 \end{cases} \qquad (3\text{-}32)$$

where τ_ℓ denote the roots of the polynomial $T_{m+1}(\tau)$ given by equation (3-30). Thus, in the formation of the normal equations matrix (A^TA) there exists a tendency for cancellations among the products of different degree Chebychev polynomials according to the equation (3-32). This tendency prevents the numerical problems associated with the inversion of the normals and it justifies the term "nearly orthogonal" often used when the Chebychev polynomials constitute the base functions in a least-squares adjustment.

The effectiveness of the data-snooping procedure to edit laser range observations is shown below for only two passes. Extensive experimentation, however, with sparse and dense data sets recorded by many different stations, indeed confirms that the results for these two passes are indicative for the overall performance of the data-snooping procedure. Fig. 1 shows the residuals, computed with equation (3-9), for two passes observed by stations 7114 (Owens Valley) and 7115 (Goldstone) on October 31, 1979. These residuals indicate that erroneous observations with blunders as large as 350 m do exist in the original data set. Rejection of the erroneous observations is carried out by the data-snooping procedure (see Fig. 2). This figure shows the distribution and the magnitude of the residuals after the application of the data-snooping procedure. It is evident that a rejection of less than 10% of the the observations not only eliminates the blunders and makes random the residuals but also reduces the RMS from about 46 m down to 0.11 m.

A close inspection of Fig. 1 and 2 also reveals that observations having 20 m residuals not only survived in the data-snooping process but also reduced their residuals down to the 0.10 m level. This not only demonstrates the dependence of the residuals on the number and the magnitude of the blunders affecting the observations but also shows how difficult it would be to detect and reject erroneous observations by testing the individual residuals v_i alone. The data-snooping process overcomes this difficulty by testing the normalized residual (i.e., $v_i/\hat{\sigma}_{v_i}$) instead. Furthermore, Fig. 2 shows that about three percent of the residuals have an absolute magnitude greater than 0.40 m while the rest of them are randomly distributed about zero with an RMS of 0.12 m. Thus, it was decided to edit out the observations with residuals of absolute magnitude greater than 0.40 m. A plot of the residuals for the remaining observations is shown in Fig. 3. These residuals have a random distribution about zero with an RMS ranging from 0.10 m to 0.12 m. These RMS values are consistent with the expected accuracy of the observing stations thereby confirming our claim that these observations form a clean (i.e., no presence of blunders) data set. Although the

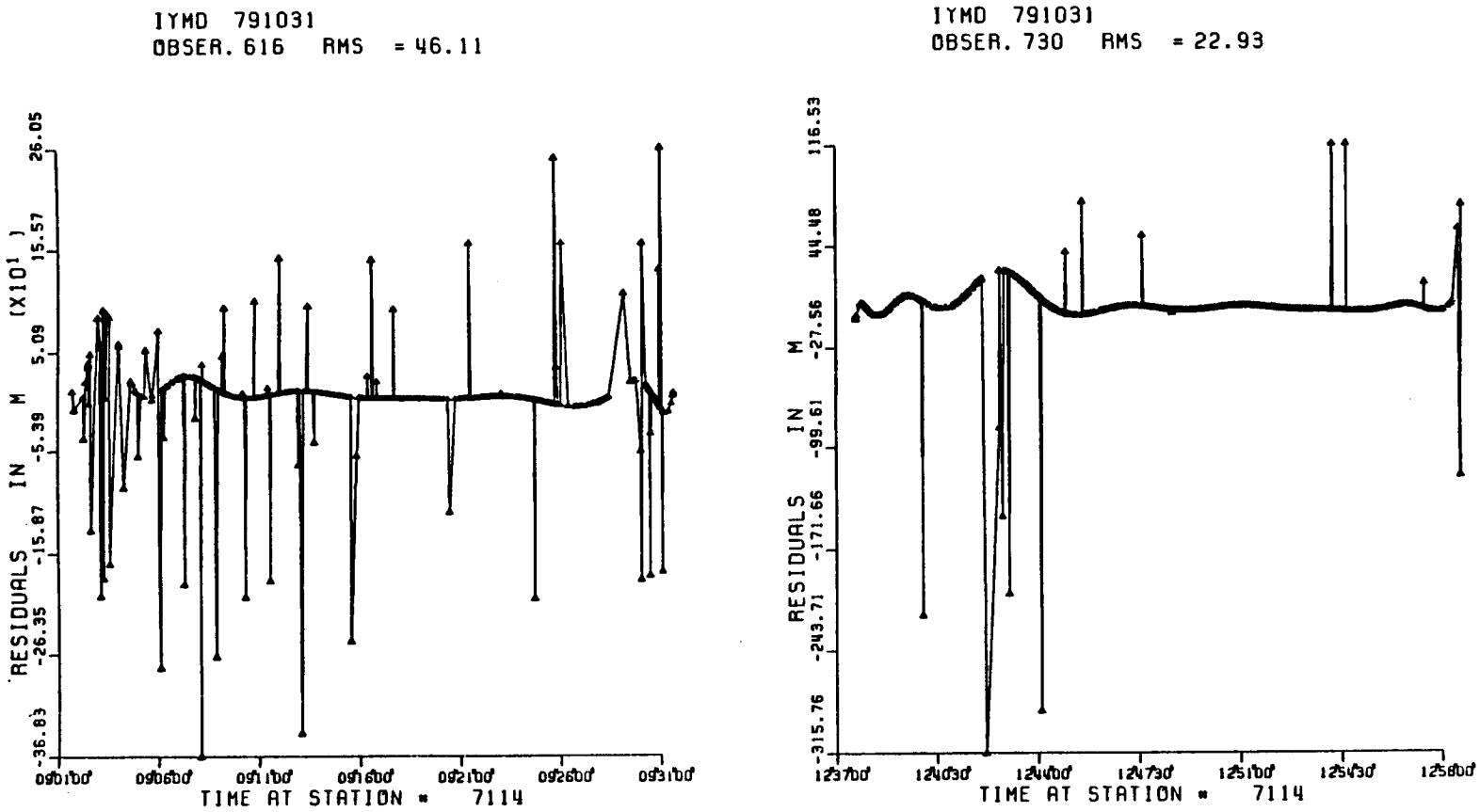

Fig. 1 Residuals of Chebychev interpolation (before data snooping).

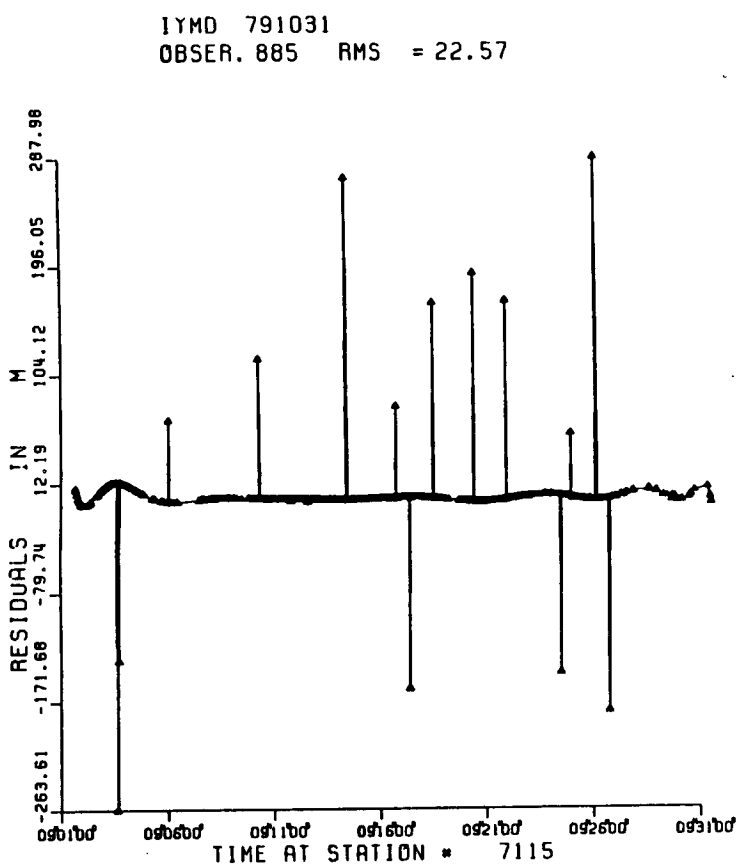
IYMD 791031
OBSER. 885 RMS = 22.57
RESIDUALS IN M
287.98
196.05
104.12
12.19
-79.74
-171.66
-263.61
TIME AT STATION * 7115

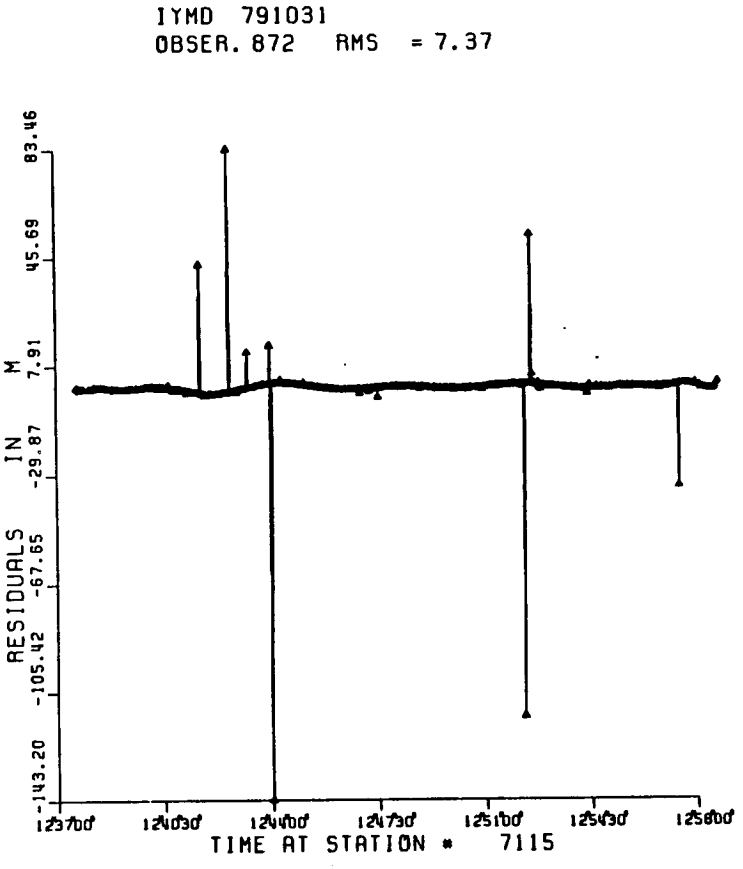
IYMD 791031
OBSER. 872 RMS = 7.37
RESIDUALS IN M
83.46
45.69
7.91
-29.87
-67.65
-105.42
-143.20
TIME AT STATION * 7115

Fig. 1 (cont'd)

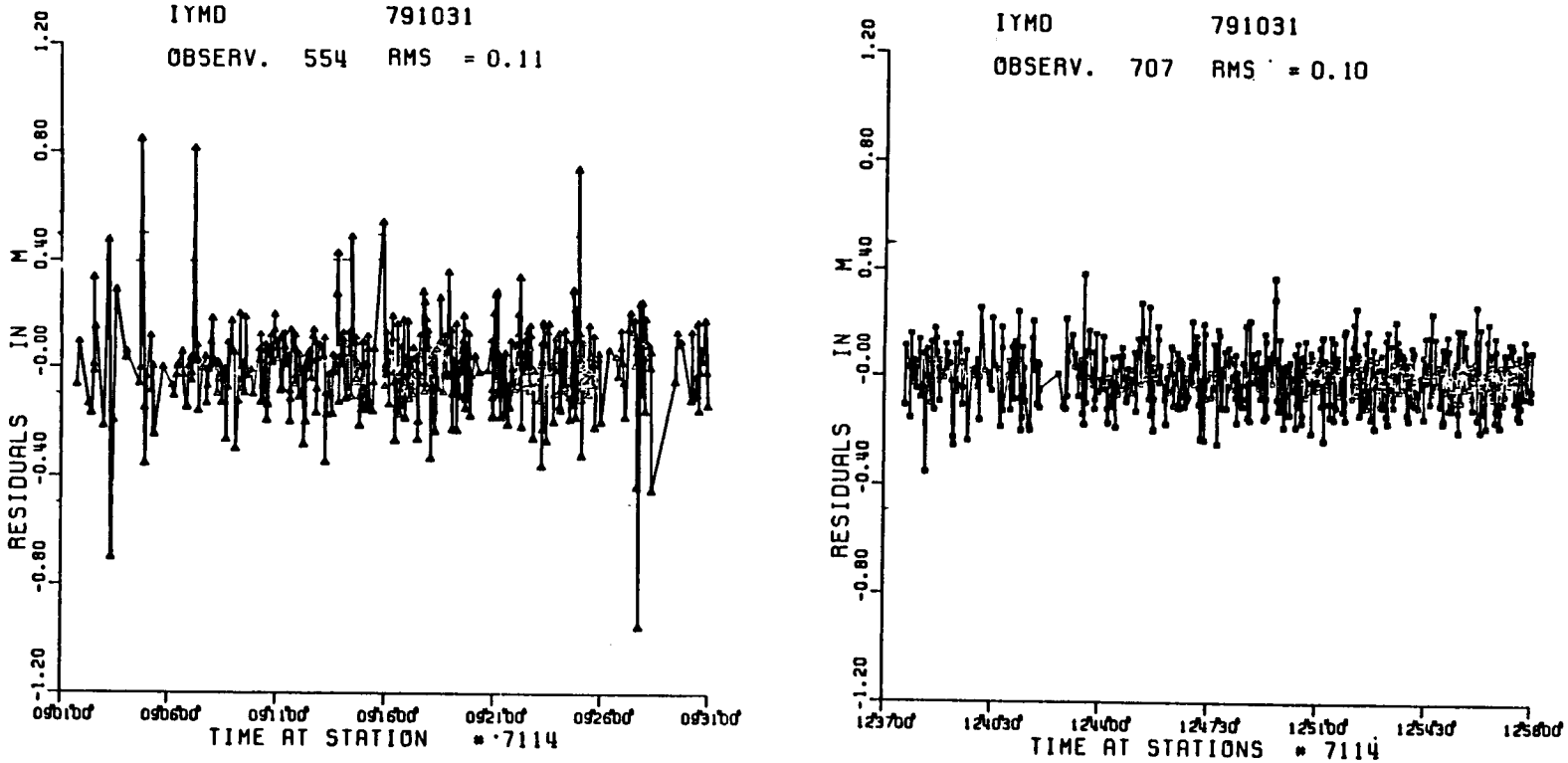

Fig. 2 Residuals of Chebychev interpolation (after data snooping).

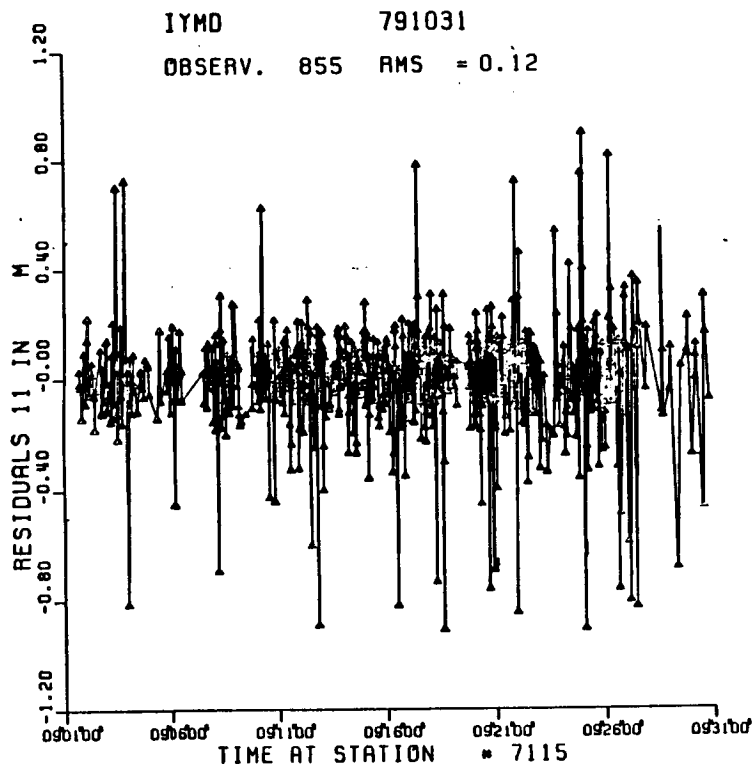
IYMD 791031
OBSERV. 855 RMS = 0.12
RESIDUALS 11 IN M
1.20
0.80
0.40
-0.00
-0.40
-0.80
-1.20
TIME AT STATION * 7115

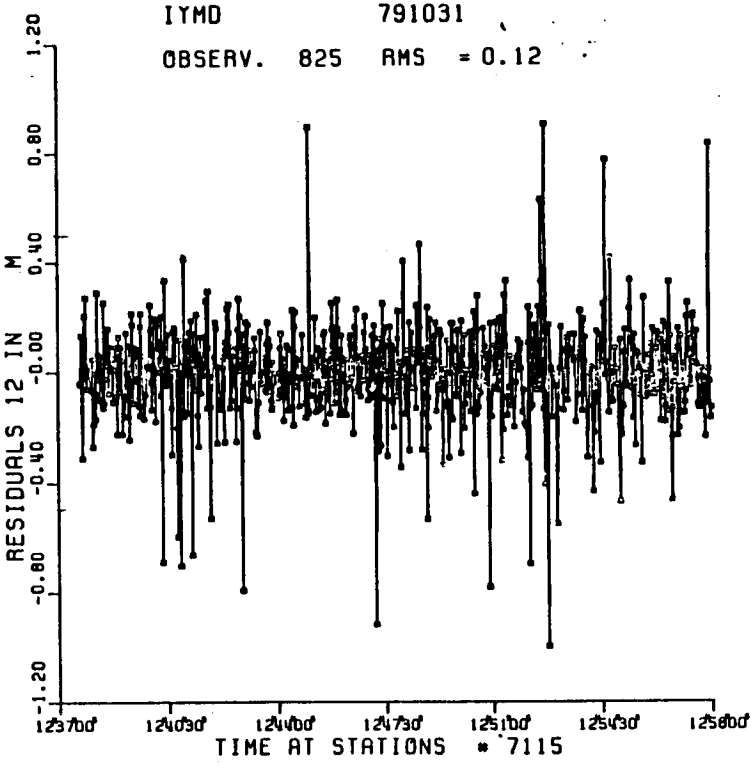
IYMD 791031
OBSERV. 825 RMS = 0.12
RESIDUALS 12 IN M
1.20
0.80
0.40
-0.00
-0.40
-0.80
-1.20
TIME AT STATIONS * 7115

Fig. 2 (cont'd)

data-snooping procedure is very effective, it is relatively slow and therefore very expensive since five to six iterations are needed for the editing process to finish. Alternative ways to speed up this process have been developed by various investigators (Pope, 1976; Gruen, 1979). Finally, we should keep in mind that constant and time dependent biases, no matter how large, cannot be detected by the described procedure simply because if such biases do exist they will be absorbed by the recovered coefficients of the Chebychev polynomials.

3.6 GENERATION OF SIMULTANEOUS RANGES AND SIMULTANEOUS RANGE DIFFERENCES

Since Lageos is a passive satellite, it is quite unlikely for the coobserving stations to record strictly simultaneous observations even if the same part of the the Lageos orbit is coobserved. This happens because for each observing site the tracking starts at a different epoch, each laser instrument has a different repetition rate and last but not least there will always be synchronization errors among the coobserving sites. Implementation of the geometric and the SRD methods requires strict simultaneity, and therefore, an interpolation of the observed laser ranges is necessary.

Simultaneous observations for the geometric solution are obtained by first identifying passes continuously coobserved (i.e., data gaps smaller than 60 seconds) by four or more stations (see Sections 3.6.2 and 3.6.3). For each of those passes the station with the least number of observations is identified. At its observing epochs simultaneous observations for all the remaining stations are generated through an interpolation.

Simultaneous Range-Differences for the SRD method are obtained by dividing the observing stations into pairs with quasi-simultaneous observations. For each of these pairs the station with the least number of observations is identified. Subsequently, at its observing epochs interpolated ranges for the alternate station are generated. The SRD observables are finally obtained by subtracting the actually observed

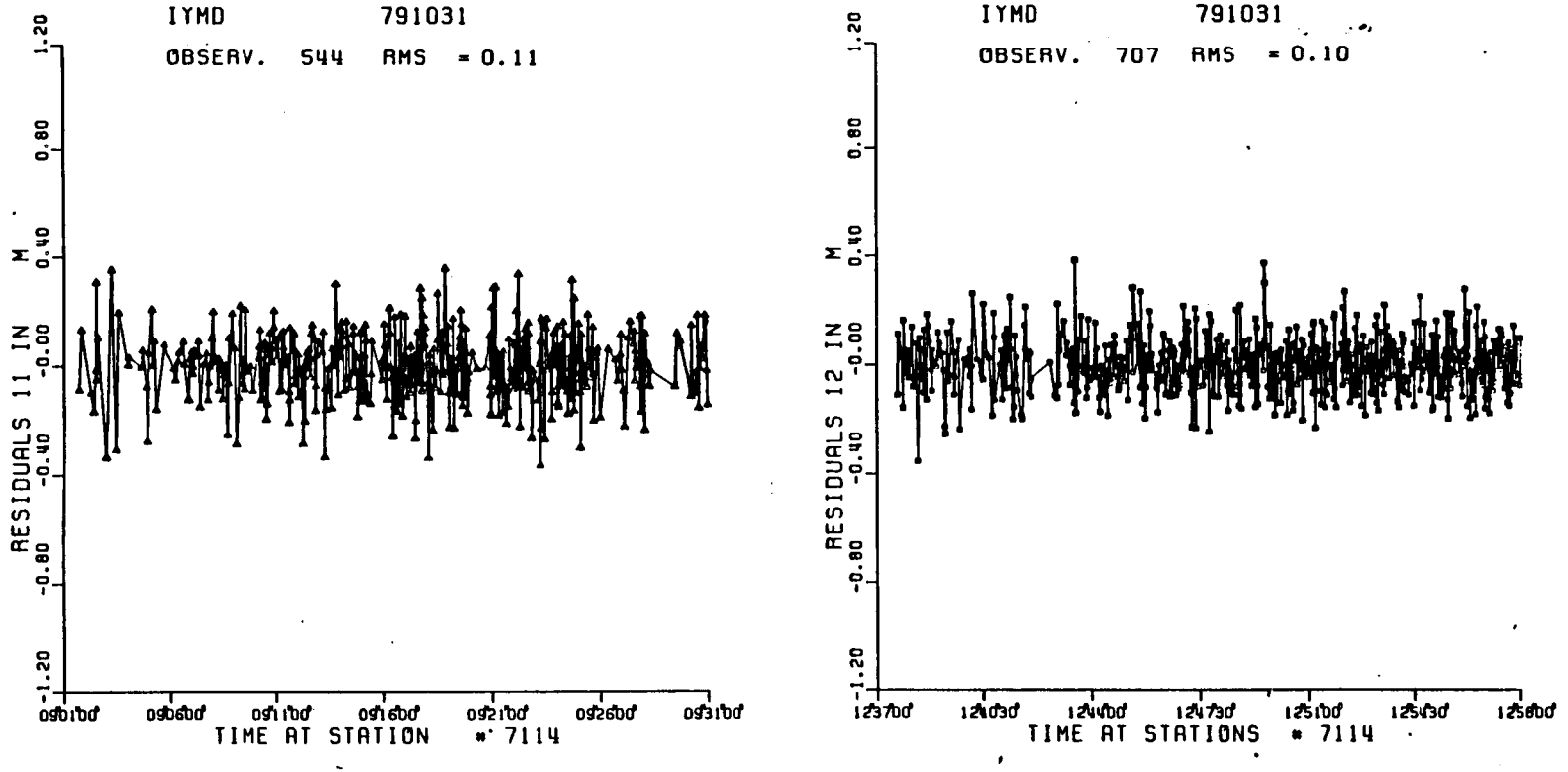

Fig. 3 Residuals of Chebychev interpolation (after data snooping and editing residuals greater than 0.4 m).

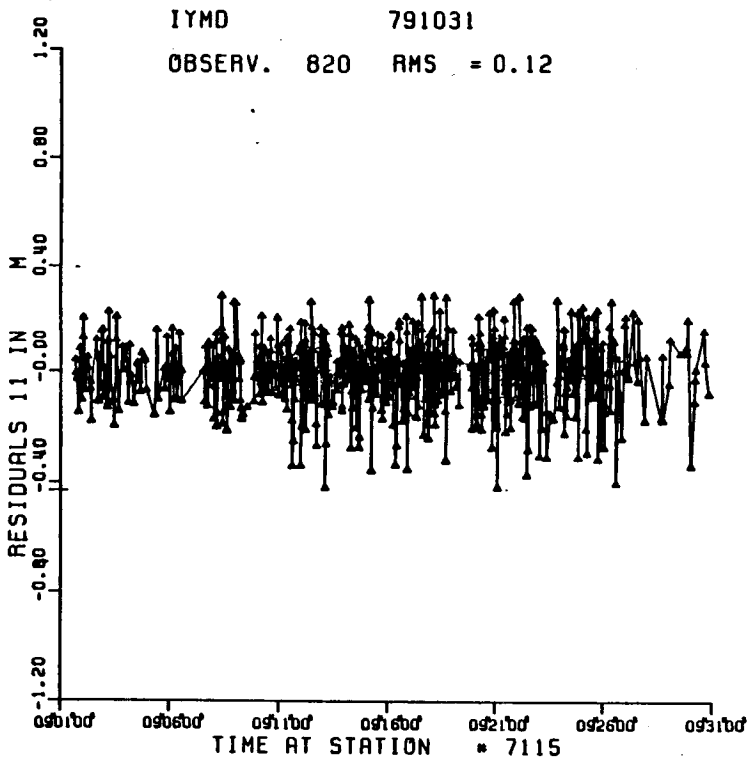
IYMD 791031
OBSERV. 820 RMS = 0.12
RESIDUALS 11 IN M
1.20
0.80
0.40
-0.00
-0.40
-0.80
-1.20
09010d
09060d
09110d
09160d
09210d
09260d
09310d
TIME AT STATION * 7115

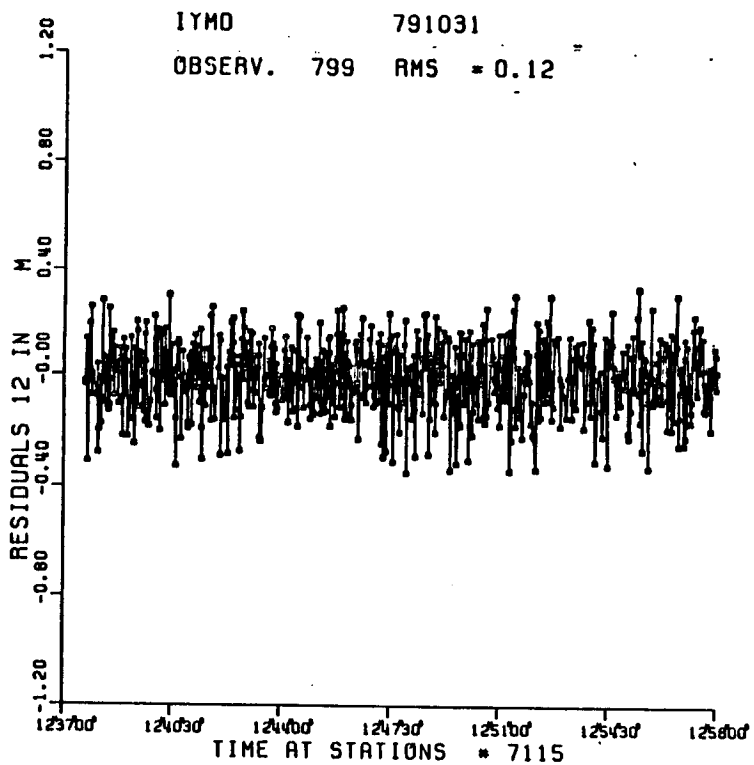
IYMD 791031
OBSERV. 799 RMS = 0.12
RESIDUALS 12 IN M
1.20
0.80
0.40
-0.00
-0.40
-0.80
-1.20
12370d
12403d
12440d
12473d
12510d
12543d
12580d
TIME AT STATIONS * 7115

Fig. 3 (cont'd)

ranges of the station with the least number of observations from the corresponding interpolated ranges of the alternate station.

Therefore, it is essential for the success of this study to select an interpolation method that is capable of generating laser ranges with an accuracy compatible to that of the observations.

3.6.1 Chebychev Polynomials and Spline Functions in the Context of Global and Piecewise Interpolation

A survey of the interpolation methods shows that these methods may be divided into two basic categories:

- the global interpolation methods, and
- the piecewise interpolation methods.

With the global interpolation methods, a function is approximated over the entire interval of approximation by the same linear combination of a selected set of base functions. The function being approximated may be known either analytically or quantitatively at a small number of base points. The latter case depicts the situation in the present study since the ranges to the satellite, apart from measurement errors, are known only at each of its observing epochs. With a piecewise interpolation method, a specific function whose values are given at a specified set of base points is approximated by dividing the base points into successive subsets, each of which contains two, three or more base points. Within each subset the function is approximated by a different linear combination of (possibly) different base functions. Boundary conditions are imposed on the common points of adjacent subsets to make the interpolating function continuous with (possibly) continuous first- and/or second-order derivatives over the interval of approximation. Thus, with a piecewise interpolation method one obtains a continuous interpolating function consisting of pieces, each of which is composed from a different linear combination of (possibly) different base functions.

The approximating function of a ***global interpolation method***, on the other hand, generates approximate values with a relatively strong dependence on the values the approximated function assumes at each

base point. This is a desired property for our study because we would like to obtain interpolated ranges that reflect to the highest degree of accuracy the overall information inherent in the actually observed ranges. Furthermore, the effect of the gaps (i.e., distances between successive base points) should be effectively controlled, and if possible, kept down below the noise level of the observations. In global interpolation methods these effects of unevenly distributed gaps are uniformly distributed over the interval of approximation provided that the gaps are not large enough to corrupt the effectiveness of the global interpolating function (see Section 3.6.2). With global interpolators the generated approximate values exhibit strong correlations because the same linear combination of base functions is used to generate approximate values over the entire interval of approximation. Moreover, the closer the approximated values the stronger the correlations are. Strong correlations are not welcomed in the present study since the generated SR and SRD observables will be considered uncorrelated in the final adjustment when the station coordinates and baselines will be estimated (see Sections 3.6.2, 4.3 and 4.4). The effectiveness of the global interpolation methods is largely dependent not only on the choice of the base functions but also on their implementation to "best" represent the given set of data points.

The base functions most often encountered in practice are the monomials, the Chebychev polynomials, the Fourier series, the exponentials, etc. (Carnahan et al., 1969; Davis, 1975). Linear combinations of either monomials or Chebychev polynomials are by far the most important and most popular approximating functions. These polynomials are easily operated on by addition, multiplication, integration, differentiation, scaling and shifting and more importantly they are closed with respect to any of these operations. Other base functions also possess some or all of the above properties, and therefore the polynomials would not be so important if it were not for the Weierstrass approximation and uniform approximation theorems (Davis, 1975; pp. 24 and 107).

The choice of the base functions depends on the behavior of the function being approximated. For instance, functions with certain periodicities can be best approximated with Fourier base functions $\sin(k\tau)$, $\cos(k\tau)$, $k = 1, \ldots n$, while functions with exponential behavior are best described with exponential base functions. A combination of Fourier series and exponentials would also be effectively used if the behavior of the approximated function exhibits such a pattern. In the present study, since the laser range observations are affected by periodic and secular perturbations caused mainly by the gravity field it is only fair to choose for their representation periodic base functions supplemented with monomials of degree zero, one, and possibly two. Chebychev polynomials exhibit such a behavior not only because of their $\cos(n\theta)$ origin (see Section 3.5.2) but also because the Chebychev polynomials of degree zero and one coincide with the monomials of the same degrees. In addition to this, the optimal properties of the Chebychev polynomials (see Section 3.5.2) make them ideal base functions for an effective global representation of the observed laser ranges.

Having chosen a set of base functions, their linear combination should be determined to "best" approximate the function implied by the given set of data (i.e., function of the observed laser ranges). The best representation of this function is determined on the basis of a chosen criterion. Such a criterion may be chosen to either reproduce the function at its base points or to reproduce the function and its derivatives at a given point. We may also choose to either minimize the maximum error of the approximation (i.e., minimax principle) or to minimize a weighted sum of the squares of the residuals at the base points (i.e., least squares approximation).

Reproducing the function at n base points results in an interpolating polynomial of degree (n-1). Thus approximation of the laser ranges with an interpolating polynomial would result in a polynomial of degree ranging anywhere between 200 to 12000. Use of such a high-degree polynomial is completely out of the question. Reproducing the function and its derivatives at a given point or minimizing the maximum error of approximation are also ruled out

because for the former criterion the derivatives needed are not available while for the latter the base points should coincide with the roots of the minimax polynomial. Such a choice is not feasible in our study simply because we have no control over when the laser ranges will be recorded. However, if such a choice would have been possible it would result in a minimax polynomial of very high degree, and therefore it would have been ruled out again. Minimizing a weighted sum of the squares of the residuals (i.e., least squares principle) constitutes a very good alternative not only because we can statistically select a relatively low degree for the approximating polynomial but also because the least squares do not reproduce the observations. The former property prevents instability problems usually associated with the polynomial interpolation, while the latter is desired because the observed laser ranges are always contaminated by measurement errors. Therefore, the functional representation of the observed laser ranges with Chebychev polynomials whose coefficients are estimated with a least squares adjustment, constitutes an alternative having many of the desired properties necessary for a successful interpolation (see Section 3.6.2).

The ***piecewise interpolation methods*** generate approximate values that are sensitive to the values of the approximated function in the neighborhood of the interpolating point but largely insensitive to the values of this function a little farther away from that point. Furthermore, the effects of the gaps in the piecewise interpolation methods are not uniformly distributed over the interval of approximation. Thus, approximation errors committed closer to big gaps are substantially larger than those committed closer to smaller gaps (see Section 3.6.2). Such behavior of the approximation errors cannot be easily controlled because their functional dependence on the magnitude and the distribution of the gaps is not known. Direct evaluation of this functional dependence requires laser ranges between adjacent observations which of course are not available. The inability to effectively control the effect of the gaps in the piecewise interpolation methods constitutes a major drawback when these methods are compared to the global interpolation methods (see Section 3.6.2).

The generated approximate values via piecewise interpolation methods are largely uncorrelated because a different linear combination of a (possibly different) set of base functions is used to generate the approximate values between different pairs of successive observations. This property differentiates the piecewise interpolation methods from the global interpolation methods and constitutes a desired property for the present study because the generated SR and SRD observables will be considered uncorrelated in the final least squares adjustment when station coordinates and baselines are estimated (see Sections 4.3 and 4.4).

With the piecewise interpolation methods a relatively small number of base functions (usually three to five) is needed to represent the data between adjacent data points. The choice of the base function should be made along the same lines discussed in the global interpolation methods. The coefficients of the different linear combinations of the (possibly) different set of base functions for each subset of adjacent base points are determined by imposing boundary conditions to reproduce the functional values (i.e., observed ranges) and to obtain a continuous interpolating function with continuous first and/or second derivatives. One may also choose not to reproduce the observed ranges but rather to introduce a weight function that would reflect a desired relation between the predicted and the actually observed laser ranges. The introduced weight function may be derived according to the measurement errors and to the distribution of the gaps in the neighborhood of the base points (i.e., observing epochs). Use of weight functions with cubic splines leads to the weighted cubic splines interpolation (Spath, 1974). Estimating the weight function is a difficult task, and this function may not be valid for different cases. Therefore it was considered appropriate not to introduce any weight function but rather to reproduce the functional values (i.e., observed ranges) at each base point (i.e., observing epoch). This would enable the evaluation of the overall performance of the piecewise methods in regard to their ability to generate good approximate values when relatively large gaps exhibit an uneven distribution over the interval of approximation (see

Section 3.6.2). For this evaluation we made use of the easy-to-handle cubic splines.

A cubic spline s(t) where t is in the interval $[t_1, t_n]$ is defined as a set of third-degree polynomials, each defined in the interval $[t_k, t_{k+1}]$ ($k = 1, \ldots n-1$). These polynomials are joined at the base points (t_k) so that the resulting cubic spline is twice differentiable at each base point. A cubic spline defined on an interval with n base points consists of (n-1) third-degree polynomials. Thus, its unique determination requires 4(n-1) independent sets of equations. The requirement to have a twice differentiable cubic spline in the interval $[t_1, t_n]$ introduces a set of 2(n-2) independent equations which results from the continuity conditions required for the existence of the first and second derivatives at the base points t_2 through t_{n-1}. The requirement to reproduce the functional values (i.e., observed laser ranges) at the base points (i.e., observing epochs) introduces another set of [2(n-2) + 2] independent equations bringing up to (4n-6) the total number of independent equations. The two additional equations, necessary for the unique determination of a cubic spline, are obtained from the boundary conditions specified for both ends of the approximation interval (i.e., at the base points t_1 and t_n). Since the observed laser ranges vary slowly within a few seconds of time, we have adopted in the present study the following conditions:

$$s''(t_1) = s''(t_2) \tag{3-33}$$

$$s''(t_n) = s''(t_{n-1}) \tag{3-34}$$

Such an arbitrary choice influences the results very slightly in the neighborhood of the end points (Spath, 1974; Pavlis, 1982). The independent set of equations used to determine the (4n-4) coefficients of a cubic spline is given in (Spath, 1974; Pavlis, 1982). The next section contains an evaluation of the relative performance of the least squares Chebychev and cubic spline interpolators. This evaluation is based on their ability to effectively interpolate the observed laser ranges.

3.6.2 Chebychev Polynomials vs. Cubic Spline Functions in the Functional Representation of Laser Ranges

Least-squares approximation of the laser ranges with Chebychev polynomials requires a priori knowledge for the degree of the resulting algebraic polynomial

$$Ra(\tau) = \alpha_0 + \alpha_1 T_1(\tau) + \ldots + \alpha_k T_k(\tau) \qquad (3\text{-}35)$$

The degree of the algebraic polynomial $Ra(\tau)$ coincides with the degree of the k^{th} Chebychev base function $T_k(\tau)$. This degree should be chosen to represent the data "sufficiently" in the sense that an extension of equation (3-35) to include higher-degree Chebychev polynomials will represent the data with the same accuracy. There is a limit as to what degree we can go to because after a certain degree has been reached instability problems will deteriorate the solution substantially. With Chebychev polynomials there exists a wide range of degrees that can be used to represent the data with the same accuracy. This is possible because Chebychev polynomials are not seriously affected by instability problems (see Section 3.5.2). This property will be very useful in our study because in the generation of the SR and SRD observables it reduces the computing time substantially (see Section 3.6.3).

The lowest-degree Chebychev polynomial that sufficiently represents the available data is conveniently determined through statistical testing. To construct this test it was assumed that the coefficients of the equations (3-35) were estimated together with the weighted sum of the squares of the residuals

$$R_k = (V^T P V)_k \sim \sigma^2 \chi^2_{n-k-1} \qquad (3\text{-}36)$$

through a least-squares adjustment. At this point we would like to statistically test if the coefficient (α_k) is significantly different from zero. To accomplish this, we perform another adjustment supplemented with the constraint that the coefficient (α_k) is zero. If in this adjustment the computed weighted sum of squares of the residuals is

C-2

R_{k-1}, then the weighted sum

$$R_C = R_{k-1} - R_k \tag{3-37}$$

caused by the constraint ($\alpha_k = 0$) is distributed as $\sigma^2\chi_1^2$ [$= \sigma^2 N^2(0, 1)$] independently from R_k (Hamilton, 1964). Thus, the percentage change of the weighted sum of the residuals

$$P = \frac{R_C}{R_k} \cdot (n-k-1) = \frac{R_{k-1} - R_k}{R_k} \cdot (n-k-1) \sim \frac{\chi_1^2}{\chi_{n-k-1}^2} = F_{1,n-k-1} = t_{n-k-1}^2 \tag{3-38}$$

caused by the constraint ($\alpha_k = 0$) is distributed as t_{n-k-1}^2. Having P and its distribution it is possible to set up a hypothesis test based on the percentage change of the weighted sum of the residuals

H_o: $\alpha_k = 0$ (=: not significant change in P)

H_1: $\alpha_k \neq 0$ (=: significant change in P)

The critical region of the test is obtained through the following equation

$$P(F_{1,n-k-1} > P_{cr}) = \alpha \leftrightarrow P(|t_{n-k-1}| > (P_{cr})^{1/2}) = \frac{\alpha}{2} \tag{3-39}$$

where α is the significance level (i.e., Type I error) of the test. Specifying a value for α of 0.01 (1%) we can determine P_{cr} for $n > 200$ with the help of a t table and equation (3-39) (DeGroot, 1975)

$$(P_{cr})^{1/2} = 2.576$$

resulting in the critical region

$$C = \{P \in R: \quad P > (2.576)^2\} \tag{3-40}$$

Thus the hypothesis H_o is rejected if

$$P > (2.576)^2 \tag{3-41}$$

thereby suggesting that a higher degree is needed at the 1% significance level. This process continues up to the degree for which

H_0 cannot be rejected. With this test at our disposal we have the means to determine the least squares Chebychev polynomial that "sufficiently" represents the observed laser ranges. Therefore, we can proceed with the relative evaluation of the cubic spline and Chebychev interpolators. This evaluation is based on the ability of these interpolators to "adequately" represent the laser ranges.

The relative performance of these interpolators is based on a quantitative analysis of the orbit residuals obtained with two identical semidynamic orbit adjustments. The SRD observables input to those adjustment were generated through the cubic spline and the Chebychev interpolators using the edited observations of the station pair 7114 and 7115. These observations correspond to the same two passes whose Chebychev residuals are shown in Fig. 3. The generated cubic spline and Chebychev SRD's were processed with the help of

- Lageos initial state vectors predicted, through numerical integration, for the starting epochs of both passes
- the shortened version of the DE/LE200 lunar planetary ephemeris file covering the time span of the observations, and
- the coordinates of the pole with the variations in UT1 at each observing epoch

through two separate orbit least squares adjustments implemented by the GEOSPP software. This software was developed by Pavlis (1982) and during the course of this study was not only modified to comply with the MERIT standards but also was corrected to successfully operate in the real data environment (see Chapter 2). The TRF and the CRF frames for each of the above adjustments are realized through the implicit constraints discussed in Chapter 2 supplemented with the following weighted constraints (see Section 4.1):

- coordinates of station 7114 were held fixed (i.e., $\sigma x = \sigma y = \sigma z =$ 0.0001 m)
- coordinates of station 7115 were moderately weighted (i.e., $\sigma x = \sigma y = \sigma z =$ 10.0 m)
- initial state vectors were moderately weighted (i.e., $\sigma x = \sigma y = \sigma z =$ 20 m; $\sigma \dot{x} = \sigma \dot{y} = \sigma \dot{z} =$ 0.02m/s)

The relative evaluation of the cubic spline and Chebychev interpolators is based on the comparison of the orbit residuals obtained with the cubic spline and Chebychev SRD observables. The cubic spline and Chebychev orbit residuals for the same two passes depicted in Fig. 3 are shown in Figs. 4 and 6. The generation of the cubic spline SRD's and the Chebychev SRD's is based on the interpolation of the station having the larger number of observations.

A comparison of Figs. 4 and 5 shows a strong correlation between the cubic spline orbit residuals and the data gaps of station 7115. However, this strong correlation exists only for the pass whose successive data gaps reach a maximum value of 60 seconds (see left plots of Figs. 4 and 5). For the other pass, whose gaps are not larger than 10 seconds, the correlation of the cubic spline orbit residuals with the successive data gaps is not strongly pronounced. This happens because the small magnitude data gaps are evenly distributed over the entire pass (see right plots of Figs. 4 and 5). On the contrary, the correlation of the Chebychev orbit residuals with the successive data gaps of station 7115 is very low (compare Figs. 6 and 5). Furthermore, it is quite clear that the cubic spline residuals are noisier than their Chebychev counterparts. In fact, the RMS of the cubic spline residuals for the passes shown in Figs. 4 and 6 is 0.41 m and 0.23 m respectively, while for the same two passes the RMS of the Chebychev orbit residuals is 0.12 m and 0.11 m respectively. The noisy behavior and the high RMS of the cubic spline orbit residuals is traced to the piecewise nature of the cubic spline interpolation. This assessment is confirmed by computing the differences between the cubic spline and the Chebychev SRD's. These differences are shown in Fig. 7, and they seem to exhibit an almost identical behavior with the cubic spline orbit residuals (see Fig. 4), thereby confirming the anticipated fact, namely, that these residuals are primarily caused by the cubic spline interpolator. This result is not surprising since the piecewise nature of the cubic spline interpolator makes it sensitive to the magnitude and distribution of the data gaps. On the contrary, the global nature of the Chebychev interpolator makes it insensitive to the magnitude and the distribution

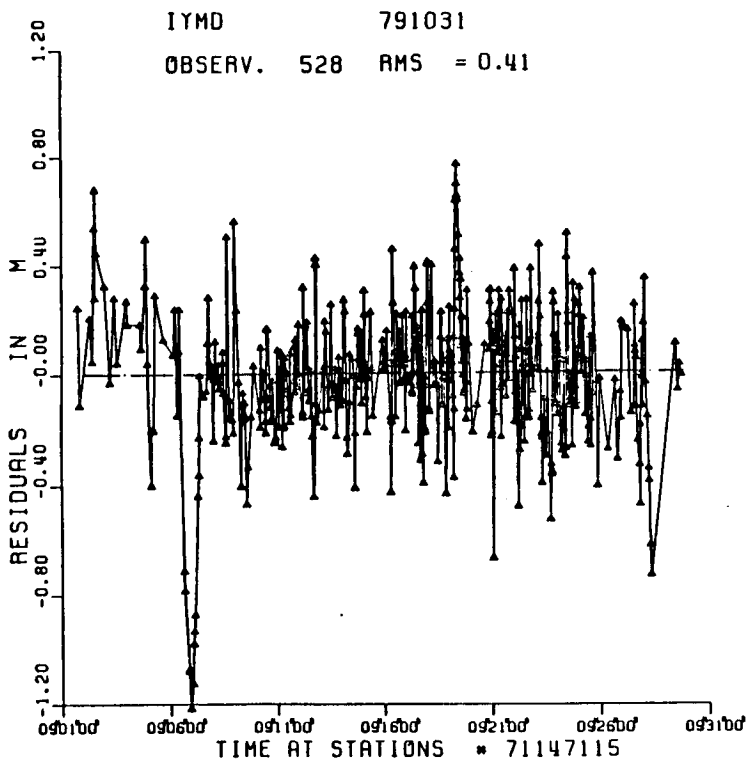

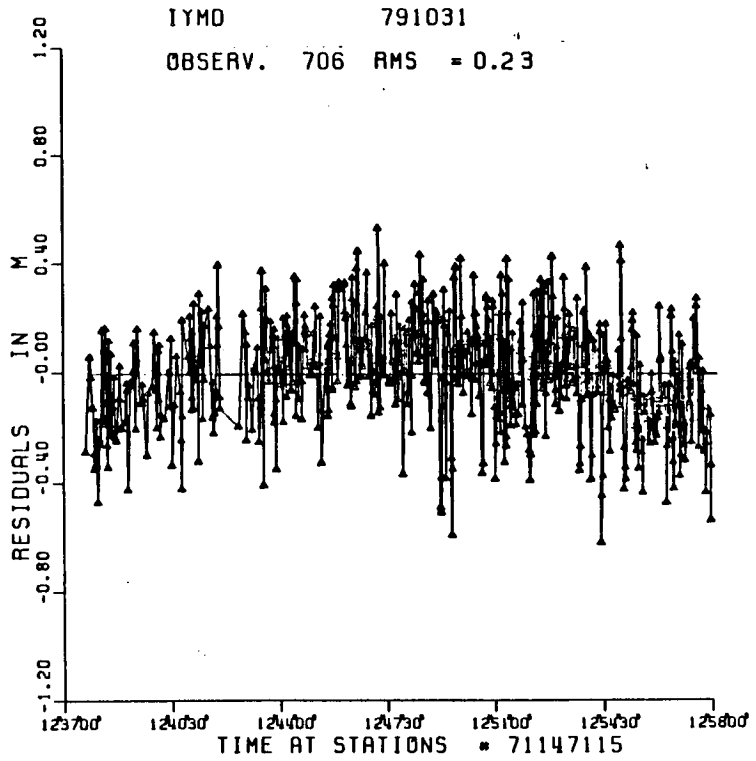

Fig. 4 Orbit residuals (cubic spline SRD's).

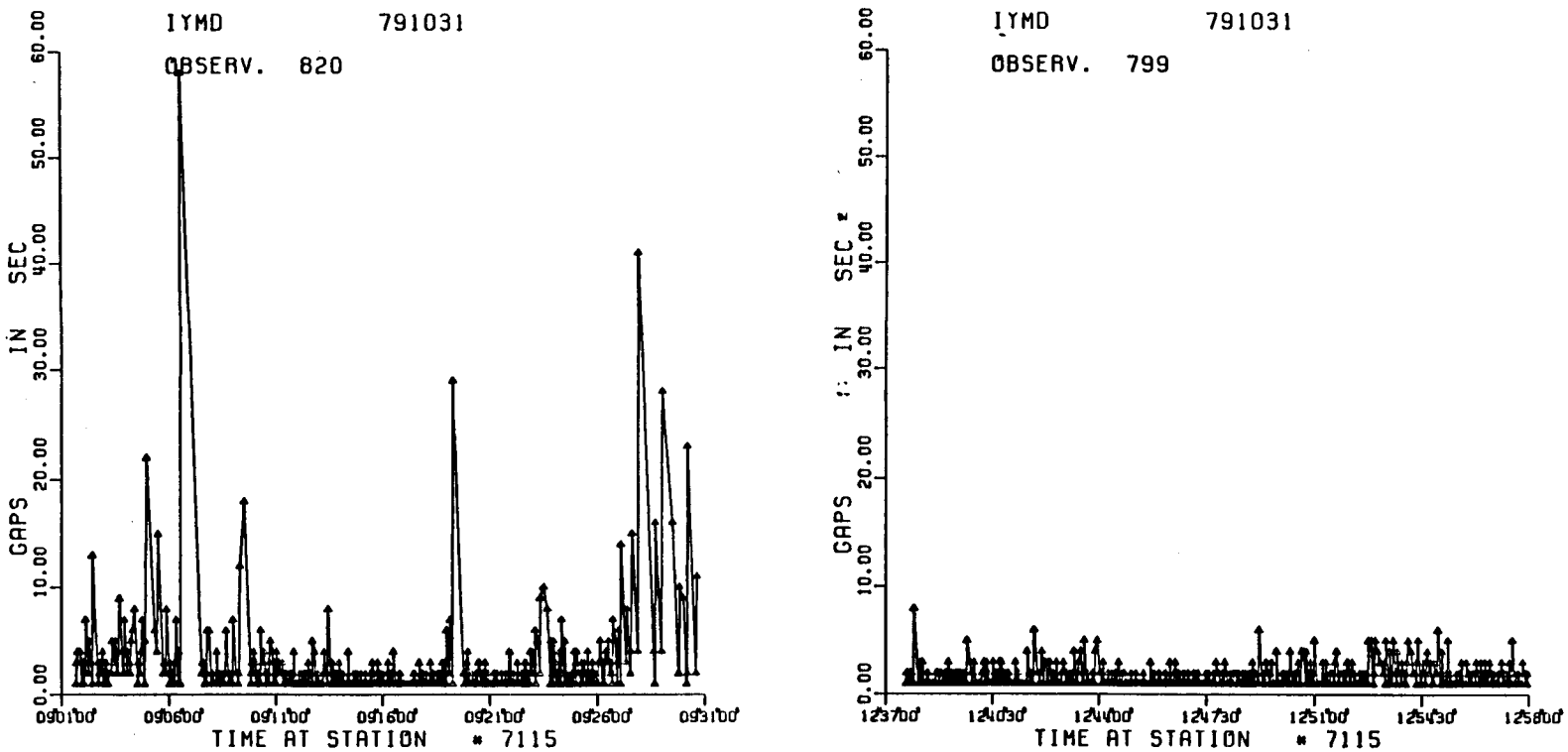

Fig. 5 Successive data gaps for station 7115.

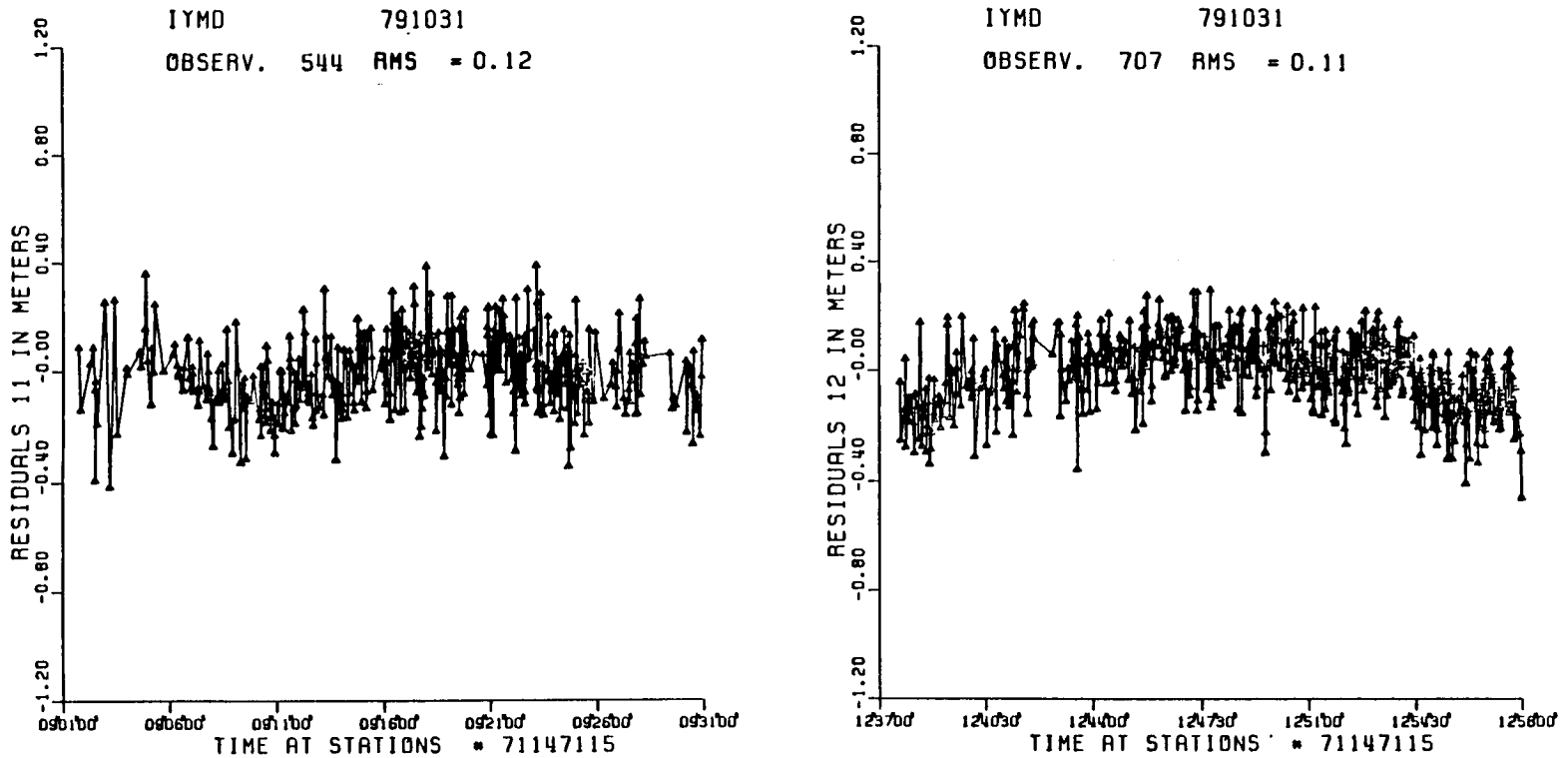

Fig. 6 Orbit residuals (Chebychev SRD's).

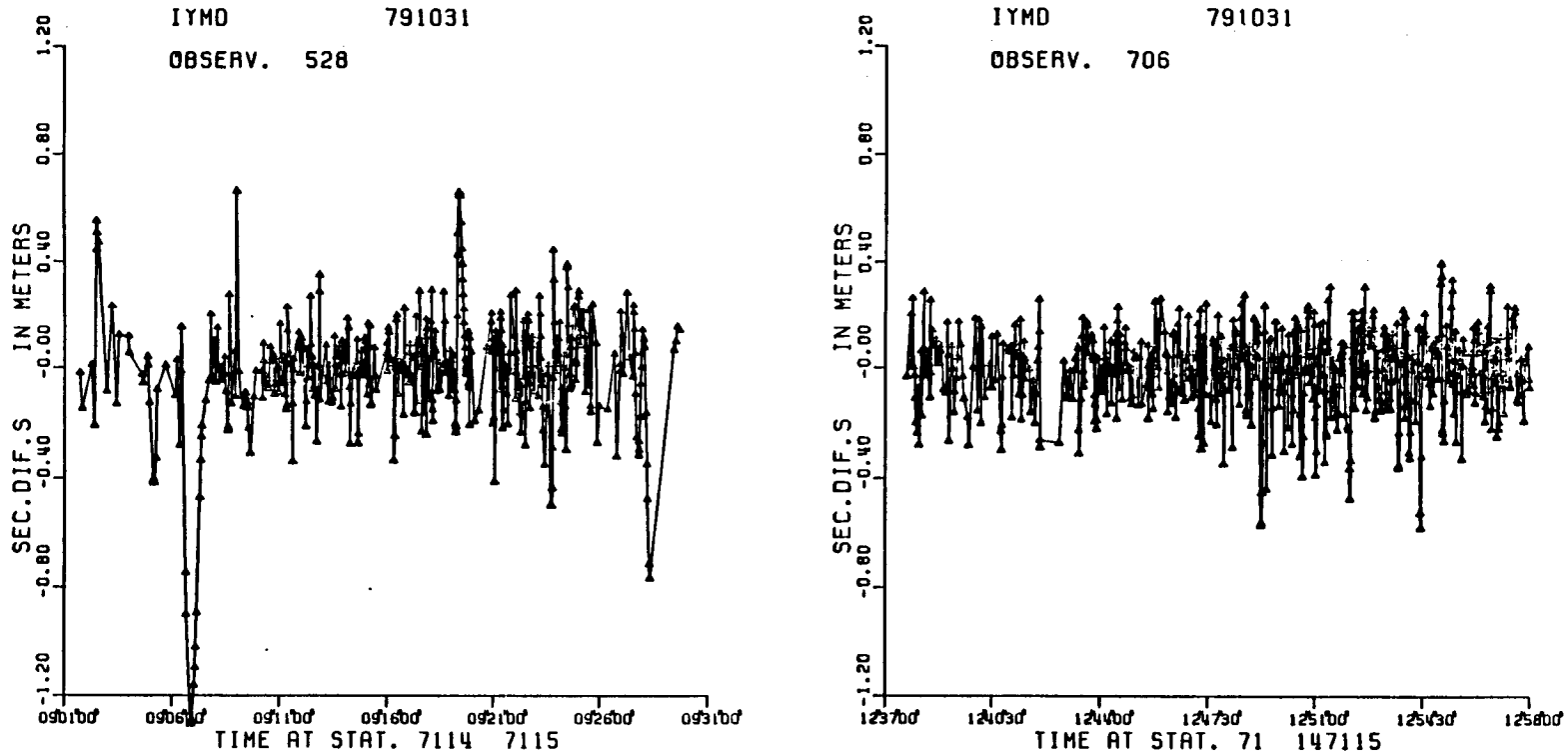

Fig. 7 Differences between cubic spline and Chebychev SRD's.

of the data gaps provided that these gaps are not larger than 60 seconds. On the other hand, the 0.11 m and 0.12 m RMS of the Chebychev orbit residuals is consistent with the expected accuracy of stations 7114 and 7115 respectively. Thus one can safely assume that the errors caused in the generation of the Chebychev SRD's by the up-to-60-second data gaps are not larger than the noise level of the observations. Extensive experimentation with dense and sparse data sets has revealed that gaps larger than 60 seconds tend to be several minutes long, thereby implying that the corresponding station ceased to observe due to calibration, weather problems, etc. (see Section 3.6.3). Thus, from now on we say that a station observes continuously if and only if successive data gaps are not larger than 60 seconds. Furthermore, interpolation is performed only over time intervals with "continuous" coverage of observations.

The above discussion demonstrates that interpolation of the laser ranges with Chebychev polynomials is superior to that of the cubic splines. Thus, for the MMC data set all the SR and SRD observables have been generated through a Chebychev least squares approximation. The interpolation is performed only over observing intervals with gaps smaller than 60 seconds (see next section).

3.6.3 Data Selection for the Generation of the Simultaneous Ranges and the Simultaneous Range Differences

In the present study a considerable amount of time and effort was devoted to generate the Simultaneous Range (SR) and the Simultaneous Range Difference (SRD) observables. These two observables constitute the input to the geometric and to the SRD methods respectively. A geometric solution, apart from special cases, is possible if at least six satellite positions are being coobserved by at least four stations generally distributed in space (i.e., not lying on the same plane). If the ground stations either form a plane (or close to forming a plane), a geometric solution is possible only if six or more stations are involved and each satellite position is coobserved by at least four stations (see

Section 2.1.3). An SRD solution, apart from special cases, is possible if at least one pair of stations is coobserving (see Section 2.2.6).

The only data set having the potential to best fulfill the above reqirements is the MMC SLR data set (see Section 3.4). This data set contains the satellite laser range observations collected during the MERIT Main Campaign. Presently, a large amount of simultaneous laser range observations are recorded in the WEGENER/MEDLAS project.

The MMC data set was received upon request from the CDDB data bank on nine-track magnetic tapes, each containing a month's worth of observations collected either by all or by some of the MERIT stations. In each tape the information relevant to a specific observation is stored in records in the Seasat Decimal (SSD) format (see Section 3.4). Each record contains the observed laser range, the epoch of the observation, systematic corrections and indicators for the corrections that have been applied and for those that have yet to be applied (Schutz, 1983b). Some observations, however, were missing from the received tapes due mainly to data problems and delays. Thus, it was necessary at first to identify for each of the received tapes the ID's of the observing stations, the number of passes per station and the number of observations per pass. This information was compared against the same information published in the monthly SLR reports issued for the entire MERIT Main Campaign by the Center of Space Research (CSR) at the University of Texas (UTX). These monthly reports contained the number of passes together with the total number of observations recorded by each of the stations involved. Any observations missing from the received tapes were obtained through a subsequent request issued only if the utilization of those observations was considered critical for the successful implementation of either the geometric or the SRD methods. Upon this request, new tapes identified with the release letters A, B, C, etc. were received from the CDDB data bank. These tapes contained the missing observations together with those received in previous releases.

When the software necessary to process the laser range observations was ready, it was decided not to wait any longer but rather to use whatever releases were available up to that date (i.e.,

Spring 1985). These releases are listed in Table 3, and they were finally employed in our investigation. For each of those releases the passes containing arcs coobserved by two or more stations were identified and isolated. In the context of the present study a pass is defined as a satellite passage whose blind spots are shorter than 2.2 hours. With blind spots we designate the periods during which the satellite was not observed by any of the stations involved. An arc, on the other hand, denotes an observing period during which the successive data gaps are shorter than 60 seconds. An arc overlap of a Lageos pass recorded by American stations is shown in Figure 8 (left plot).

The abscissae in these two plots denote the observing epochs relative to the starting epoch of the pass shown on the top of these plots. The starting epoch (84082442132) shown on the top of the left plot reads 84 (1984), 08 (August), 24 (-th day), 4 (hours), 21 (minutes) and 32 (seconds). The ordinates on the right-hand side designate the numeric station ID's (see Table 2 in Section 3.2.4). The ordinates on the left-hand side of these plots designate in ascending order the observing sequence of the stations involved. The solid horizontal lines indicate that for the period they cover the stations whose numerical ID is shown on the right-hand side of this line have data gaps shorter than 60 seconds. The dotted horizontal lines indicate that for the period they cover the corresponding station was not observing. The number above the starting point of each solid line denotes the number of observations whose successive data gaps are shorter than 60 seconds. Fig. 8 confirms the assertion made in the previous section, namely, if the gaps are larger than 60 seconds they tend to be several minutes long. It is evident from the left plot of Fig. 8 that all of the stations involved except 7086 have a good continuous coverage, thereby making it possible to effectively interpolate their ranges. There is no need to interpolate the ranges of station 7086 since this station has recorded the least number of observations (see Section 3.6). The observing pattern shown in the left plot of Fig. 8 is indicative for the performance of the American stations during the MERIT Main Campaign. On the contrary,

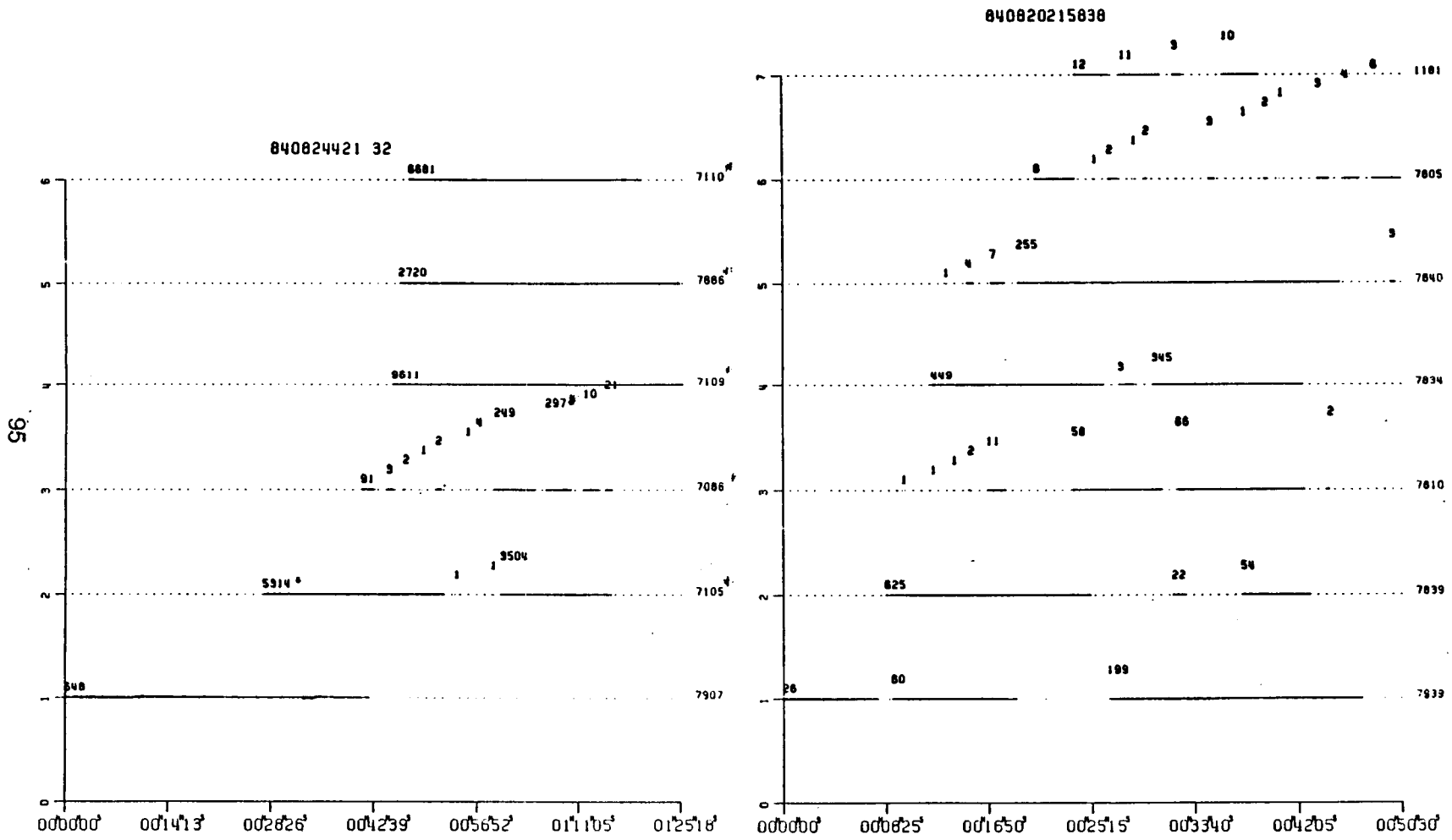

Fig. 8 Arc overlap of two Lageos passes recorded by American stations (left plot) and European stations (right plot) respectively.

the performance of the European stations is not quite as good. This is seen in the right plot of Fig. 8. This plot confirms the extended overlap expected among the visibility regions of the European stations. In spite of this, we can hardly interpolate the laser ranges for any of the coobserving stations simply because each of the arcs involved contains a small number of observations. Thus the question as to how many continuous observations (i.e., observations with successive data gaps shorter than 60 seconds) are enough for an effective interpolation is examined next. This question will be investigated by analyzing the errors committed in the recovery of ground truth observations. The recovery errors are computed by taking out a subset of observations, referred to as ground truth observations, in such a way that the data gaps of the observations left remain shorter than 60 seconds. The observations left are then used to determine a least-squares Chebychev polynomial which is subsequently employed to recover the ground truth observations, that is, the observations not considered in its determination. Finally, by subtracting the recovered ground truth observations from the actually observed ones we obtain the recovery errors mentioned above. A sample plot of such errors for station 7210 is shown in Fig. 9 together with the distribution of the ground truth points used in the computation of those errors (i.e., left- and right-hand-side plots respectively).

These errors were computed for 285 ground truth observations obtained from a total of 1427 available observations by taking out every fourth observation. The ones left (i.e., 1142 all together) formed the basis to determine the least-squares Chebychev polynomial which was in turn employed to recover the ground truth observations. The abscissae for both of the plots shown in Fig. 9 designate the epochs of the ground truth observations relative to 0^h UT of the day shown on the top of the figure. The ordinates of the left plot designate the recovery errors (i.e., Range - Rint.) while the ordinates of the right plot designate the laser ranges after they have been scaled and shifted for plotting purposes. The RMS of these errors is 0.03 m which is exactly equal to the expected precision of station 7210.

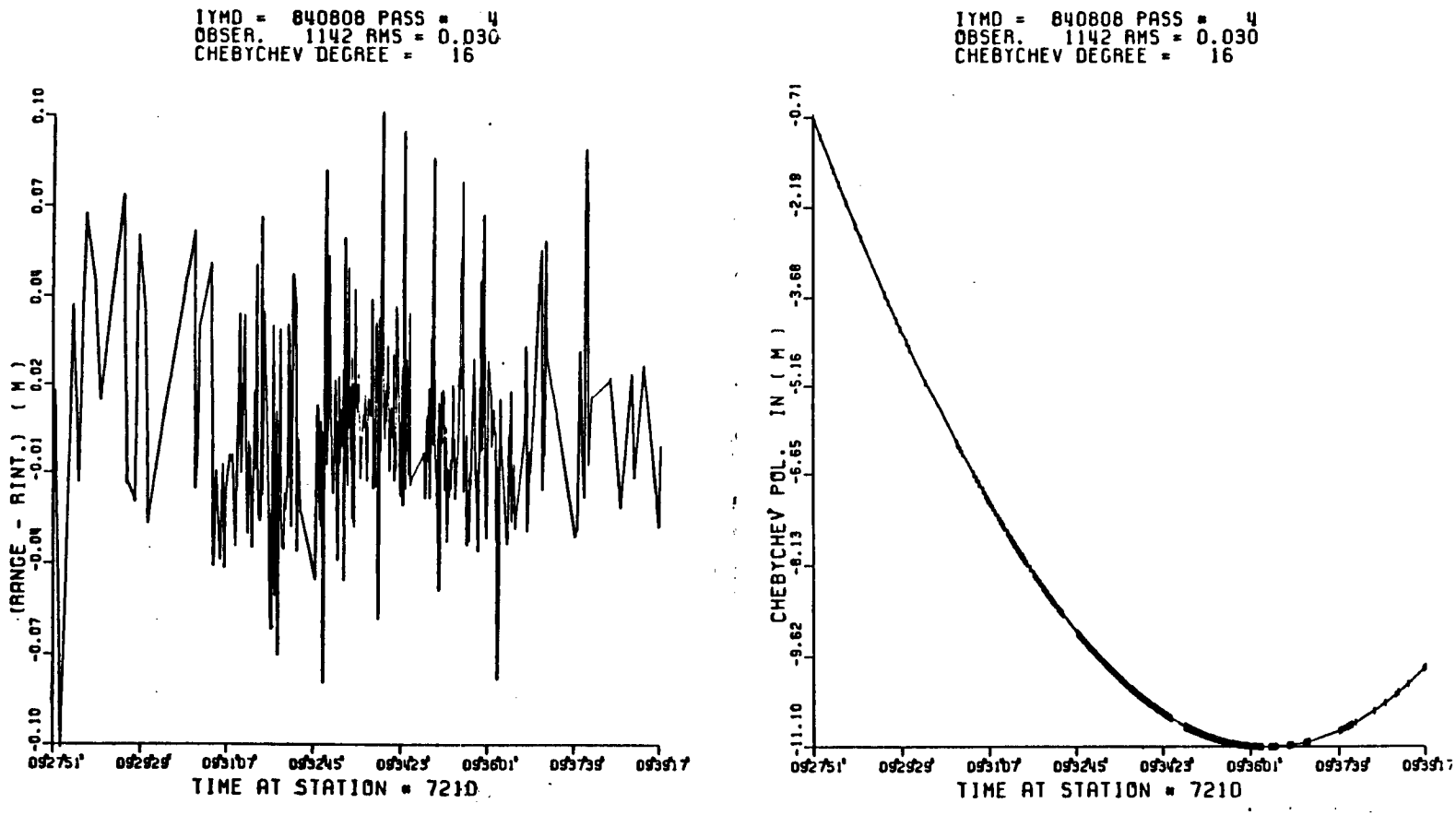

Fig. 9 Recovery errors and distribution of ground truth observations (dense data).

Using a different arc observed by the same station and in the same month we again have computed the recovery errors for 47 ground truth observations obtained from a total of 283 observations by taking out every sixth observation. These errors, together with their distributions, are shown in Fig. 10.

The RMS of these errors is about 23% worse than the expected precision of station 7210 (Analysis of Lageos Range Data, August 1985). Extensive experimentation with American stations has indeed confirmed that on the basis of less than 500 observations the interpolated ranges are affected by errors which are 15% to 20% worse than the noise level of the observations. On the contrary, using more than 500 observations the errors caused by the interpolation hardly ever reach the noise level of the observations.

The distribution of the ground truth points shown in Figs. 9 and 10 reflects for each arc the distribution of the available observations because the ground truth observations were obtained from the available observations by taking out either every sixth or every fourth observation. With this in mind a closer inspection of Figs. 9 and 10 clearly reveals that small recovery errors are distributed around the denser parts of these two arcs while for the denser arc shown in Fig. 9 the recovery errors are considerably smaller. Although the small recovery errors are distributed around the denser parts of these two arcs, there exist in those parts recovery errors having an absolute magnitude of 0.10 m which is about three times larger than the expected accuracy of station 7210. Thus, the question arises as to whether these large recovery errors are caused by the procedure used to compute them or by errors affecting the actually observed ranges.

To examine this we have plotted in Fig. 11 the Chebychev residuals for both arcs shown in Figs. 9 and 10. These Chebychev residuals have been computed by using all of the 1142 and 283 available observations for both arcs. Comparison of the recovery errors shown in Figs. 9 and 10 with the corresponding Chebychev residuals shown in Fig. 11 clearly shows their high correlation and the equality of their RMS values as well. Moreover, the large recovery errors seem to have their

ORIGINAL PAGE IS
OF POOR QUALITY

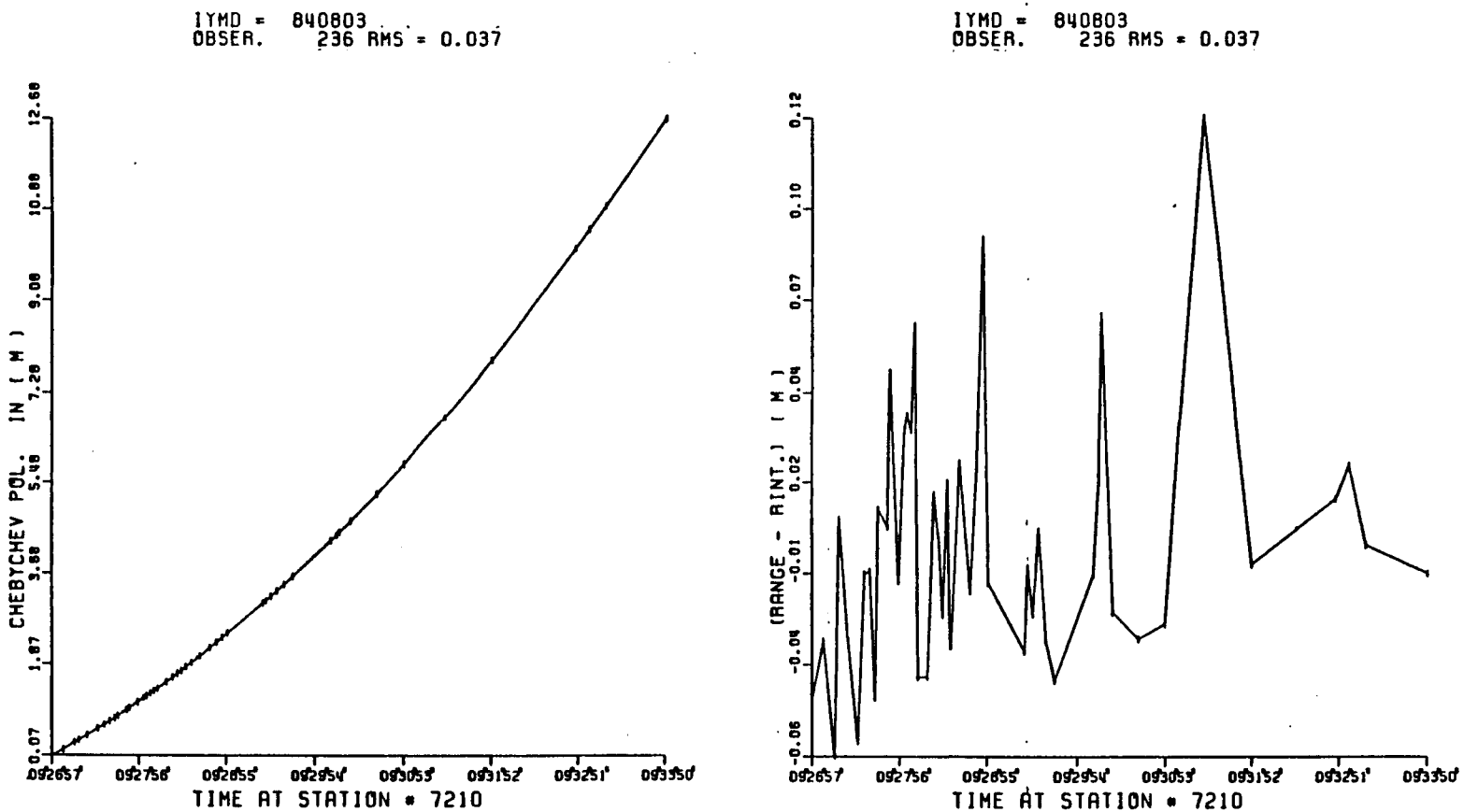

Fig. 10 Recovery errors and distribution of ground truth observations (sparse data).

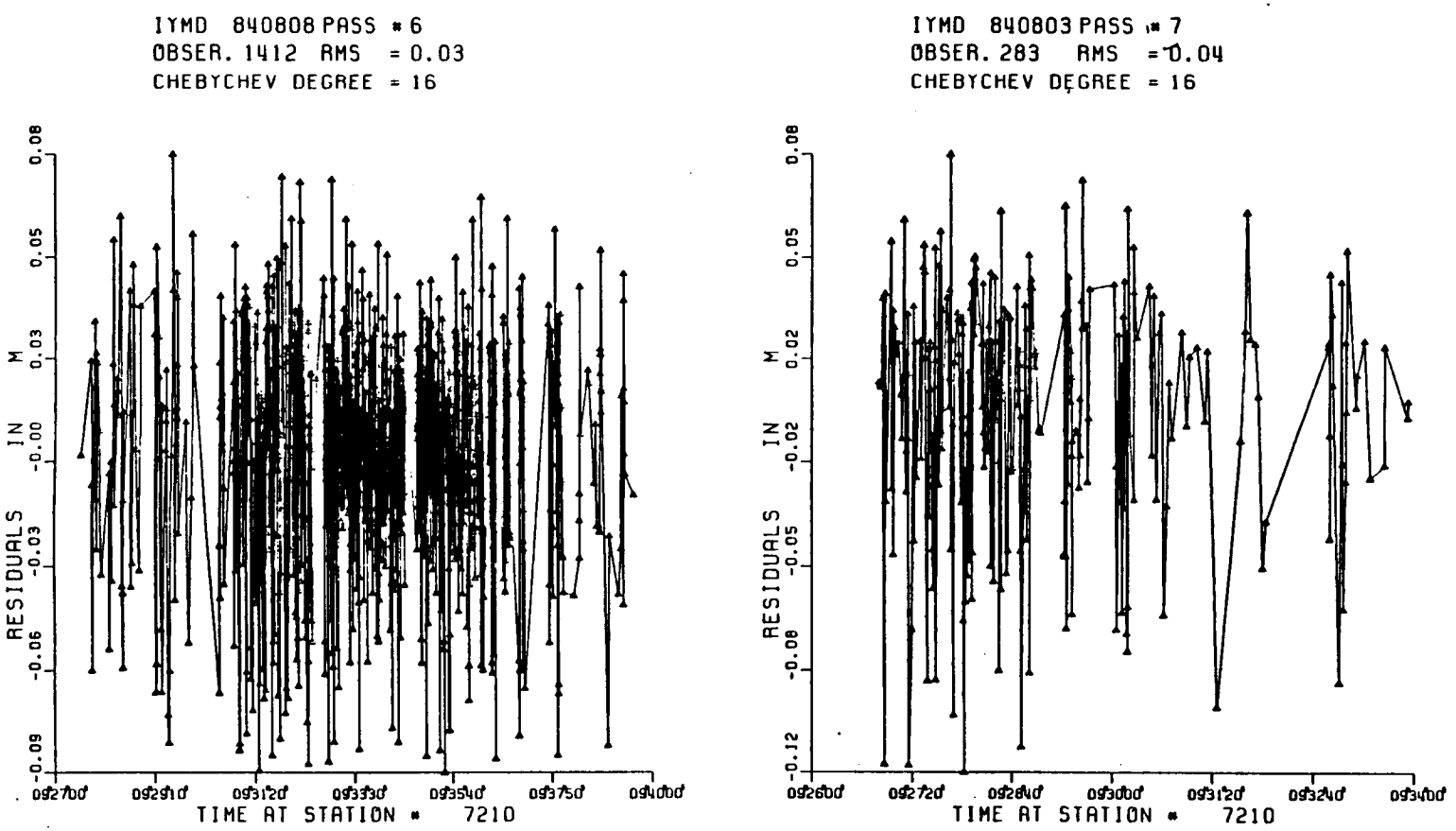

Fig. 11 Chebychev residuals.

counterparts in the Chebychev residuals thereby suggesting that the large recovery errors have originated from errors affecting the actually observed ranges. More importantly the equality of the RMS values between the recovery errors and the Chebychev residuals suggests that analysis of the Chebychev residuals will give a good qualitative measure for the accuracy of the interpolated ranges. This important result used in the present study to control the quality of the interpolated ranges has also been confirmed from the analysis of the orbit residuals (see Section 4.4). Thus, we can safely state that interpolated laser ranges based on a relatively dense data set (i.e., with more than 500 observations) will be affected on the average by approximation errors that are smaller than the noise level of the observation. Since the Chebychev polynomials are nearly orthogonal, deterioration due to numerical instability ceases to exist as the number of observations increases 11,000, 12,000 or more. Thus, since the recovery errors are smaller for denser data sets it is preferable to interpolate dense rather than sparse data sets provided that at least 500 observations with gaps shorter than 60 seconds are available.

Inspection of the left and right plots of Fig. 8 reveals that the American stations fulfill the above requirements (i.e., to have more than 500 observations with gaps shorter than 60 seconds) while the European stations hardly ever fulfill such a requirement. The American station 7086, on the other hand, seems to have experienced several problems during the pass shown in the left plot of Fig. 8. The observing pattern, however, of this station was more or less the same for the entire MERIT campaign thereby making its observation inappropriate for interpolation, Fortunately, out of all the American stations used in this investigation only two of them, station 7086 (Texas) and 7112 (Colorado), seem to consistently have so many interruptions within all of their observed passes. More specifically, the interruptions of station 7086 are traced to the need of calibrating the laser within any of its observed passes. Furthermore, for most of the passes coobserved by four or more American stations, there exist at least three stations with dense enough observations to be effectively interpolated. This is the

necessary requirement only for the geometric solution since the required four-station events are obtained by interpolating the observations from three stations at the observing epochs of the fourth station for which the actual ranges are used. For an SRD solution, the observations of only one station are interpolated at the observing epochs of the alternate station.

The European stations, on the other hand, seem to have experienced several interruptions for most of their observed passes. These interruptions have forced most of them to record relatively sparse observations. Therefore, it is difficult to find passes having arcs coobserved by four or more stations out of which three have dense enough observations that can be effectively interpolated. For instance, for the arc overlap shown in the right plot of Fig. 8 the observations from stations 7839, 7834 and possibly from 7840 can be effectively interpolated while the observations from any of the remaining stations are inappropriate for interpolation. Since this is the case for most of the passes coobserved by the European stations, it was considered appropriate to drop these stations from their implementation in the geometric solution. However, simultaneous observations collected in (WEGENER/MEDLAS) project have the potential to effectively implement the SRD method.

In other parts of the world there may exist two or three stations coobserving. Overlap, however, for four or more stations is quite unlikely to occur anywhere else except over North America and Europe because only in these two parts of the world there exists a large number of operating laser ranging stations. This and Lageos' high altitude orbit are the main reasons why most of the passes recorded during the MERIT Main Campaign by American stations were coobseved by at least two of them. This resulted in a large number of American station pairs with quasi-simultaneous observations, and therefore it was possible to generate a large enough number of SRD observables that have led to a steady state response of the semidynamic solutions (see Chapter 4). Since the purpose of the present study is not to compute all possible baselines but rather to study the performance of the SRD

and geometric methods in baseline determinations, it was considered appropriate to employ the laser ranges recorded only by the American stations for both the SRD and the geometric methods. Fig. 12 shows the locations for those stations.

Since for each station the observing pattern in terms of data gaps and observational density is relatively homogeneous from pass to pass, we've shown in Fig. 13 three additional arc overlaps involving stations that are shown in Fig. 12 but not in Fig. 8. A comparison of Figs. 8 and 13 confirms our assertion that the observing patterns of stations 7109, 7110 and 7122 which are involved in more than one pass are homogeneous from pass to pass. Furthermore, the RMS of the Chebychev residuals for each of the stations involved shows very small fluctuations from arc to arc. This, however, is not true for stations such as 7122 that were upgraded during the MERIT Main Campaign. Table 4 lists the monthly mean RMS values of the Chebychev residuals obtained by interpolating the edited with the data-snooping-procedure laser range observations. The RMS values listed in Table 4 are in close agreement with those computed by the CSR at UTX listed in Table 2 in Section 3.2. This close agreement confirms once again the effectiveness of the data-Snooping procedure to edit the laser range observations.

For each observing station the quality of the interpolated ranges as reflected through the qualitative pattern of the Chebychev residuals is relatively homogeneous for all of the arcs recorded during the MERIT Main Campaign. Thus, in order to get a feeling for the quality of the interpolated ranges we have plotted in Figs. 14 and 15 the Chebychev residuals for those arcs of Figs. 8 and 13 which have been marked with an asterisk next to their numeric station ID's. If a specific station has observed more than one of the arcs shown in Figs. 8 and 13, then the arc whose Chebychev residuals are shown in Fig. 14 or 15 is also marked just above its starting point with an asterisk. Table 5 lists, for the same arcs shown in Figs. 14 and 15, the RMS values of the Chebychev residuals together with the number of the available observations before and after the data-snooping procedure was applied. The condition numbers also shown in this table refer to the normal

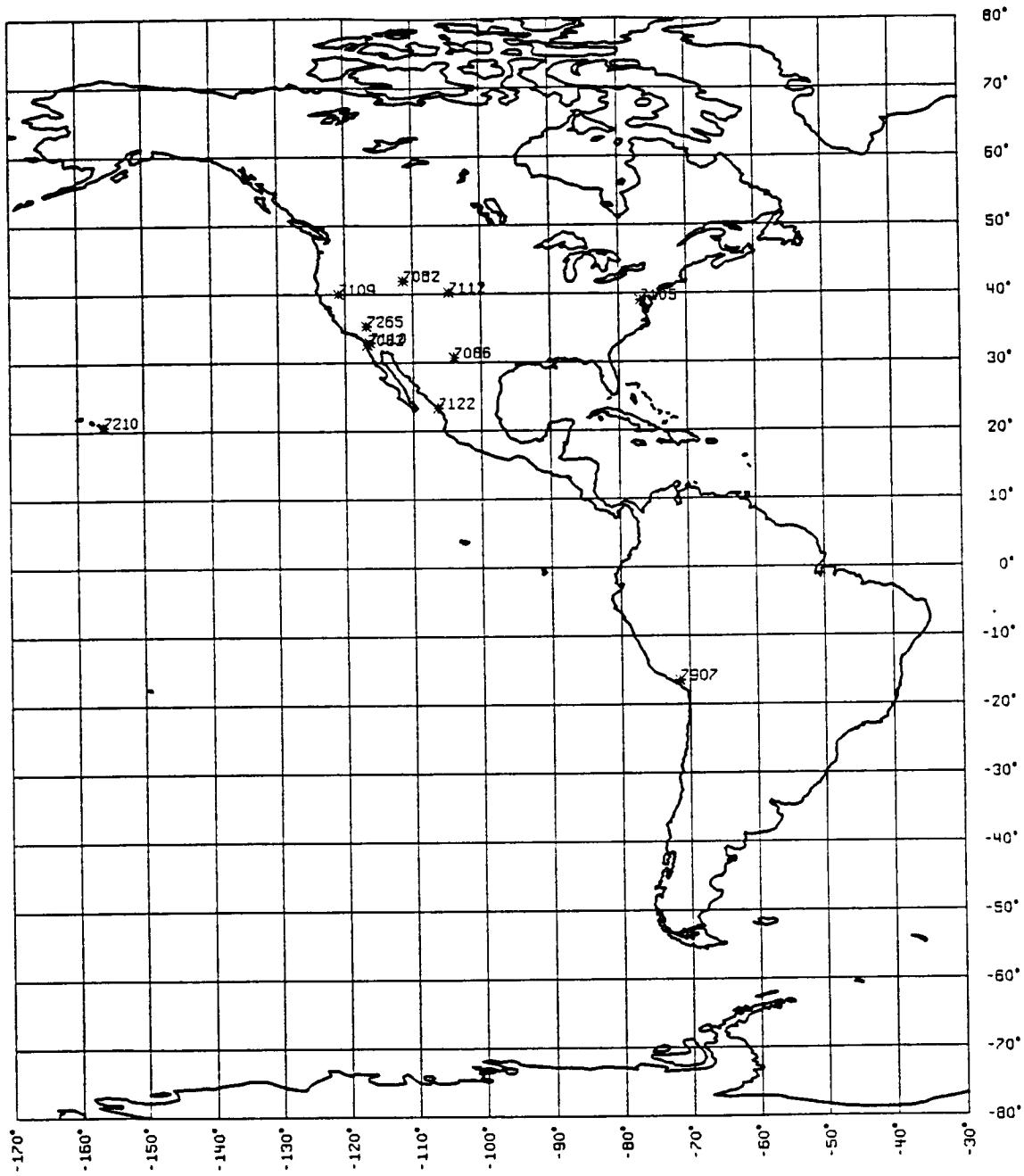

Fig. 12 Location of the American stations used in the present study.

ORIGINAL PAGE IS
OF POOR QUALITY

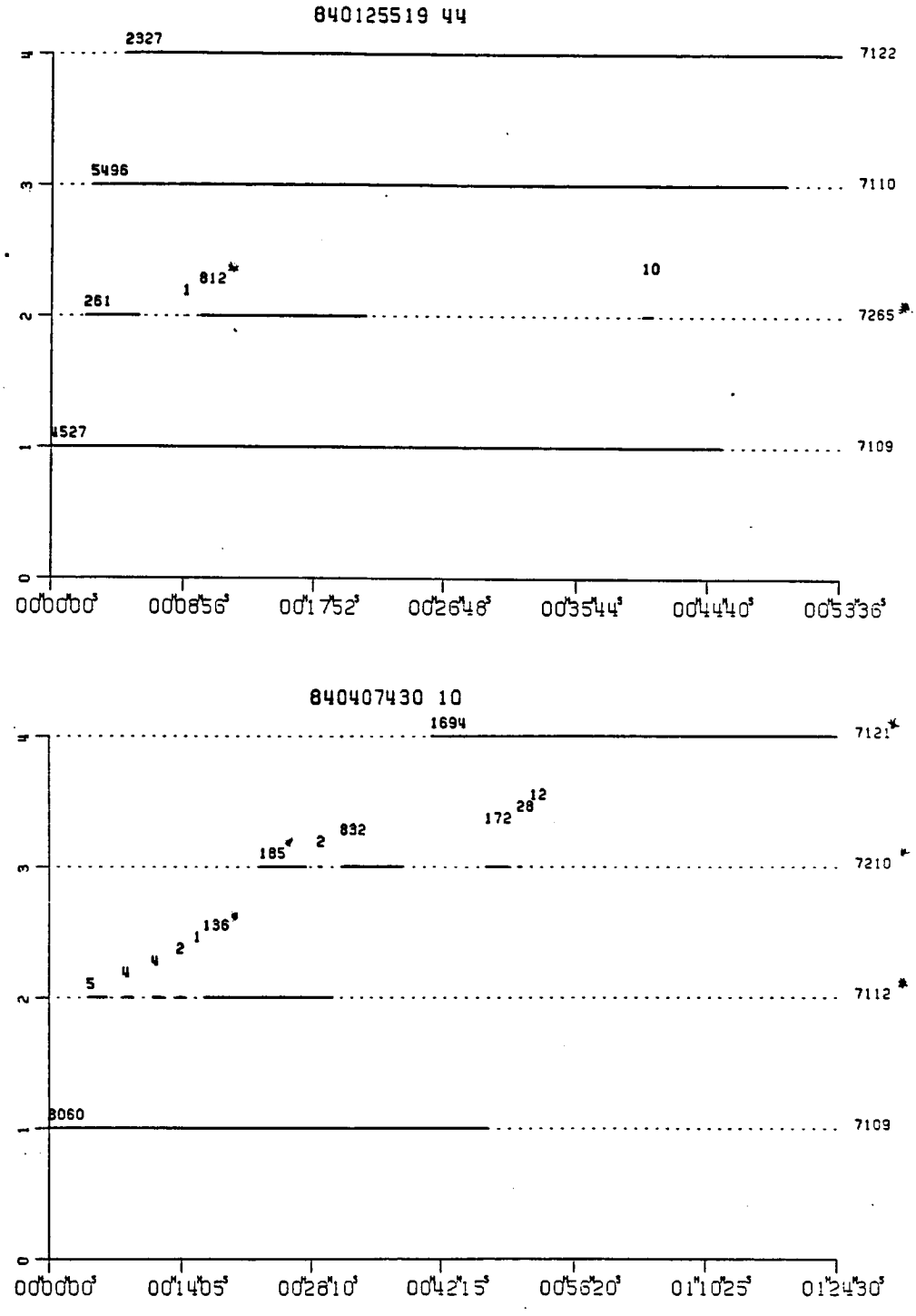

Fig. 13 Arc overlap of three Lageos passes (American stations).

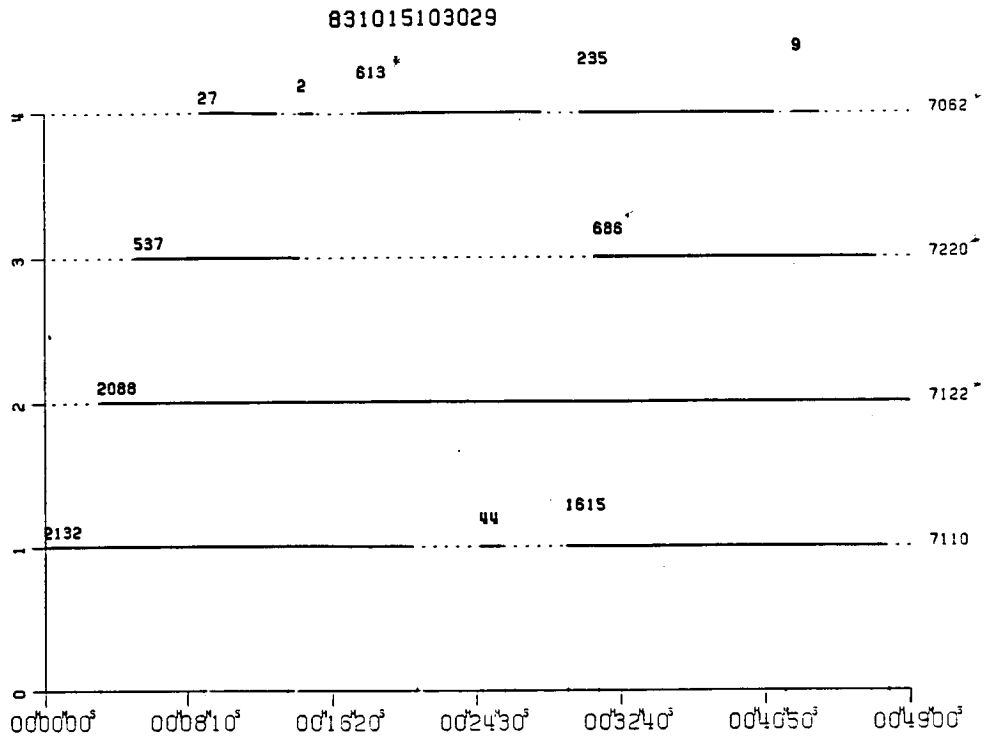

Fig. 13 (cont'd)

equations matrix that was used to estimate the coefficients of the least-squares Chebychev polynomial. The condition numbers missing from this table correspond to the stations whose actual ranges were used to generate both the SR and SRD observables. It is evident from this table that for some stations rejection of less than 10% of their observations reduces the RMS of the Chebychev residuals from unacceptable levels down to the expected accuracy of the observations. Furthermore, the large condition numbers associated with stations 7210 and 7121 are caused by the strong irregularities in the distribution of the data gaps. These strong irregularities usually occur when malfunction of the laser instrument has resulted in concentrated erroneous observations which in turn are rejected by the data-snooping procedure. For instance, the observations of stations 7210 and 7121 for the arcs shown in Fig. 15 are affected by four large gaps and one large gap respectively. The word large is used here in the sense that although the data gaps are usually shorter than 60 seconds they are still large as compared to the other gaps affecting the remaining observations.

Table 4. Monthly Precision Estimates (cm) for the American Stations (Chebychev Fitting/After Data Snooping)

	1983				1984									
Station ID	Sep.	Oct.	Nov.	Dec.	Jan.	Feb.	Mar.	Apr.	May	Jun.	Jul.	Aug.	Sep.	Oct.
7109	2.8	2.9	3.5	3.0	3.0	3.0	2.9	2.8	2.6	2.8	2.5	2.4	2.4	2.6
7110		3.9	3.8	3.8	3.7	3.7	3.8	3.6	3.0	3.1	2.7	2.4	2.4	2.5
7122	12.7	11.8	10.1	14.1	14.8	15.6	12.2		4.3	3.8		5.3	7.1	3.2
7105	3.4	3.4	3.2	5.3	4.8	3.9	4.4	3.1	2.8	2.7	2.5	2.5	2.5	2.9
7112	15.0	14.3	14.5	13.5		11.0	11.6	12.1	11.5	11.4	12.1	12.2	11.8	10.8
7086	16.7	13.2	6.4	7.1	6.5	6.9	7.0	7.4	7.1	6.8	7.1	6.9	7.9	9.4
7265					8.8	7.2	7.0							
7062	10.0	8.5												
7886											7.1	6.4	6.7	6.7
7220	8.3	8.4												
7210	4.7	4.8	5.4	5.0	5.4		4.1	4.5	4.7	3.3	4.1	3.1	2.9	2.9
7121	9.9	10.5	10.7	10.4	14.5	10.9	9.4	9.0	8.2	7.4	8.2	8.2	6.9	7.2
7907	14.0	14.8	14.4	14.7	14.4	12.8	15.4	15.7	14.5	14.3	14.6	14.4	14.9	14.7

ORIGINAL PAGE IS
OF POOR QUALITY

ORIGINAL PAGE IS
OF POOR QUALITY

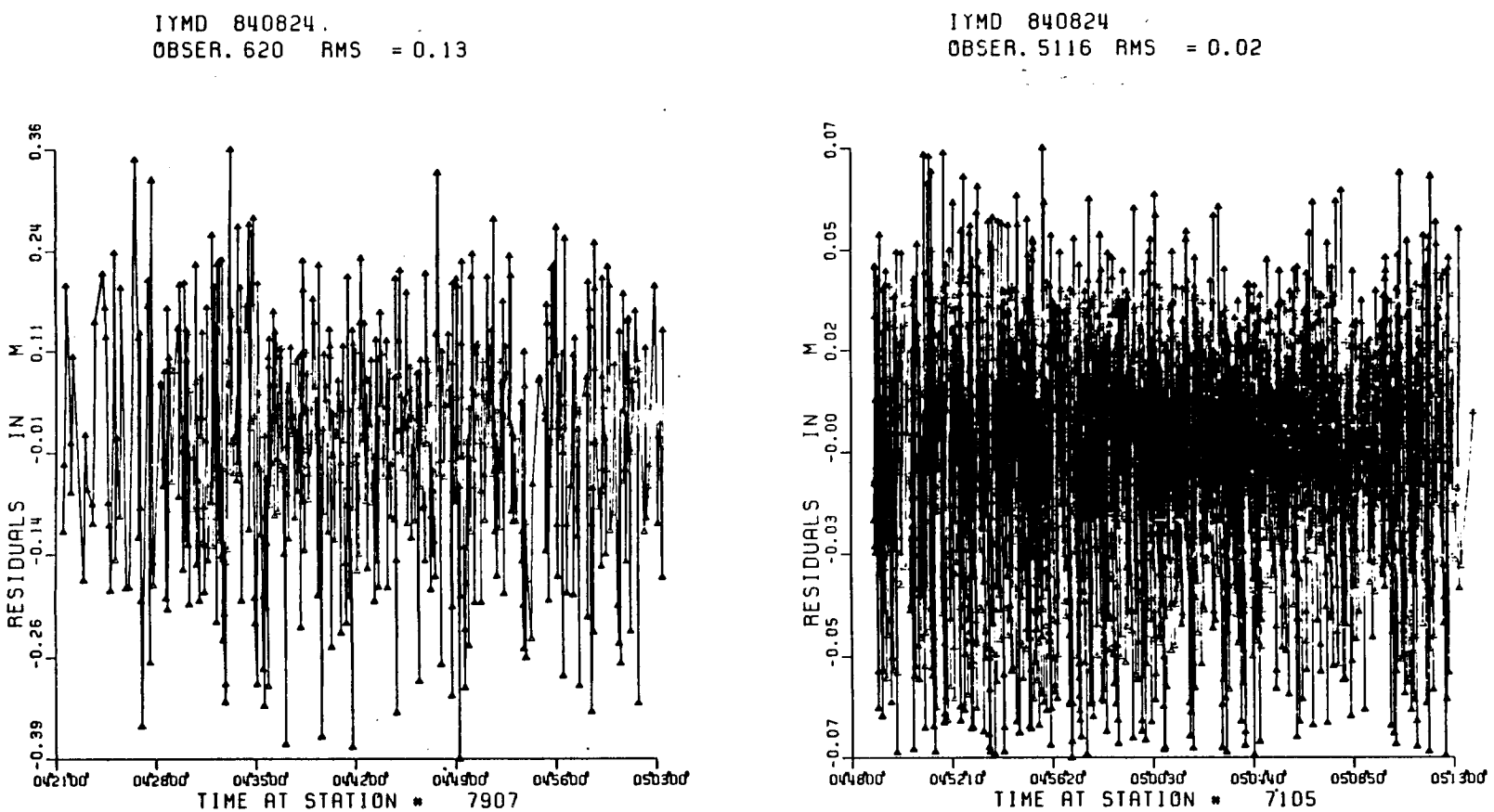

Fig. 14 Chebychev residuals for stations 7907, 7105, 7086, 7109, 7110, 7886 (after data snooping).

ORIGINAL PAGE IS
OF POOR QUALITY

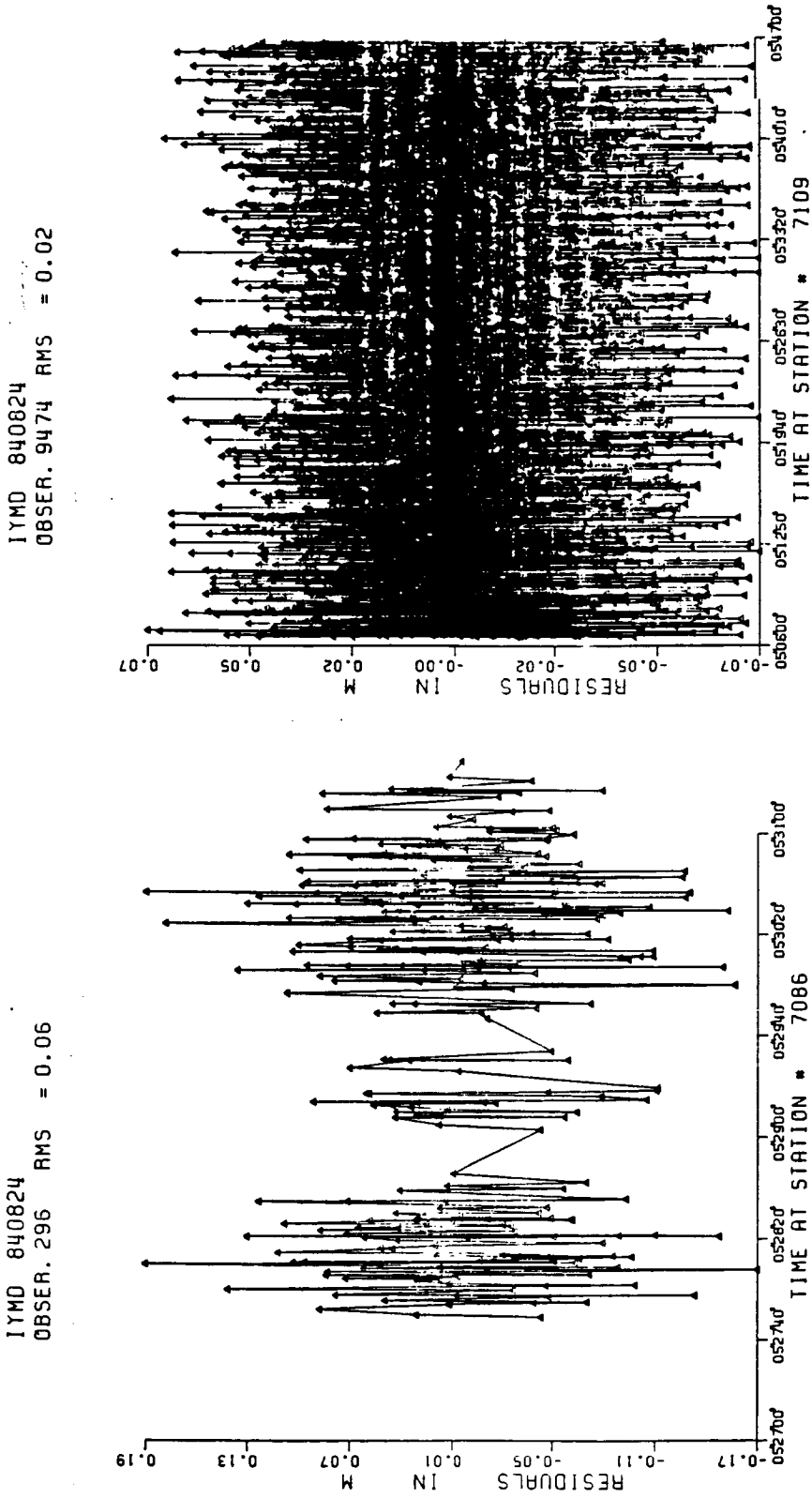

Fig. 14 (cont'd)

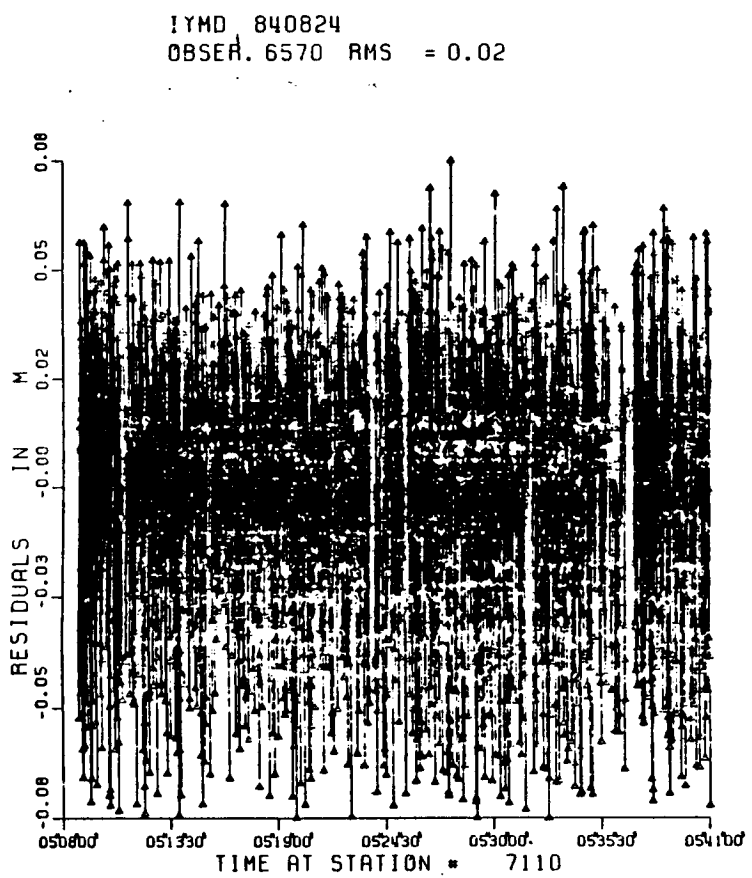
IYMD 840824
OBSER. 6570 RMS = 0.02
RESIDUALS IN M
0.08
0.05
0.02
-0.00
-0.03
-0.05
-0.08
05060d
05133d
05190d
05243d
05300d
05353d
05410d
TIME AT STATION * 7110

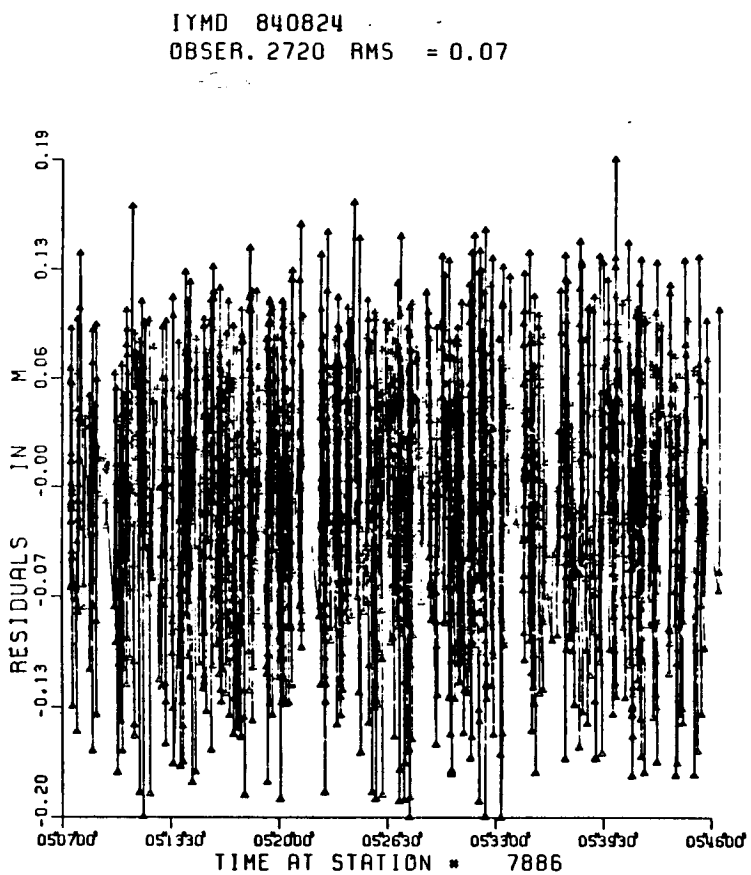
IYMD 840824
OBSER. 2720 RMS = 0.07
RESIDUALS IN M
0.19
0.13
0.06
-0.00
-0.07
-0.13
-0.20
05070d
05133d
05200d
05263d
05330d
05393d
05460d
TIME AT STATION * 7886

Fig. 14 (cont'd)

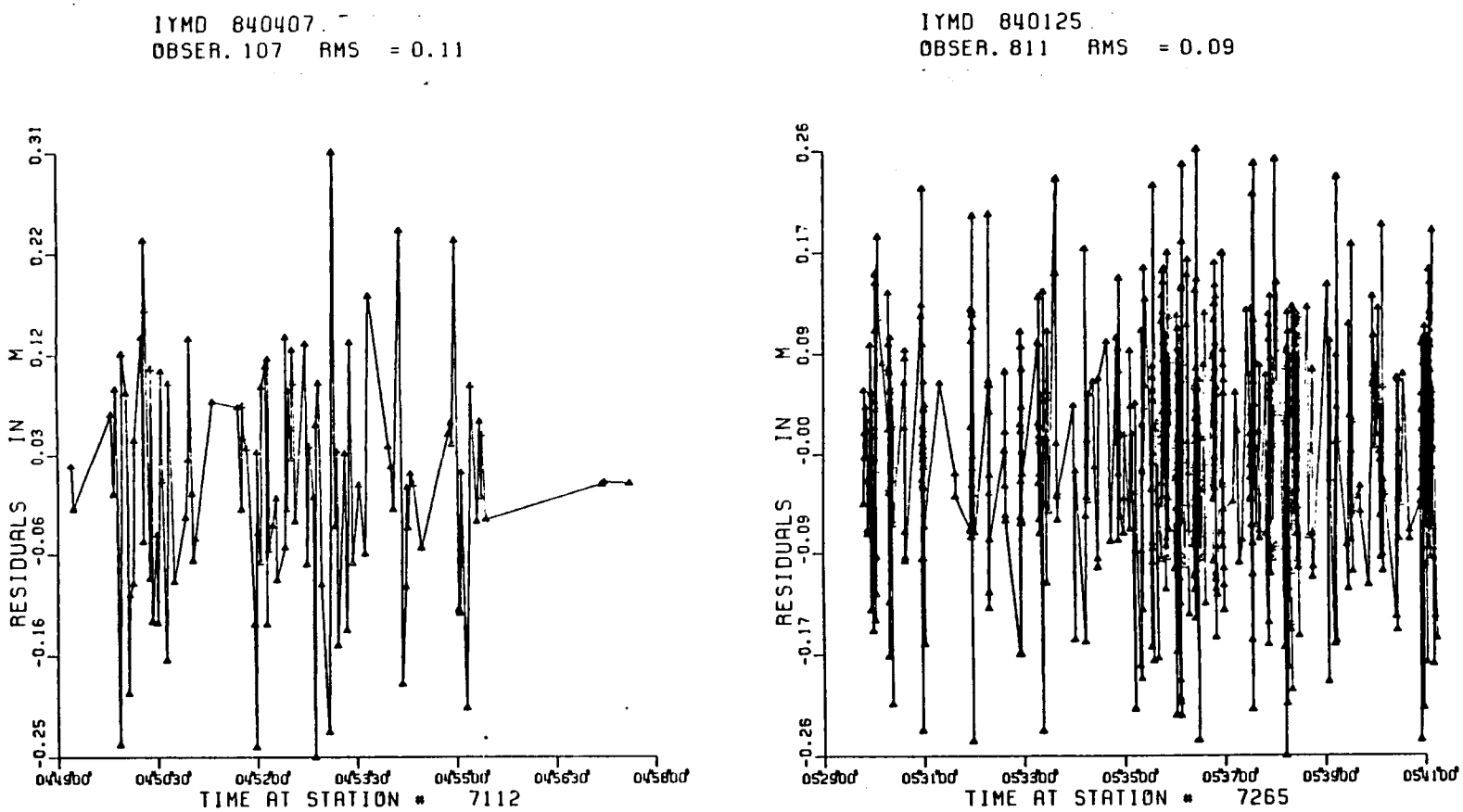

Fig. 15 Chebychev residuals for stations 7112, 7265, 7121, 7210, 7220, 7122, 7062 (after data snooping).

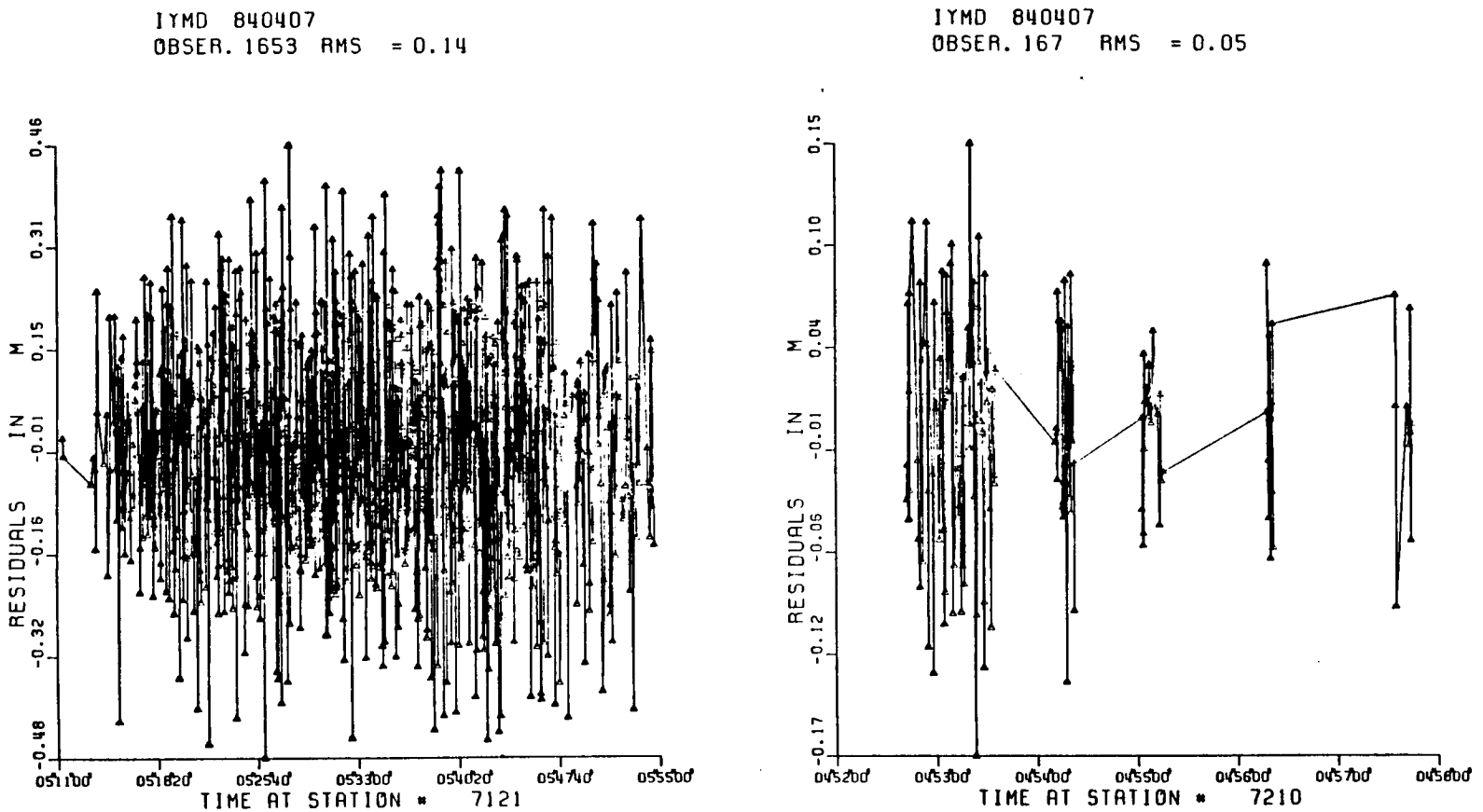
IYMD 840407
OBSER. 1653 RMS = 0.14
RESIDUALS IN M
0.46
0.31
0.15
-0.01
-0.16
-0.32
-0.48
05110d
05182d
05254d
05330d
05402d
05474d
05550d
TIME AT STATION * 7121
IYMD 840407
OBSER. 167 RMS = 0.05
RESIDUALS IN M
0.15
0.10
0.04
-0.01
-0.06
-0.12
-0.17
04520d
04530d
04540d
04550d
04560d
04570d
04580d
TIME AT STATION * 7210

Fig. 15 (cont'd)

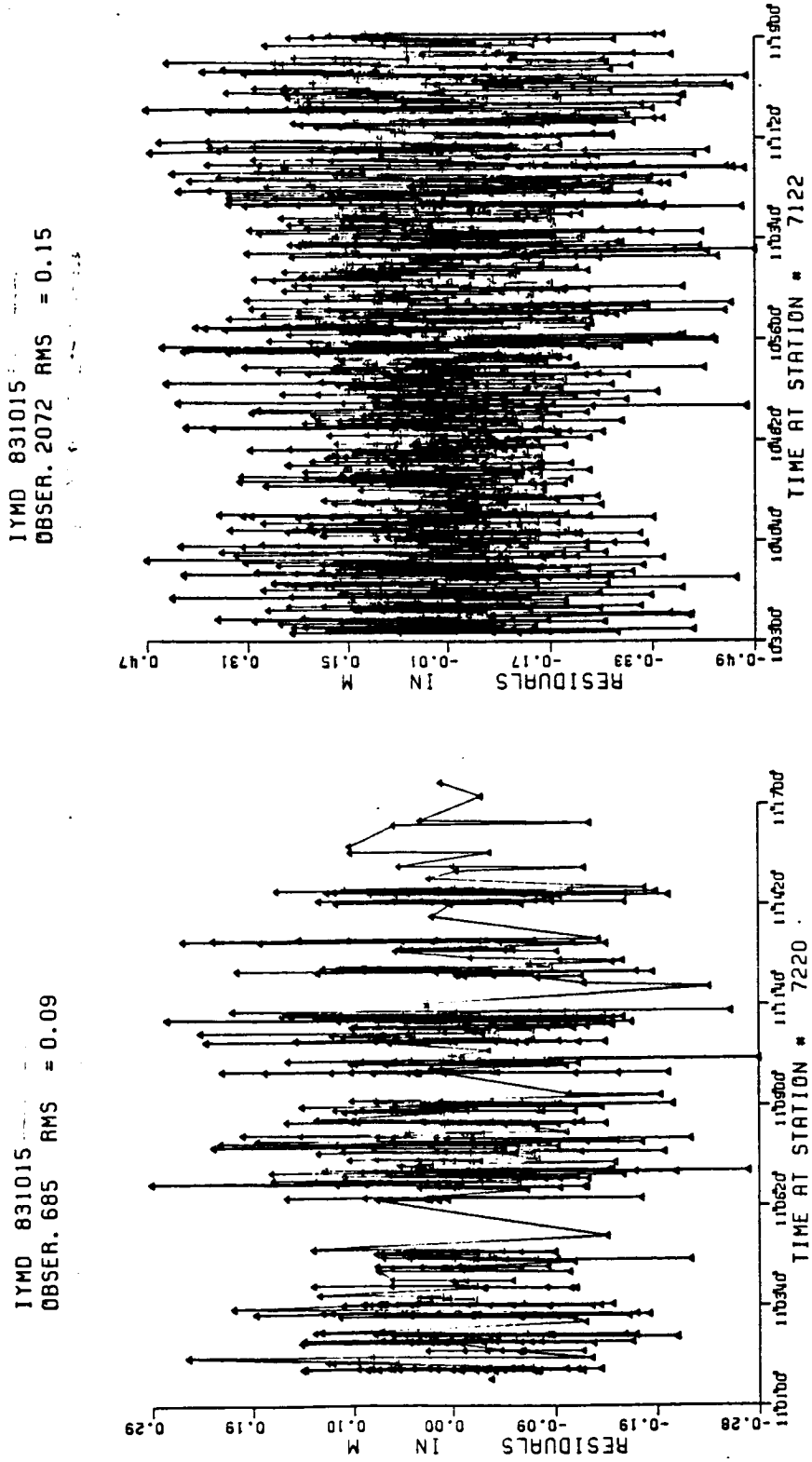

Fig. 15 (cont'd)

ORIGINAL PAGE IS
POOR QUALITY

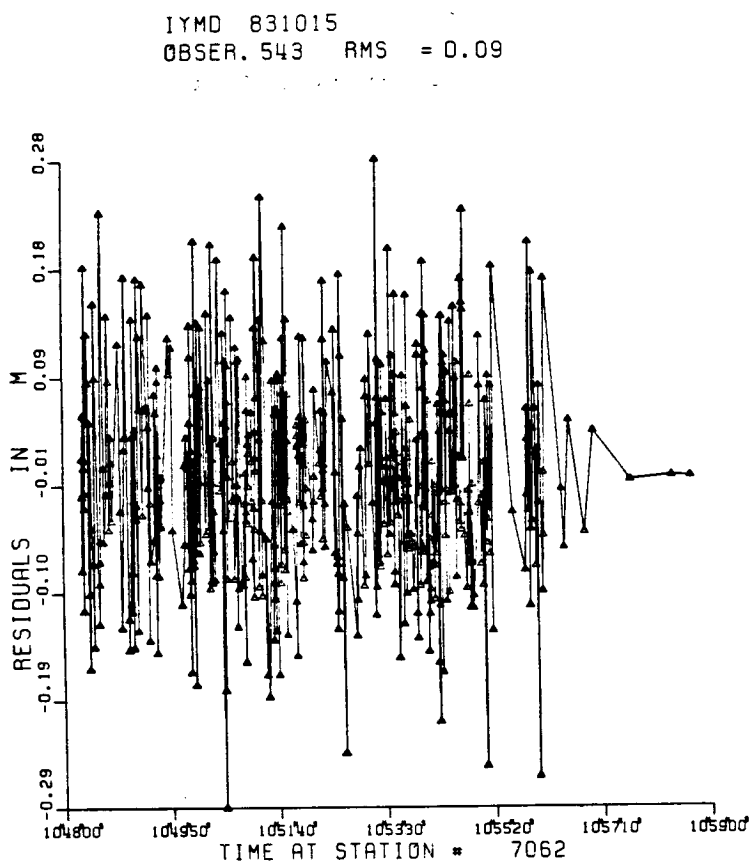

Fig. 15 (cont'd)

The large condition numbers, caused by the strong irregularities in the distribution of the gaps, might deteriorate the precision of the interpolated ranges since the number of the significant digits lost in the inversion of the normals is approximately equal to the base 10 logarithm of the condition number (Forsythe et al., 1967). Even if the numerical instability is not bad enough to affect the quality of the interpolated ranges there might still exist large approximation errors in the neighborhood of the large gaps. Therefore, it was decided to either reject those arcs or to break them down into several subarcs with even distribution of gaps (i.e., small condition number) provided that for each subarc there are enough available observations to be effectively interpolated.

Sufficient representation of a relatively large number of observations requires a high-degree Chebychev polynomial. Determination of its coefficients through a least-squares adjustment does not cause any numerical instability, as might have been expected,

ORIGINAL PAGE IS
OF POOR QUALITY

Table 5. Precision of Chebychev Interpolation (Before and After Data Snooping).

Station IDs	RMS before D.S.*(m)	No. of obs. before D.S.	RMS after D.S. (m)	No. of obs. after D.S.	Condition Number	Reference figures
7907	26.9	648	0.13	620	600	8, 14
7105	7.35	5314	0.02	5116	561	8, 14
7086	0.07	297	0.06	296	-	8, 14
7109	0.04	9611	0.02	9474	31	8, 14
7886	0.07	2720	0.07	2720	102	8, 14
7110	0.23	6681	0.02	6570	34	8, 14
7122	0.16	2088	0.15	2072	48	13, 15
7220	0.09	686	0.09	685	106	13, 15
7062	0.70	613	0.09	543	-	13, 15
7265	0.09	812	0.09	811	-	13, 15
7112	23.18	136	0.11	107	-	13, 15
7210	0.07	185	0.05	167	4249	13, 15
7121	15.88	1694	0.14	1653	1058	13, 15

*Data snooping

because of the near orthogonality properties of the Chebychev polynomials (see Section 3.5.2). For instance, to sufficiently represent 9474 observations of station 7109, a 22-degree Chebychev polynomial is required. In this case the condition number of the normals has a very small value (i.e., 31, from Table 5), and therefore numerical instability and ill-conditioning associated with large condition numbers (ibid.) are not a concern in spite of the fact that a high-degree Chebychev polynomial was used.

All the information acquired in regard to the interpolation of the laser ranges was implemented in the locally developed software that was subsequently used to generate the SR and SRD observables. With this software the passes containing arcs coobserved by two or more stations were identified and isolated together with the starting and ending epochs of each of the arcs involved. More specifically, for the MERIT Main Campaign there have been identified 536 such passes observed by the American stations shown in Fig. 12. For each of these passes the observations recorded within an arc by all of the stations involved were edited by using the data-snooping procedure and by taking into

consideration all of the necessary precautions in regard to the magnitude, the distribution of the gaps, and the resulting numerical instability. However, effective editing of the laser ranges requires knowledge of the degree of the Chebychev polynomial that would sufficiently represent the laser ranges recorded within any of the arcs involved. This is accomplished with the help of a statistical test which is explicitly outlined in Section 3.6.2. According to this test, any adjustment for which the hypothesis H_0 is rejected leads to another adjustment (see Section 3.6.2). To eliminate these additional adjustments, and therefore to reduce the computing time, it was decided to determine a priori the degree of Chebychev polynomials that sufficiently represent the observations of any of the stations involved in our study (see Fig. 12). Accordingly, if the number of available observations recorded by a specific station falls into a certain window then for that station an appropriate degree of the Chebychev polynomial is assigned (see Table 6). These degrees are predetermined for specified windows and for all of the stations involved on the basis of the actually observed ranges. Table 6 lists for prespecified windows and for all of the stations involved the degree of the Chebychev polynomials that sufficiently represent the ranges falling into any of those windows.

Next the software proceeds with the identification of the passes containing arcs that have been coobserved by four or more stations. For each of those passes the exact overlapping times of the arcs involved are identified and subsequently Simultaneous Ranges (SR) are generated along the guidelines described in Section 3.6. For instance, stations 7110, 7122 7220 and 7062 have arcs with quasi-simultaneous observations (see Fig. 16). It is obvious from Fig. 16 that quasi-simultaneity for all four stations occurs only in the intervals (bc) and (hi). The epochs b and c designate the starting and ending epochs of the first arc of station 7062, while the epochs h and i designate the starting epoch of the second arc and the ending epoch of the fourth arc of stations 7220 and 7062 respectively. Since station 7062 recorded the least number of observations for both arcs bc and hi respectively,

Table 6. Degree of Chebychev Polynomials.

No. of obs. / Station IDs	0 - 500	500 - 1000	1000 - 2000	2000 - 3000	3000 - 5000	5000 - 9000	> 9000
7907	16	17	17	18	19	21	22
7105	12	16	16	18	19	21	22
7086	12	17	17	18	19	21	22
7109	12	17	17	18	19	21	22
7886	12	13	15	17	17	21	22
7110	12	16	16	19	20	21	22
7122	14	19	19	20	21	21	22
7220	11	11	14	14	16	21	22
7062	16	18	18	19	19	21	22
7265	11	13	15	18	19	21	22
7112	14	19	19	20	21	21	22
7210	11	19	19	20	21	21	22
7121	14	19	19	20	21	21	22

the four station events (i.e., exact simultaneous observations from four stations) for these two arcs were generated by interpolating all the available observations from the corresponding arcs of stations 7110, 7122 and 7220 respectively. Although in Fig. 16 we have only four-station arc overlaps, there may exist arc overlaps including five, six or even seven stations. In such cases all possible seven-, six-, five- or four-station events are generated, provided that any duplication that may occur is to be avoided.

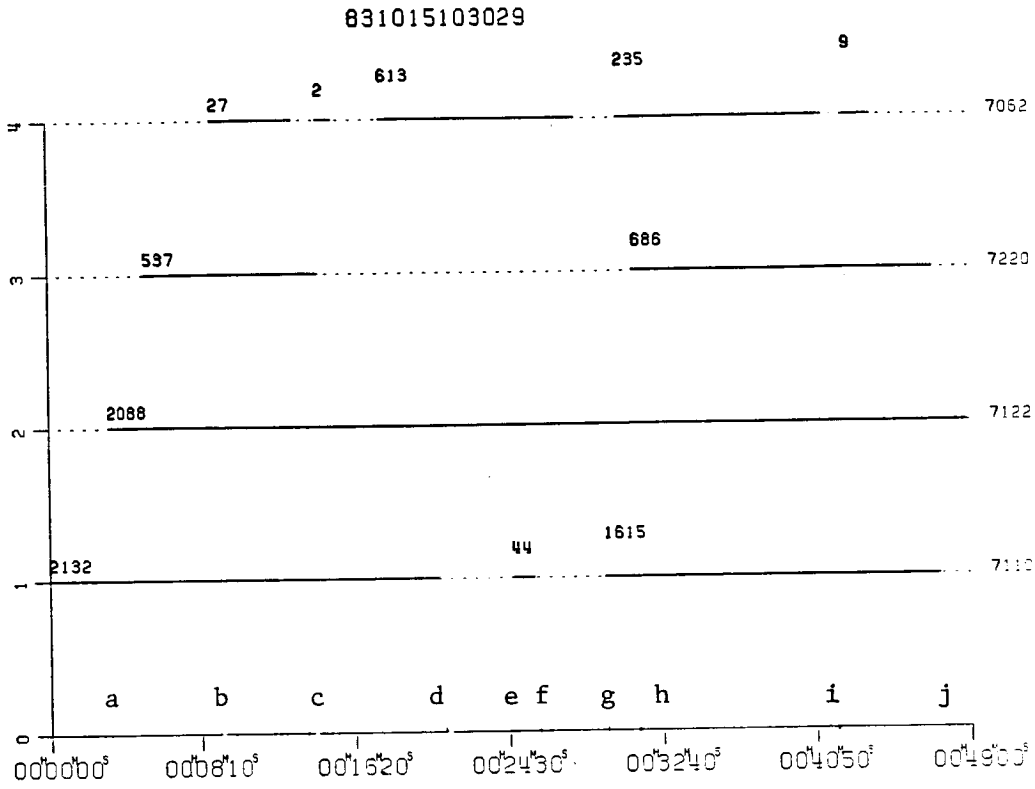

Fig. 16 Arc overlap of a Lageos pass involving four American stations.

Finally all the passes with quasi-simultaneous observations from two or more stations were employed to generate the SRD observables. For instance, the station pair 7122-7110 shown in Fig. 16 has quasi-simultaneous observations for the intervals (ad), (ef) and (gj) respectively (see Fig. 16). For the first interval (ad) the SRD observables are generated by interpolating the observations of the first arc of station 7110 at the observing epochs of station 7122, while for the intervals (ef) and (gj) the SRD observables are generated by interpolating all the available observations of station 7122. Thus, having all possible four-, five-, six- and seven-station events together with all possible SRD's, the baselines are estimated through the geometric and SRD methods respectively. This is the subject of the next chapter.

ORIGINAL PAGE IS
OF POOR QUALITY

Chapter 4

BASELINE ESTIMATION

4.1 BASELINE ESTIMABILITY

Baseline estimability in connection with satellite geodesy is very closely related to the concept of estimable parameters. In fact, if optimum geometric configurations are fulfilled and enough observations are available, the baselines can be estimated with a precision compatible to that of the observations. This is possible only because the baselines form a set of estimable parameters. This is true for both the range geometric mode and the SRD semidynamic/dynamic mode methods. In general, baselines estimated through either geometric or dynamic mode methods are estimable only if through the appropriate adoption of the necessary constants and units the scale is implied by the measurement system being employed. In such cases the baselines estimated with a dynamic mode method are referred to as best estimable parameters. The use of this term is justified since out of all possible estimable parameters associated with either semidynamic or dynamic mode methods, the baselines are recovered with substantially reduced a posteriori variances (i.e., an order of magnitude) (Van Gelder, 1978).

4.2 STEADY STATE RESPONSE OF THE GEOMETRIC AND SRD METHODS

The nature of as well as the spatial and temporal distribution of the available observations quantify the inherently present information for each of the estimable parameters involved (Sections 2.2, 4.3 and 4.4).

The process of recovering estimable quantities from any given set of observations is referred to as an inversion process. This process is effectively realized via an estimation method such as a least squares adjustment (Sections 2.1.2 and 2.2.6). The available set of observations

forms the input to the inversion process, while the recovered estimable quantities constitute the response (i.e., the output) of this process to the given set of observations.

Different inversion processes have different responses to a specific set of observations and adjusted quantities. Nevertheless, as far as satellite geodesy is concerned, these responses cannot be meaningfully differentiated in the light of the current observational distribution and accuracy.

The steady state response of an estimation method has been reached if extension of its input with additional observations does not contribute any additional information to the estimable quantities being recovered. In the present study, steady state responses of both the geometric and the SRD methods is sought through the extension of their input with more and more observations. This process continues up to that point where additional observations do not affect the recovered baselines beyond the level of accuracy implied by the sophistication of the models employed and by the accuracy of the available observations. With the assumption that the accuracy of the baselines, recovered from laser range observations collected during the Main MERIT Campaign, cannot exceed the 1 cm level, the steady state response of both the SRD and the geometric methods is said to have been reached if additional observations do not affect the recovered baselines at the 1 cm accuracy level. Furthermore, we refer to "steady state response of the SRD method" if the input observables are the dynamically modeled SRD observables, while we refer to "steady state response of the geometric method" if the input observables are the geometrically modeled simultaneous ranges (see Chapter 2).

In many circumstances the steady state response of either the geometric or the SRD methods may not be possible because their response either diverges or oscillates. Such a response, however, can be reached if the geometric and/or physical characteristics of either the geometric or the SRD methods are changed accordingly.

In the geometric method, for instance, near singularity cases (Section 2.1.3) result in an extremely ill-conditioned normal equation matrix which in turn leads to a divergent response. Divergence is reversed to convergence if the input of the geometric method is extended to include more and more observations collected by stations located well away from the critical surfaces and the critical curves (Blaha, 1971). However, if the distribution and number of available observations is not good enough to warrant a steady state response, then such a response can be reached via the implementation of appropriately chosen constraints. This is accomplished either by constraining baselines in the geometric method (Section 4.3.2) or by increasing the lengths of continuous integration in the SRD method (Section 4.4.2).

Increasing the length of continuous integration in the implementation of the SRD method results in a "faster" steady state response in regard to baseline estimation. The term "faster" is used to indicate that the steady state response of the SRD method is reached on the basis of a substantially reduced number of observations compared to those needed to reach this steady state response via the short arc solutions (Section 4.4). This is the result of the geometric strength implied by the long integration periods and manifested in the reduced order of the normal equation matrix and in the larger values of its corresponding diagonal elements.

Long integration periods constitute a potential source of "instability" of the normal equation matrix. The term "instability" is used to express the existence of high correlations among the adjusted parameters. High correlations (greater than .99) raise the warning flag of ill-conditioning of the normal equation matrix and a possible divergent response of the SRD method. Employing long integration periods independently of what the baseline pass geometry is, the state vectors of the passes that are days away from the corresponding adjusted initial state vector are largely insensitive to that initial state vector. Therefore, for those passes there exists a tendency for linear dependence among the corresponding columms of the state transition

matrix Y*(t) (equation 2-63). This tendency further contributes to the instability of the normal equation matrix. The instability of the normal equation matrix gets even worse when single long baselines (longer than about 4000 km) are estimated via the SRD method. For those baselines there is a tendency for the coobserved passes to concentrate in the areas between the end points of the baseline (Section 4.4.1).

With the weather-dependent laser range observations it is very likely that the stations consitituting the end points of the estimated baseline have coobserved only one pass falling within a specific integration period. Under these circumstances the length of continuous integration will be reduced to that of the duration of one single pass which lasts about one hour for the Lageos satellite. Such short integration lengths implemented in the same solution with integration lengths of up to one week (Section 4.4) constitute a potential source of instability because of the resulting inhomogeneity in the structure of the normal equation matrix. In the design matrix, this inhomogeneity manifests itself by the many zero entries affecting the columns associated with the initial state vectors of those short arcs. Therefore, care should be exercised to avoid extreme circumstances that may result in an algorithmically singular normal equation matrix (Section 4.4.2). This can be avoided either by employing homogeneous integration lengths and/or by incorporating in the same SRD solution observations from many stations. This would improve the stability of the normals because of the strength implied by the geometry of the additional observations. This, however, is true only if four or more stations are involved since as it was mentioned in Section 2.1.3, at least four stations and six targets are generally necessary for a nonsingular range geometric solution. Therefore, in the single baseline solutions the stability of the normals is mainly controlled by the constraint imposed on the satellite to move along a six-parameter orbit (Chapter 2).

In the present study only single baseline solutions via the SRD method have been performed. This was decided upon because, for moderate baseline lengths (<3500 km), the single SRD baseline solutions seem to be simple, fast and very accurate.

The maximum length of continuous integration in the implementation of the SRD method should be chosen not only to assure the steady state response of the SRD method but also to warranty minimum propagation of the accumulated residual orbital biases into the recovered baselines. These biases are the ones not eliminated by the nature of the SRD observables which reduces substantially the accumulated orbital biases with an almost total cancellation of the accumulated radial biases (Pavlis, 1982). Consequently, the choice of the integration lengths is limited only to those which result in an a posteriori standard deviation of unit weight the value of which is close to unity. Thus, in seeking the steady state response of the SRD method we start out with short arc solutions. If with short arc solutions the available observations are not enough to warranty a steady state response, the integration lengths are steadily increased up to those resulting in a steady state response. If the a posteriori standard deviation of unit weight approaches unity before such a response has been reached, then the corresponding baseline is not estimated. However, any integration lengths leading to a steady state response will be adopted even if the a posteriori standard deviation of unit weight is smaller than one. This simply means that the baselines via the SRD method are estimated on the basis of the minimally required integration lengths.

The effectiveness of the a posteriori standard deviation of unit weight to control the maximum length of continuous integation in the single SRD baseline estimation depends heavily on the assumption of having weighted the observations properly. This assumption has been elaborated on and it has also been well justified in Chapter 3.

4.3 BASELINE ESTIMATION VIA THE STEADY STATE RESPONSE OF THE GEOMETRIC METHOD

In the absence of ill-conditioning that may result from nearly critical configurations, the steady state response of the geometric method will be reached if a large enough number of observations is available. This is a consequence of the fact that the weight coefficient matrix ($Q_{\hat{X}}$) of the adjusted parameter vector "improves" as additional observations are

incorporated into the geometric solution (Blaha, 1971). The term "improves" is used to indicate that with the same adjusted parameter vector the matrix $(Q_{\hat{X}} - Q_{\hat{X}}^{a})$ is a positive (semi) definite matrix where $(Q_{\hat{X}})$ and $(Q_{\hat{X}}^{a})$ denote the weight coefficient matrices of the adjusted parameter vector before and after the inclusion of additional observations. Since $(Q_{\hat{X}} - Q_{\hat{X}}^{a})$ is a positive (semi)definite matrix, it follows that (ibid.)

$$\mathrm{Tr}\ (Q_{\hat{X}}^{a}) \leq \mathrm{Tr}\ (Q_{\hat{X}}) \qquad (4\text{-}1)$$

indicating that the precision of the adjusted parameters improves only if the additional observations are drawn from the same population, thereby making it possible to assume that the a priori variance of unit weight is the same for both solutions and it is equal to one. Since the mathematical model employed in the minimum constraint geometric adjustments is an almost error free model, the a posteriori variance of unit weight tends towards one at the steady state. If these a posteriori variances of unit weight are very close to unity so they preserve the relative structure of the weight coefficient matrices of eq. (4-1), the a posteriori variance of the adjusted parameters decreases. In the geometric mode adjustments, the adjusted parameters are the Cartesian coordinates of the ground stations.

In the present study we are particularly interested in estimating baseline lengths and therefore the a posteriori variances of the Cartesian coordinates have been mapped back into the estimated baselines. As the a posteriori variance of the estimated Cartesian coordinates improves with the incorporation of additional observations, the a posteriori variance of the estimated baselines will also improve only if the nonlinearity of the model employed allow such an improvement to take place. Therefore, by including additional observations into the geometric solutions a point will be reached where the estimated baseline length will not change beyond the 1 cm level.

It turns out that before reaching the steady state, the a posteriori standard deviations of the estimated baselines do not reflect the change of their length as additional observations are incorporated into the

solution. For instance, it is possible for an estimated baseline, the a posteriori standard deviation of which is 5 cm, to change its length by as much as 76 cm with the incorporation of additional observations (Table 8, baseline 7110-7122). This means that before reaching the steady state response, the a posteriori standard deviations of the estimated baselines do not reflect their accuracy but rather they indicate how far away the solution is from its steady state. If, however, the steady state response has been reached, the corresponding a posteriori standard deviations assume millimeter-level values (Table 8). Therefore, in the present study the a posteriori standard deviation of the estimated baselines are used only as indicators showing whether or not the steady state response has been reached. Successful utilization of these indicators assumes close to unity a posteriori variances of unit weight so they preserve the relative structure of the weight coefficient matrices of the recovered parameters as additional observations are incorporated into the solution (eq. 4-1).

If steady state has been reached, it is furthermore assumed that the corresponding baseline has been determined at the 1 cm accuracy level. This is well justified only if the following three assumptions are fulfilled: (1) the motion of the observing stations has been properly modeled for the time span of the observations, (2) the steady state response implies strong geometry, and (3) the accuracy of the available observations allows recovery of the baselines at the 1 cm level (see Section 4.2). As of the geometric modeling itself, the only errors affecting it arise from using the three-dimensional Euclidean space formulation rather than the four-dimensional post-Newtonian formalism (Moyer, 1971; Bjerhammar, 1985) which of course does not affect the estimated baselines at the 1 cm level (Moritz, 1979).

4.3.1 Geometric Strength of the Available Observations

In the geometric approach the observed satellite positions are treated as auxiliary independent points in space (see Section 2.1); therefore the strength of any minimum constraint geometric solution depends entirely on the geometric strength implied by both the amount and the distribution of the available observations. Thus, any meaningful

interpretation of the results obtained in geometric mode adjustments should be preceded by an analysis aiming to assess the strength of the geometry involved in each of those adjustments.

The analysis of the geometry involved in the geometric adjustments, presented later in this section, is based on the examination of Table 7. The first column of this table lists the ID of the stations involved, the second, third and fourth columns contain the number of observations per station when all the simultaneous events from Sept. 1983 to May 1984, from Sept. 1983 to Aug. 1984, and from Sept. 1983 to Oct. 1984 are considered respectively. The bottom part of the second and third columns contain the total number of observations, the degrees of freedom and the a posteriori variance of unit weight obtained from minimum constraint solutions on the basis of the data shown in the corresponding column. The bottom part of the third column contains the same information for two types of solutions, one minimum constraint and one overconstraint obtained using the data listed in that column.

The geometric strength in each of the above solutions is primarily drawn from the stations having the most observations. In assessing this strength we assume that stations 7886 and 7220 coincide with stations 7109 and 7110 because they are 8 m and 15 m away from each other. With this in mind it can be easily deduced from Table 7 that 86% of the available observations has been recorded by stations 7105, 7109, 7110 and 7122. A geometric solution, the strength of which is primarily drawn from four stations, tends to be sensitive to how close these stations are from their best fitting plane (Blaha, 1971) because with stations close to forming a plane six are needed for a nonsingular space range network (see Section 2.1.3). Thus, when six or more stations are involved the solutions are not sensitive to the closeness of those stations from the best fitting plane.

In the geometric solutions shown in Table 7 the additional 11% of the available observations has been recorded by stations 7112, 7086 and 7265. Therefore, 97% of the observations has been recorded by seven stations. The existence of these three additional stations reduces the sensitivity of the solutions to how close stations 7105, 7109, 7110 and

Table 7 Global Statistics of the Geometric Adjustments

Station ID	No. of Observations[1]		
	Sep 83 - May 84	Sep 83 - Aug 84	Sep 83 - Oct 84
7105	7143	18990	19214
7109	10198	22784	23936
7112	2884	3467	3467
7122	10996	11284	12212
7220	1969	1969	1969
7110	11549	24200	25352
7062	841	841	841
7086	1412	4400	4624
7907	176	245	245
7082	299	299	299
7210	712	756	1684
7265	4395	4395	4395
7886	—	11859	11859
	N = 52574 DF = 14519 σ_0^2 = 1.18	N = 105489 DF = 29478 σ_0^2 = 1.03	N = 110097 DF = 30630 σ_0^2 = 1.03 DF = 30631[2] σ_0^2 = 1.05[2]

(1) Minimum constraint solution, coordinates fixed[3]: X,Y,Z for 7109; X,Y for 7122; Z for 7105.
(2) Overconstraint solution, coordinates fixed[3]: X,Y,Z for 7109; X,Y,Z for 7122; Z for 7105.
(3) Coordinates fixed to those of (CSR)85L01 (Section 4.4.2)

N = total number of observations
DF = degrees of freedom
σ_0^2 = a posteriori variance of unit weight

7122 are from their best fitting plane. The remaining four stations, 7062, 7907, 7082 and 7210, have contributed only the last 3% of the available observations. Therefore, their contribution to the geometric strength is very minor as compared to that of the previous stations.

Next we assume that stations 7112, 7086 and 7265, which contribute the 11% of the available observations, make the geometric adjustments insensitive to how close stations 7105, 7109, 7110 and 7122 are from their best fitting plane. Even if this were true, the strength of the geometric solutions tends to still be weak because the stations that have

Table 8 Baseline Steady State Response of the Geometric Solution

Baseline	No. of Observ.	Correlation ≥ 0.80	Length (m)	Data Set [1]	Solution Type [2]
7109-7110	9,186	None	883601.637 ± 0.02	A	1
	21,772	"	.608 ± 0.02	B	1
	22,924	"	.661 ± 0.02	C	1
	"	"	883601.661 ± 0.02	C	2
	"	"	883602.245 ± 0.009	C	3
7109-7265	3,363	"	627043.412 ± 0.02	A	1
	"	"	.452 ± 0.01	B	1
	"	"	.535 ± 0.01	C	1
	"	"	.535 ± 0.01	C	2
	"	"	.988 ± 0.005	C	3
7109-7886	11,859	None	7.746 ± 0.002	B	1
	"	"	.746 "	C	1
	"	"	.746 "	C	2
	"	"	.746 "	C	3
7109-7122	8,644	None	2280712.335 ± 0.07	A	1
	8,932	"	2.700 ± 0.05	B	1
	9,860	"	3.188 ± 0.05	C	1
	"	"	3.188 ± 0.05	C	2
	"	"	4.949 ± 0.0005	C	3
7110-7122	10,060	$\rho_{Z_F Z_S}$=0.998	1437137.428 ± 0.05	A	1
	10,348	"	.780 ± 0.04	B	1
	11,276	"	8.187 ± 0.03	C	1
	"	$\rho_{X_F X_S}$=0.996	8.187 ± 0.03	C	2
	"	None	9.288 ± 0.009	C	3
7110-7220	1,576	$\rho_{X_F X_S}$=0.801 $\rho_{Y_F Y_S}$=0.990 $\rho_{Z_F Z_S}$=0.998	15.225 ± 0.006	A	1
	"	$\rho_{Y_F Y_S}$=0.987 $\rho_{Z_F Z_S}$=0.998	.221 ± 0.005	B	1
	"	$\rho_{Y_F Y_S}$=0.981 $\rho_{Z_F Z_S}$=0.997	.218 ± 0.005	C	1
	"	$\rho_{X_F X_S}$=0.997 $\rho_{Y_F Y_S}$=0.975 $\rho_{Z_F Z_S}$=0.800	.218 ± 0.005	C	2
	"	$\rho_{Y_F Y_S}$=0.965	.208 ± 0.005	C	3
7110-7265	3,866	$\rho_{Y_F Y_S}$=0.91 $\rho_{Z_F Z_S}$=0.996	274069.453 ± 0.01	A	1
	"	$\rho_{Y_F Y_S}$=0.887 $\rho_{Z_F Z_S}$=0.995	.383 ± 0.008	B	1
	"	$\rho_{Y_F Y_S}$=0.850 $\rho_{Z_F Z_S}$=0.994	.355 ± 0.008	C	1
	"	$\rho_{X_F X_S}$=0.994	.355 ± 0.008	C	2
	"	None	.474 ± 0.007	C	3

Table 8 (cont'd)

Baseline	No. of Observ.	Correlation > 0.80	Length (m)	Data Set [1]	Solution Type [2]
7110–7886	11,859	None	883605.698 ± 0.02	B	1
	"	"	.751 ± 0.02	C	1
	"	"	.751 ± 0.02	C	2
	"	"	6.335 ± 0.009	C	3
7122–7265	4,184	$\rho_{Z_F Z_S}$=0.995	1663980.848 ± 0.05	A	1
	"	=0.994	1.161 ± 0.04	B	1
	"	=0.993	1.555 ± 0.04	C	1
	"	$\rho_{X_F X_S}$=0.993	1.555 "	C	2
	"	None	2.823 ± 0.005	C	3
7122–7886	0	None	2280718.021 ± 0.05	B	1
	0	"	.509 ± 0.05	C	1
	0	"	18.509 ± 0.05	C	2
	0	"	20.269 ± 0.002	C	3
7220–7265	0	$\rho_{Y_F Y_S}$=0.90 $\rho_{Z_F Z_S}$=0.994	274066.158 ± 0.010	A	1
	0	$\rho_{Y_F Y_S}$=0.874 $\rho_{Z_F Z_S}$=0.993	.090 ± 0.009	B	1
	0	$\rho_{Y_F Y_S}$=0.833 $\rho_{Z_F Z_S}$=0.991	.064 ± 0.008	C	1
	0	$\rho_{X_F X_S}$=0.991	.064 ± 0.008	C	2
	0	None	.189 ± 0.007	C	3
7265–7886	0	None	627048.351 ± 0.01	B	1
	0	"	.434 ± 0.01	C	1
	0	"	.434 ± 0.01	C	2
	0	"	.887 ± 0.006	C	3

[1] Data Sets: A Sep 83 – May 84
B Sep 83 – Aug 84
C Sep 83 – Oct 84

[2] Solution Type:
1 Minimum constraint solution, Cartesian coordinates fixed: X,Y,Z for 7109; X,Y for 7122; Z for 7105

2 Minimum constraint solution, Cartesian coordinates fixed: X,Y,Z for 7109; Y,Z for 7122; Z for 7105

3 Overconstraint solution, Cartesian coordinates fixed: X,Y,Z for 7109 and 7122; Z for 7105

recorded the 91% of the observations (i.e., 7105, 7109, 7122, 7220, 7110, 7062, 7265 and 7886) are concentrated around two intersecting lines defined by station 7109 with 7122 and 7122 with 7105 (see Fig. 8). Since

two intersecting lines belong in the family of second-order curves, it is reasonable to expect that near singularity B (Section 2.1.3) tends to weaken the strength of those solutions. If we furthermore assume that the 9% of the observations recorded by stations 7082, 7086, 7112, 7907 and 7210 which are located well away from these two intersecting lines, make the geometric solutions insensitive to the previously mentioned near singularity B, it is still possible that near singlarity C might be present. This is a consequence of employing a network of relatively large extent. With such a network the simultaneously observed satellite positions tend to concentrate on the area extended above the middle part of the network and therefore to be closer to a plane. This in turn would lead to near singularity C because off-plane targets are needed to avoid this type of singularity (Section 2.1.3).

It is evident from the above discussion that the geometric strength implied by the available observations is relatively weak. Therefore the minimum constraint geometric solutions will be strongly influenced by the distribution of the available observations thereby making it difficult to recover the relative geometry of the ground stations (next section).

4.3.2 Baseline Results

On the basis of the data listed in the last three columns of Table 7, we have performed five least squares geometric mode adjustments. Four of these adjustments are based on minimum constraints, and the fifth is based on constraining one additional Cartesian coordinate than those required for a minimum constraint solution. More specifically, the first three minimum constraint geometric adjustments have been obtained by using all the events from Sept. 1983 to May 1984, from Sept. 1983 to Aug. 1984 and from Sept. 1983 to Oct. 1984. An event occurs when four or more stations observe the same satellite position. In these three adjustments, the same mimimum constraints have been used as they are implied by fixing the X,Y,Z Cartesian coordinates of station 7109, the X and Y coordinates of station 7122, and the Z coordinate of station 7105. The fourth adjustment was obtained by using all the available events and by fixing the Y and Z rather than X and Y coordinates of station

7122. This adjustment was necessary to confirm further the weakness of the geometry that seriously affects the minimum constraint geometric solutions. Finally, the overconstraint solution performed on the basis of the data listed in the fourth column of Table 7 was necessary to reach the steady state response for longer baselines. The results for all of the adjustments decribed above are listed in Tables 7 and 8. Table 8 contains for each baseline and for all of the solutions performed the number of observations per baseline, the correlations that are greater than or equal to 0.80 and the estimated baseline lengths followed by their a posteriori standard deviations. Out of all of the estimated baselines, only those are listed for which the a posteriori standard deviations in the overconstraint solution have reached the millimeter level. The symbol $\rho_{Z_F Z_S}$, in Table 8, designates the correlation between the Z coordinate of the first (F) station and the Z coordinate of the second (S) station of the corresponding baseline.

A close inspection of the minimum constraint solutions clearly reveals that the estimated baselines whose a posteriori standard deviation is at the centimeter level change their length by as much as 70 cm to 80 cm when additional observations are incorporated into the solutions (baselines 7110-7122 and 7122-7265). The number of additional observations incorporated in each solution as compared to the previous one is easily deduced from the information given in Table 7 for each one of those solutions.

The baselines whose length is smaller than 1000 km change their length to within -10 cm to 12 cm with a tendency of positive increase. This positive increase, which is clearly pronounced for the longer baselines (7110-7122 and 7122-7265) takes place toward the correct length of the corresponding baselines. This is easily seen by comparing these lengths with the ones obtained in the overconstraint adjustment (i.e., Solution C 3). The fact that the lengths of the baselines, which have been estimated at millimeter precision level via the overconstraint adjustment are very close to their true lengths is elaborated on at the end of this section, and it has also been confirmed by comparing their lengths with those obtained via the SRD method as well as with those

computed by other computational centers such as CSR and ZIPE via dynamic long-arc solutions (see next section).

The geometry implied by the number and the distribution of the available observations manifests itself in the minimum constraint solutions shown in Table 8. This geometry is not strong enough to warrant a steady state response since all the baselines but 7110-7220 and 7109-7886 change their length by several centimeters with the incorporation of additional observations. The existence of weak geometry is the result of the expected near singularities described in the previous section. This weak geometry is also confirmed by the high correlations prevailing among the station coordinates that were not constrained in the implementation of the minimum constraint solutions. This weakness is further confirmed by using all the available events from Sept. 1983 to Oct. 1984 and by changing the minimum constraints from (1) to (2) (Table 8). In solution (2) the correlations prevail among the X coordinates of the stations for which the correlations in solution (1) were high among their Z coordinates. It is interesting to note that the correlations among the X coordinates in solution (2) are almost the same as those among the corresponding Z coordinates of solution (1). This is the result of fixing the X and Y coordinates of station 7122 in solution (1) and the Y and Z coordinates of the same station in solution (2). The reduction of the correlations among the Y coordinates of the corresponding stations from (1) to (2) simply reveals that the minimum constraints (2) have better stability characteristics than those of minimum constraint (1).

The correlations among the coordinates of station 7110 and 7220 are also high because these stations are very close to each other, about 15 m apart. This, in light of weak geometry, makes their separation difficult thereby bringing the corresponding correlations to high levels. The correlations among the coordinates of station 7886 and the coordinates of all of the other stations involved are small because 7886 is only about 8 m away from 7109 which was held fixed in the implementation of both solutions (1) and (2). The estimated baseline lengths and their a posteriori standard deviations remained of course

the same for both solutions because the baselines are invariant quantities under any minimum consraints and as such their estimated lengths together with their variances should not change from one minimum constraint solution to the next.

The above discussion evidently reveals that the geometry implied by all of the simultaneously observed satellite positions is weak thereby making the minimum constraint solutions susceptible to the distribution of the available observations. For reasons mentioned in the previous section, the simultaneously observed satellite positions tend to concentrate on the area extended above the middle part of the employed network (see Fig. 12). This observational coverage together with the weak geometry will imply, via the minimum constraint solutions, a range space network with a tendency to shrink towards its center and more specifically towards the area where most of the available observations are concentrated. This simply means that the scale of the recovered range space network is not properly implied by the geometric strength of the available observations. This fact is also confirmed by the positive increase of the longer baselines when additional observations are incorporated into the minimum constraint solutions. Implementation of the scale in the geometric solution has been attempted by fixing the third coordinate of station 7122 (solution (3)) in addition to the coordinates fixed in the implementation of the minimum constraint solutions. By fixing the third coordinate of this station we implicitly fix the length of baseline 7109-7122.

As mentioned earlier in this section, Table 8 contains the results only for those baselines for which the a posteriori standard deviations in the overconstrained solution are smaller than 1 cm. Although all of the remaining baselines have been estimated in all solutions shown in this table, they are not included there because the steady state response for those baselines is assumed not to have been reached. The reason for claiming this is based on the fact that baselines 7110-7220 and 7109-7886 are the only ones that do not change their lengths at the centimeter level either when additional observations are incorporated into the solution or when additional constraints are applied.

Furthermore, only these two baselines have been estimated in the minimum constraint solutions with an a posteriori standard deviation at the milimeter level thereby suggesting that a steady state response in the geometric mode environment assumes millimeter level a posteriori standard deviations of the estimated baselines.

Application of an additional constraint brings the a posteriori standard deviation of all the remaining baselines shown in Table 8 to the millimeter level thereby implying that for those baselines the steady state response has been reached via the implementation of the scale in the resulting range space network.

This was expected because in the geometric solutions the baselines constitute a set of estimable quantities and as such constraining one of them (i.e., 7109-7122) will lead, apart from nonlinear terms, to reduced unscaled standard deviations for the remaining baselines. Their scaled standard deviations (i.e., a posteriori standard deviations) will also be reduced if the scaling factors (i.e., the a posteriori standard deviations of unit weight) are close enough to unity so they preserve the relative structure of the corresponding unscaled standard deviations. In fact the a posteriori standard deviation of unit weight in the overconstrained solutions is 1.05, just slightly larger than that of the corresponding minimum constraint which is 1.03, making it possible to preserve in those solutions the same relative structure of the scaled variance-covariance matrices as that of their corresponding weight coefficient matrices (Table 8). This simply means that the additional constraint did not distort the geometry but rather made it stronger, and therefore it was possible to reach through the solution (3) steady state response for longer baselines.

Since the geometric solutions are not affected by the erroneous modeling of either the satellite motion or the motion of reference frames, we have taken solution (3) to constitute the standards of comparison in assessing the effectiveness of the SRD method versus the dynamic mode methods. Solution (3) was chosen over the corresponding minimum constrained solutions because, of all of the available events, the steady state response for more than the two very short baselines (i.e.,

7110-7220 and 7109-7886) was not possible via the minimum constrained solutions (Table 8).

The only errors affecting solution (3) result from the ineffectiveness to implement the ill-defined scale by fixing the third coordinate of station 7122 to that of the (CSR)85L01 solution (see Section 4.4.2). This, however, is difficult to assess, but on the basis of the results presented in the next section it can be safely stated that the scale along a band in the direction of baseline 7109-7122 has been properly defined by constraining this baseline. In fact the value of the scale factor varies from solution C2 to that of C3, from 6.61×10^{-7} to 7.72×10^{-7} for baselines longer than 627 km while for the two baselines of about 274 km the value of the scale factor drops down to 4.5×10^{-7}. This dependency of the scale factor on the baseline lengths is expected since for shorter baselines the implied geometry is stronger.

4.4 BASELINE ESTIMATION VIA THE STEADY STATE RESPONSE OF THE SRD METHOD

The incorporation of additional observations into the SRD solutions will lead to a steady state response for the same reasons mentioned in the previous section. This response is even faster if observations of "improved quality" are available. The term improved quality indicates improvement of the weight coefficient matrix. For instance, from two sets of observations (a) and (b) having identical sizes, the set (b) is of improved quality if the difference $(P_b - P_a)$ of their weight matrices is a positive (semi)definite matrix. Based on this, it is a trivial exercise to prove that the matrix $(Q_{\hat{X}}^{a} - Q_{\hat{X}}^{b})$ is positive (semi)definite if the design matrix is the same for both sets of observations (a) and (b) and of full rank. $Q_{\hat{X}}^{a}$ and $Q_{\hat{X}}^{b}$ denote the weight coefficient matrices of the same adjusted parameter vector obtained on the basis of sets (a) and (b). Since $(Q_{\hat{X}}^{a} - Q_{\hat{X}}^{b})$ is a positive (semi)definite matrix, it follows that

$$\mathrm{Tr}(Q_{\hat{X}}^{b}) \leq \mathrm{Tr}(Q_{\hat{X}}^{a}) \qquad (4\text{-}2)$$

Although the two sets (a) and (b) are drawn from different populations, consistency between the accuracy of the models employed and the

accuracy of the observations leads to a close-to-unity a posteriori variance of unit weight, thereby reducing, as it follows from equation (4-2), the a posteriori variances of the adjusted parameter vector. This vector contains the earth-fixed Cartesian coordinates of the ground stations and the inertial initial state vectors which are treated in the present study as nuisance parameters. The adjusted station coordinates and their statistics are used to estimate the baseline lengths and their a posteriori standard deviations. Reduced variances in station coordinates, obtained from improved quality observations, yield baselines the variances of which are also reduced only if the non-linearity of the employed models allows such a reduction to take place. These reductions, taking place for most of the SRD solutions presented in the next section, imply a faster steady state response.

Constraining of estimable quantities in any SRD solution results in baselines with reduced variances thereby implying again a faster steady state response. Thus, incorporation of additional observations, improved quality observations, and constraining of estimable quantities constitute the three major factors leading to a steady state response. In the SRD solutions, this response is achieved by balancing the contribution of the first and the third factors because we have no control over the second factor since the quality of already recorded observations does not change. Furthermore, the goal has been to restrict as much as possible the contribution of the third factor because the steady state response achieved on the basis of constraining estimable quantities may be affected severely by the errors affecting those quantities. These quantities are in error because their recovery has also been based on erroneous observations. If the propagation of the errors affecting the constrained estimable quantities is not well controlled, it will lead to erroneous recovery of the adjusted parameter vector and therefore to erroneous baseline estimates. Even worse, the a posteriori variances of those estimates might also be reduced making it more difficult to reliably assess their accuracy.

4.4.1 Pass Baseline Geometry and Its Manifestation in the Design Matrix of the SRD Observable

The underlying characteristic inherently present in any factor leading to a steady state response is its ability to strengthen the geometry implied in the SRD solution under question. Thus, with stronger geometry, the steady state response will be achieved on the basis of a reduced number of observations. In other words, observations containing more information for the recovered estimable quantities will lead to a faster steady state response.

Fig. 17 shows the horizontal plane of the starting point (1) of the baseline (12). The ending point (2) of the baseline and the simultaneously observed satellite positions have been projected on this plane. This simplification is aimed at revealing the information the SRD observables contain about the estimated baseline for two characteristic geometric configurations, namely, one when the subsatellite tracks are parallel to the estimated baseline (Fig. 17a) and one when the subsatellite tracks are perpendicular to that baseline (Fig. 17b and c).

It is a matter of trivial trigonometric manipulations to confirm that with subsatellite tracks parallel to the estimated baseline the magnitude of the SRD observable tends towards the length of the estimated baseline as the subsatellite point moves away from either end of the baseline along the subsatellite track denoted by (ε) in Fig. 17a. Thus, with this geometry the SRD observable directly relates to the length of the baseline. However, as the subsatellite point moves towards the perpendicular bisector of baseline (12′), the SRD observable tends towards zero.

With the subsatellite tracks perpendicular to the estimated baseline, the SRD observable tends towards zero as the subsatellite point moves away from the projected baseline along the line (ε) in Fig. 17b and c. This observable also tends towards zero as the subsatellite track (ε) tends toward the perpendicular bisector of the projected baseline (12′). However, the SRD observable tends towards the baseline length as the subsatellite point moves toward point (I) and as this point moves in the direction of the baseline and away from it (Fig. 17c). Thus, for a faster

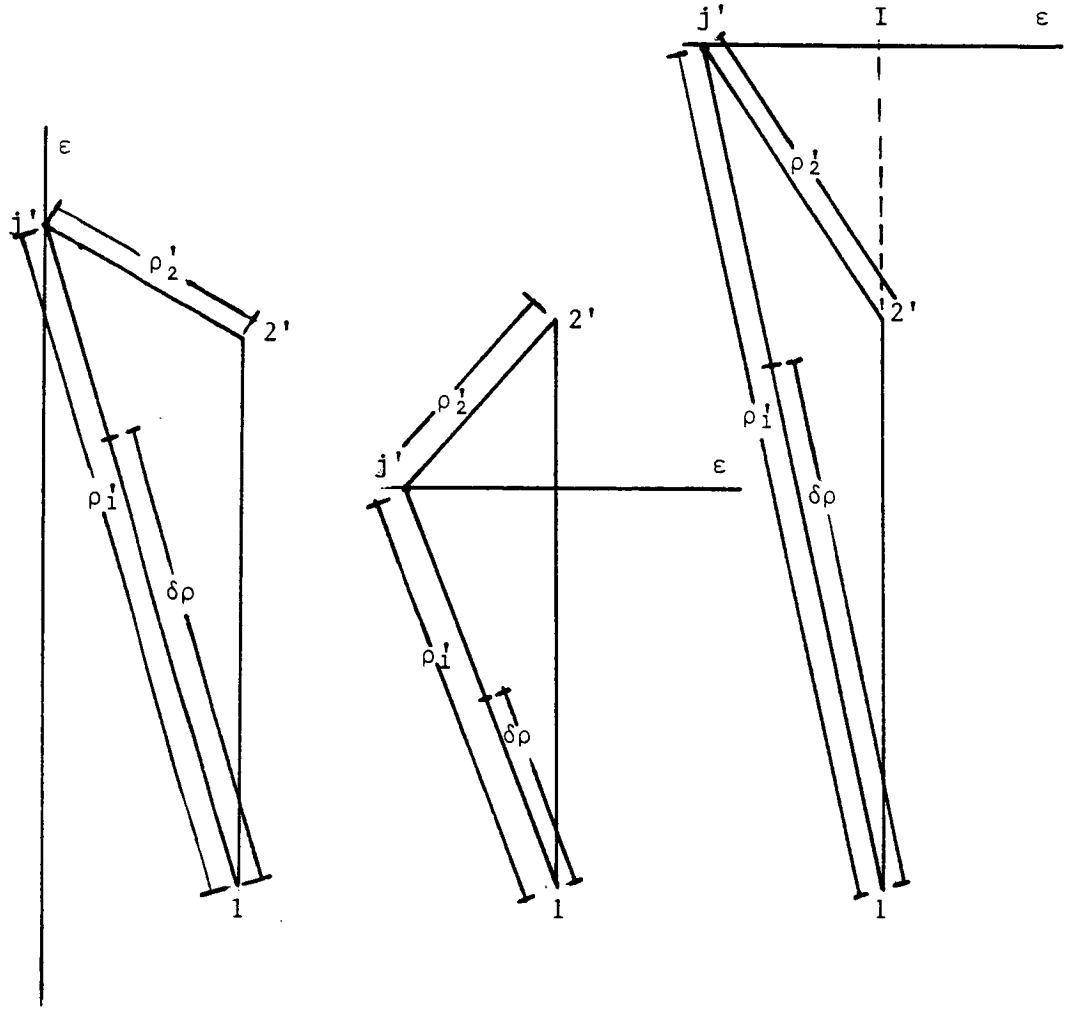

ε	subsatellite track	ρ_1'	projected observed range from 1
j′	subsatellite position	ρ_2'	projected observed range from 2
12′	projected baseline length	$\delta\rho$	projected SRD observable

Fig. 17 Subsatellite track-baseline geometry.

steady state response, parallel passes, the coobserved parts of which are extended well away from the endpoints of the baseline, should be preferred. When perpendicular passes are available, the ones located well away from the perpendicular bisector plane of the estimated baseline should be preferred.

The previously described favorable geometry manifests itself in the strong independence prevailing among the columns of the resulting design matrix. The term "strong independence" indicates the sharp variation characterizing the ratio of the corresponding entries between any two columns of the design matrix. The sharp variation resulting from favorable geometry is seen in the partial derivatives of the SRD observable taken with respect to the coordinates of one of the ground stations and to those of the inertial initial state vector (Appendix A)

$$\frac{\partial \delta \rho_j}{\partial \bar{Y}_2} = - \frac{\bar{X}_j - \bar{Y}_2}{\rho_{j2}} \tag{4-3}$$

$$\frac{\partial \delta \rho_j}{\partial X_0} = \left(\frac{\bar{X}_j - \bar{Y}_2}{\rho_{j2}} - \frac{\bar{X}_j - \bar{Y}_1}{\rho_{j1}} \right)^T (SNP) \frac{\partial \bar{R}_j}{\partial X_0} \tag{4-4}$$

where $\bar{X}_j$, $\bar{Y}_1$, $\bar{Y}_2$ are the earth-fixed position vectors of the satellite at epoch j and stations (1) and (2) respectively.

Since the partial derivatives of equation (4-3) have a common denominator, the variation of their ratios is controlled by the variations prevailing among the coordinates of the satellite as it moves along the coobserved part of the pass referred to from now on as "common part." The longer the common parts, the sharper the variations are for the ratios of the partial derivatives of equation (4-3). Common parts tend to be longer as the baseline decreases thereby resulting in sharper variations among the ratio of those partial derivatives for shorter baselines. However, these variations become sharper for both short and long baselines as more and more passes of different spatial distribution are incorporated into the solution. For long baselines (i.e., > 3500 km), the common part tends to be short if the pass is parallel to the baseline thereby reducing the variation of the ratio of those partial derivatives.

For perpendicular passes, the common parts tend to be a little longer for long baselines, allowing therefore for sharper variations in the ratio of the partial derivatives of equation (4-3).

The variations of the ratios between the partial derivatives of equation (4-4) as well as between the partial derivatives of equations (4-3) and (4-4) tend for perpendicular passes to be substantially reduced. The variations of the ratios among the partial derivatives of equation (4-4) are controlled by the changes in the observed ranges ρ_{j2} and ρ_{j1}, the changes in the satellite coordinates and the changes in the columns of the state transition matrix. When the SRD observables tend to become shorter (Fig. 17b and c), the observed ranges tend to be equal and therefore the coordinates of the coobserved satellite positions tend to cancel out. With such cancellations taking place and with the tendency to have equal denominators in those partial derivatives, the variations of their ratios are primarily controlled by those among the transformed state transition matrix ((SNP)$\cdot\partial R_j/\partial X_o$, ...), the columns of which, apart from the common denominator, tend in this case to be multiplied by the components of the estimated baseline. Thus, for shorter baselines the variations among these partial derivatives tend to be sharper than those for longer baselines (Appendix B). The unfavorable geometry associated with almost perpendicular passes manifests itself with an almost constant numerator in the partial derivative taken with respect to the station coordinate measured along the direction of the estimated baseline. This happens because in this direction the satellite coordinates change very little as the satellite moves along a pass almost perpendicular to the direction of the baseline. This geometry also leads to small variations of the numerators in the partial derivatives of equation (4-4); therefore, in the design matrix the ratio between the entries of the columns corresponding to the station coordinate, recorded along the baseline direction, and to the coordinates of the initial state vectors will exhibit very little variation because the denominators of the corresponding entries are nearly equal.

Reduced relative variations among the columns of the design matrix lead to high correlations among the corresponding adjusted parameters.

These correlations tend to increase or decrease as the homogeneity and the strength of the implied geometry decreases or increases respectively, a fact also manifested in the resulting poor or strong conditioning of the normal matrix.

The above discussion, the aim of which is to help in understanding the results presented in the next section, evidently reveals that in single SRD baseline solutions, the strength of the geometry fades away as the length of the estimated baseline increases. For longer baselines (i.e., > 4000 km), the steady state response cannot be reached because poor geometry results in an ill-conditioned normal equation matrix.

The weak geometry associated with long single baseline solutions is substantially improved through a network solution. Such a solution has not been performed in the present study because of the large number of observations and the limiting computer capabilities. If SRD normal points were available a network solution would have been possible which, however, is beyond the scope of this study.

4.4.2 Baseline Results

This section describes the process of achieving steady state response for those baselines only for which such a response, through single SRD baseline solutions, was possible on the basis of the data collected during the main MERIT campaign.

The adjusted parameter vector in single SRD baseline solutions contains the coordinates of the baseline end-points and the components of the initial state vectors for all of the arcs involved. In these solutions, obtained via a weighted least squares adjustment, the coordinates of one baseline end are held fixed while the coordinates of the other end and the components of the initial state vectors are allowed to adjust by assigning, through their weight matrix, the following standard deviations

$\sigma_x = \sigma_y = \sigma_z = 0.0001$ m (fixed baseline end)

$\sigma_x = \sigma_y = \sigma_z = 20$ m ("free" baseline end)

$\sigma_{x_0} = \sigma_{y_0} = \sigma_{z_0} = 50$ m (initial position)

$\sigma_{x_0} = \sigma_{y_0} = \sigma_{z_0} = 5$ cm/s (initial velocity)

The term "free" designates the adjusting baseline end.

The standard deviation of 20 m assigned on the coordinates of the free baseline end reflects an accuracy estimate of their approximate values. These values have been obtained by altering from 20 m to 100 m the coordinates of the (CSR)85L01 solution (Tapley et al., 1985b). The standard deviations of 50 m and 5 cm/s assigned to the approximate values of the components of the initial state vectors, reflect the accuracy of those values. They have been obtained by integrating, over a period of a month, Lageos' equations of motion using as initial state vectors those computed at EG&G for the entire main MERIT campaign (Pavlis, 1986; private communication). At the beginning of each month the EG&G estimates differ from those obtained by integrating Lageos' equation of motion over the period of the previous month because a simplified orbital modeling was used in the integration. These differences ranging from 50 m to 150 m for the position and from 5 cm/s to 13 cm/s for the velocity reflect the assigned accuracies to the components of the initial state vector.

Constraining one baseline end, by applying large weights to its coordinates, results in implicit constraining of its latitude and geocentric distance which both constitute, in the dynamic/semidynamic environment, a set of estimable quantities if the scale has been defined through the appropriate adoption of units and constants (i.e., units of time, velocity of light, etc.) and if a solution is possible through appropriately adopting physical constraints (Van Gelder, 1978). Weighting moderately the components of the initial state vectors results also in moderate implicit weighting of the estimable quantities associated with the geometric characteristics of the orbit. Adjusting only one baseline end and the initial state vectors, in either dynamic or semidynamic single baseline solutions, results in implicit and/or explicit constraining of a large number of estimable quantities. For instance constraining the C_{nm} and S_{nm} potential coefficients together with the geocentric gravitational constant (GM_E) and the mean radius of the earth (a_E) results in explicit constraining of the A_{nm} and B_{nm} coefficients which in the dynamic/ semidynamic environment constitute a set of estimable quantities (ibid.)

Erroneous constraining of estimable quantities distorts the geometric and/or physical characteristics of the dynamic environment, thus if enough time is allowed the accumulated errors can exceed the noise level of the observations to the extent that the adjusted estimable quantities will be affected by errors larger than those implied by the accuracy of the observations. Even worse with a priori variance of unit weight equal to one, the a posteriori standard deviations of these quantities will also be reduced only if the a posteriori variance of unit weight is close enough to unity so it preserves the relative structure of the weight coefficient matrices (ibid.)

Under those conditions baselines estimated on the basis of Cartesian coordinates will have their a posteriori variances reduced only if the non-linearity of the models employed allow such reductions to take place. In single SRD solutions the errors affecting the baselines, computed from the erroneously adjusted Cartesian coordinates of the free baseline end, result from the errors originated by erroneously constraining the parameters entering in the computation of the discrepancy vector L of equation (2-60). Erroneous baseline lengths with reduced variances constitute a potential source for misleading inferences in regard to the accuracy of the estimated baselines. Therefore, the a posteriori standard deviations of the estimated baselines will only be used, as in the geometric solutions, to indicate how far away the solution is from its steady state. The actual accuracy of the estimated baselines will be inferred on the basis of the comparison with the baselines estimated through geometric method (present study) and range dynamic methods (CSR at UTX and ZIPE at Potsdam) (next section).

Baselines estimated through Cartesian coordinates will also be affected in the dynamic environment by the errors commited in the implementation of the terrestrial reference frame, as it happens, for instance, when the barycenters of the observations of the baseline end stations are well apart in time (Pavlis et al., 1983). Strict simultaneity, however, implied by the nature of the SRD observable eliminates such inconsistencies in the present study.

For various baseline lengths ranging from 8 m to 4000 km, Tables 9 through 17 list the final results and those obtained at intermediate stages of the process leading to a steady state response. The a priori variance of unit weight is taken equal to one for all of the baseline solutions presented in this section. Fig. 18 shows the locations of the stations involved in the SRD solutions (lower part) together with a typical LAGEOS groundtrack for some of their coobserved passes (upper part).

The lengths of these common parts increase or decrease as the length of the baseline being estimated decreases or increases respectively.

Tables 9 and 10 contain the results of the steady state response reached for two very short baselines via both short and long arc modes. The first column lists the number of passes coobserved by the baseline end points while the second lists the number and the duration of the arcs, the position and orientation of which were adjusted to fit "best" the available observations. For instance, 6 (1h) in the first row of Table 9 indicates that six arcs were adjusted, each of one hour long, and 1 (4h) and 1 (2d) in the fifth row indicate that observations from eight passes (first column of this row) were adjusted using two arcs, one four hours long, and one two days long. The third, fourth and fifth column list the total number of the SRD observables, the a posteriori variance of unit weight and the root mean square of all of the SRD residuals respectively. The last column contains the estimated baseline length together with its a posteriori standard deviation. All of the remaining tables through 17 have the same format except for some obvious very minor differences.

For baselines 7109 - 7886 and 7110 - 7220 steady state response has been reached via both short arc and long arc solutions on the basis of 10 passes (Table 9, rows 3-7) and 17 passes (Table 10, rows 2-5) respectively. As in the geometric solutions, the steady state response is also associated with a posteriori standard deviations below the centimeter level. After the steady state, the estimated lengths of these two baselines do not change at the centimeter level either through a

ORIGINAL PAGE IS
OF POOR QUALITY

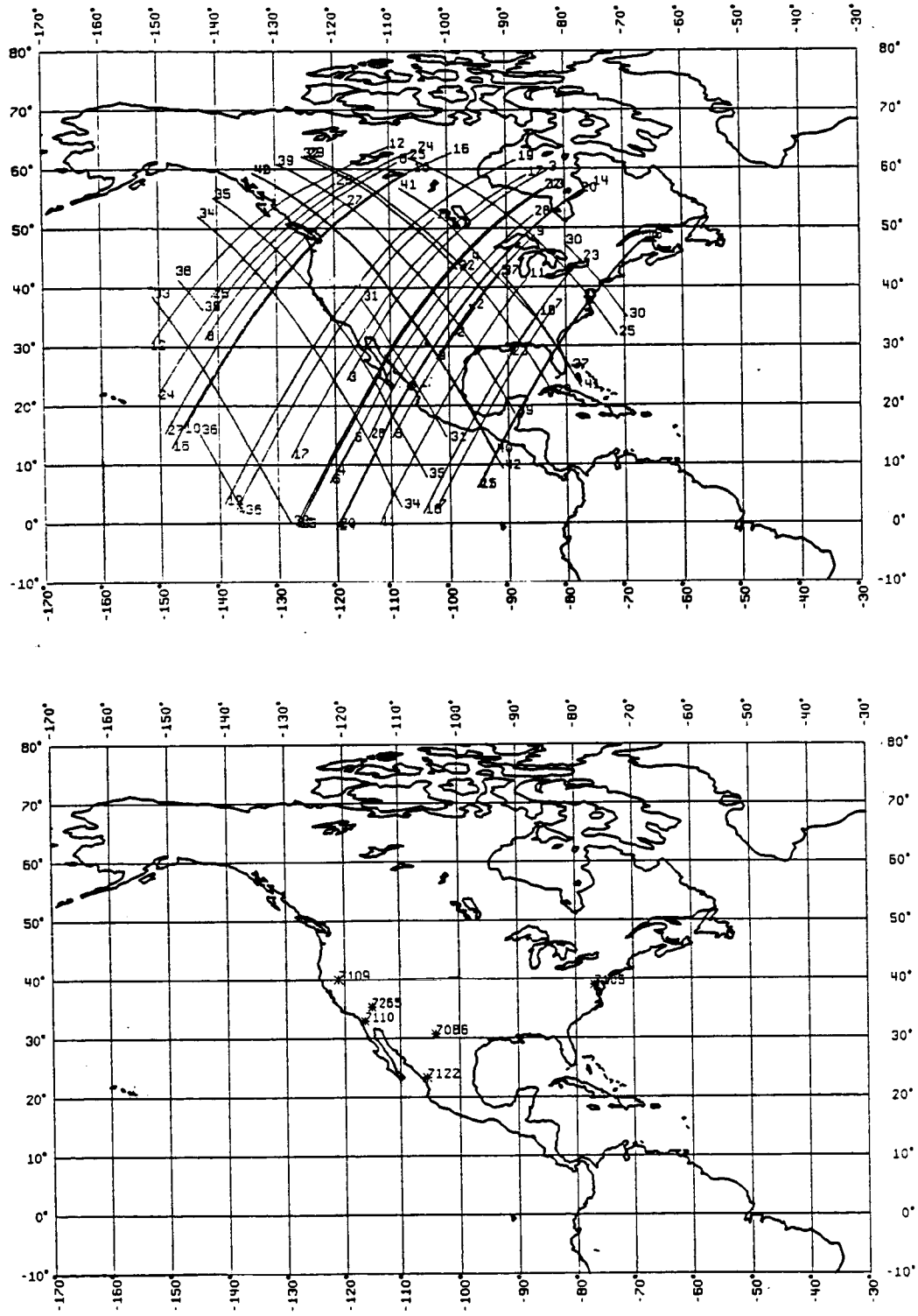

Fig. 18 Station location and Lageos groundtracks

Table 9 Steady State Response of Baseline 7109 - 7886, Parallel Passes
All length units in meters.

No. of Passes	Integration Lengths (1)	No. of Observ.	σ_0^{2} (2)	RMS of All Residuals	SRD Baseline 7._____
Short-Arc Mode					
6	6 (1 h)	8,414	0.94	0.070	.719 ± 0.002
8	8 (1 h)	12,807	0.90	0.069	.731 ± 0.002
10	10 (1 h)	18,589	0.86	0.067	.737 ± 0.001
13	13 (1 h)	25,865	0.85	0.067	.738 ± 0.001
Long-Arc Mode					
8	1 (4 h) 1 (2 d)	13,527	0.90	0.069	.733 ± 0.002
10	1 (4 h) 1 (4 d)	20,216	0.86	0.067	.741 ± 0.001
13	1 (4 h) 1 (7 d)	27,697	0.85	0.067	.738 ± 0.001

(1) k (ℓ h) = k arcs of ℓ hours
k (ℓ d) = k arcs of ℓ days

(2) a posteriori variance of unit weight

short arc or a long arc solution and furthermore these lengths are the same for both short arc and long arc solutions, thereby indicating that the accumulated orbital biases for so short baselines cancel out completely, a plausible property of the SRD observable. The correlations among the components of the adjusted parameter vector are for so short baselines substantially reduced because the lengths of the coobserved parts of the passes tend to be long and their orientation is not important since the subsatellite tracks for these short baselines are located well away from their end points (Section 4.4.1).

The 34 cm a posteriori standard deviation of the baseline solution, listed in the first row of Table 11, shows that although 17 passes of about one hour long are available, steady state response, with a short arc solution, is not possible for baseline 7110 - 7265 because the pass-baseline geometry has deteriorated as the length of the estimated

Table 10 Steady State Response of Baseline 7110 - 7220, Parallel Passes
All length units in meters.

No. of Passes	Integration Lengths (1)	No. of Observ.	σ_0^2 (2)	RMS of All Residuals	SRD Baseline 15._____
Short-Arc Mode					
11	11 (1 h)	12,040	0.95	0.084	.233 ± 0.003
17	17 (1 h)	17,971	1.09	0.091	.236 ± 0.002
Long-Arc Mode					
17	1 (4 h) 1 (1 d) 1 (2 d) 3 (3 d)	17,982	1.07	0.090	.240 ± 0.002
17	1 (1 h) 1 (3 d) 1 (4 d) 2 (5 d)	17,983	1.08	0.090	.250 ± 0.002
17	1 (1 h) 1 (3 d) 1 (6 d) 1 (7 d)	17,984	1.08	0.090	.238 ± 0.002

(1) k (ℓ h) = k arcs of ℓ hours
k (ℓ d) = k arcs of ℓ days

(2) a posteriori variance of unit weight

baseline has increased from 8 m (Tables 9) to about 274 km (Table 11). This deterioration is even worse since the geometry of the orbit is such that passes parallel to this baseline do not exist and only passes intersecting it at about ± 30 to ± 50 degrees are available creating, therefore, a geometry which is worse than that of the parallel passes and better than that of the perpendicular ones. Steady state response, however, for this solution can be reached by strengthening its geometric characteristics on the basis of constraints imposed on some additional estimable quantities. In the dynamic environment this is accomplished by increasing the maximum length of continuous integration (maximum arc length) which intensifies, through the implied geometric strength, the effect of the coefficients A_{nm} and B_{nm} on the resulting long orbital arcs. Care should be excercised not to destroy the

Table 11 Steady State Response of Baseline 7110 - 7265, Passes Within ±30° - ±50°
All length units in meters.

No. of Passes	Integration Lengths (1)	No. of Observ.	σ_0^{2} (2)	RMS of All Residuals	SRD Baseline 2740__.____
Short-Arc Mode					
17	17 (1 h)	21,767	0.77	0.0734	70.453 ± 0.335
Long-Arc Mode					
17	1 (1 d) 3 (2 d)	21,780	0.80	0.075	69.391 ± 0.012
17	2 (2 d) 1 (4 d)	21,781	0.80	0.075	69.482 ± 0.009
17	1 (2 d) 1 (3 d) 1 (7 d)	21,781	0.80	0.075	69.494 ± 0.009

(1) k (ℓ h) = k arcs of ℓ hours
k (ℓ d) = k arcs of ℓ days

(2) a posteriori variance of unit weight

accuracy of the available observations by the errors accumulated, over these long arcs, due to errors affecting the A_{nm} and B_{nm} potential coefficients.

With this in mind and on the basis of all observations, three long arc solutions have been performed by allowing maximum arc lengths of up to three, five and seven days respectively. The results of these three solutions are listed in 2nd through 4th row of Table 11. In the first long arc solution, employing one arc of one day long and three arcs of two days long, the length of the estimated baseline changed by 106 cm as compared to that of the short arc solution. Steady state response, however, for this solution has not yet been reached since the length of this baseline changes by about 10 cm when arcs up to five and seven days are allowed (Table 11, rows 3-4). However, increasing the maximum arc length from four to seven days (rows 3-4) results in a change of the estimated baseline length of about 1 cm, thereby implying that steady state response is being reached and that the baseline length of the solution listed in 3rd row of this table is the least affected by

Table 12 Steady State Response of Baseline 7109 - 7110, Parallel Passes
All length units in meters.

No. of Passes	Integration Lengths (1)	No. of Observ.	σ_0^2 (2)	RMS of All Residuals	SRD Baseline 883602.____
Short-Arc Mode					
4	4 (1 h)	11,512	0.5	0.029	.676 ± 0.30
8	8 (1 h)	36,236	0.36	0.026	.309 ± 0.04
12	12 (1 h)	59,011	0.35	0.026	.249 ± 0.03
16	16 (1 h)	69,083	0.43	0.026	.251 ± 0.03
Long-Arc Mode					
12	1 (1 h) 1 (2 d) 1 (3 d)	59,020	0.36	0.026	.220 ± 0.001
12	1 (4 h) 1 (3 d)	59,021	0.36	0.026	.224 ± 0.001
12	1 (7 d)	59,022	0.86	0.042	.217 ± 0.002
16	2 (2 d) 1 (3 d)	69,816	0.37	0.027	.225 ± 0.001
16	1 (2 d) 1 (4 d)	69,817	0.38	0.027	.226 ± 0.001
16	1 (1 d) 1 (6 d)	69,817	0.79	0.057	.219 ± 0.001

(1) k (ℓ h) = k arcs of ℓ hours
k (ℓ d) = k arcs of ℓ days

(2) a posteriori variance of unit weight

any accumulated orbital errors, because at steady state this solution employs the shorter long arcs and the a posteriori variance of unit weight is smaller than one. The correlations among the components of the adjusted parameter vector do not cause, for this baseline, any instability since almost all of them are less than 0.90 with very few just exceeding this value.

Tables 12 and 13 contain the results for the steady state response of two baselines with the same length, the same orientation, and one common end point occupied by station 7110. The observations recorded

Table 13 Steady State Response of Baseline 7110 - 7886, Parallel and Perpendicular Passes
All length units in meters.

No. of Passes	Integration Lengths (1)	No. of Observ.	σ_o^2 (2)	RMS of All Residuals	SRD Baseline 883606.____
Short-Arc Mode					
33 parallel passes	33 (1 h)	58,261	0.74	0.064	.467 ± 0.056
33 parallel + 6 perpendicular	39 (1 h)	61,037	0.75	0.064	.459 ± 0.056
Long-Arc Mode					
33 parallel passes	4 (1 h) 4 (4 h) 2 (1 d) 1 (1.5 d) 3 (2 d)	58,248	0.75	0.065	.347 ± 0.004
33 parallel passes	2 (1 h) 1 (4 h) 1 (1 d) 3 (2 d) 3 (3 d)	58,252	0.76	0.065	.342 ± 0.003
33 parallel passes	1 (4 h) 1 (2 d) 1 (3 d) 1 (4 d) 1 (4.5 d) 1 (7 d)	58,256	0.77	0.065	.335 ± 0.003

(1) k (ℓ h) = k arcs of ℓ hours
k (ℓ d) = k arcs of ℓ days

(2) a posteriori variance of unit weight

by stations 7109 and 7886, occupying the other ends of these two baselines, have an accuracy of 0.028 m and 0.070 m respectively, therefore, examination of the results presented in these two tables will show how the quality of the observations affects the speed of the steady state response (Section 4.4). Steady state response of baseline 7109 - 7110 has been reached via short arc solution on the basis of 12

passes having approximately 59,000 observations, as is confirmed by comparing the third and fourth rows of Table 12. The a posteriori standard deviation of the recovered baseline is at the 3 cm level because, in short arc solutions, the components of the initial state vectors are recovered with a relatively low precision (20 m to 50 m).

To examine the effects of using long arc solutions to achieve steady state response, we have performed six long arc solutions, three of which are based on observations from 12 passes (Table 12, rows 5-7) and three on observations from 16 passes (rows 8-10) when maximum arc lengths up to three, five and seven days are allowed respectively. The baseline lengths, estimated through all of these long arc solutions, do not change their length at the centimeter level, when either the number of observations or the maximum arc length increases and furthermore, the a posteriori standard deviation of the estimated baselines assumes millimeter level values. However, the baseline length changed from the short arc solution to the long arc solution by about 2.5 cm due to accumulation of orbital errors. The RMS of all of the SRD residuals for the long arc solutions (Table 12, rows 5-6,and 8-9) is about the same as that of the short arc ones (rows 1-4),but it is twice as much when arcs up to seven and six days are allowed in those solutions (rows 7 and 10).

Steady state reached through a short arc solution assumes a posteriori standard deviation of 3 cm (Table 12), thus, for baseline 7110-7886 shown in Table 13 such a response has not yet been reached, because a short arc solution, on the basis of all of the available observations, results in a 6 cm a posteriori standard deviation of the estimated baseline length (Table 13, row 1). This claim is also confirmed by the 10 cm change of the estimated baseline length when long arc solutions are performed (rows 3-5). The perpendicular passes incorporated in the short arc solution (2nd row), tend, in the light of weak geometry, to decrease the estimated baseline length because for those passes the SRD observable tends to become very short (Section 4.4.1). Thus, the 8 mm decrease (2nd row) on the basis of just 2,776 additional observations is another indicator confirming that steady state

response for this baseline through a short arc solution has not been reached. Consequently, such a response is sought through long arc solutions performed on the basis of arcs up to two, three, and seven days long (Table 13, rows 3-5). Since in these three long arc solutions the estimated baseline length did not change at the cm level and since its a posteriori standard deviation is below the cm level, it is assumed that steady state has been reached in those solutions.

For this baseline, although of same length and direction as baseline 7109 - 7110, steady state response was not possible on the basis of 33 passes with 58,261 observations processed via a short arc solution, because the accuracy of the observations of station 7886 is twice as large as those of station 7109. This confirms the claim, made in Section 4.4, that steady state response on the basis of improved quality observations is faster.

As of the correlations among the components of the adjusted parameter vector, they are well below the 0.90 value for all short arc solutions shown in Tables 12 and 13, except for very few of them, among the components of some of the recovered state vectors, that tend to be just a little higher than this value without, nevertheless, affecting the conditioning of the normals to the extent that could result in an algorithmically singular normal equations matrix. This behavior of the correlations is not surprising since in estimating these two baselines only parallel passes, the coobserved parts of which are extended well beyond the baseline end points, were employed, thereby, leading according to the discussion in Section 4.4.1 to a favorable geometry which is manifested in the reduced correlations among the components of the adjusted parameter vector. On the contrary, when in some of the long arc solutions shown in Tables 12 and 13, arcs of one or four hours long are employed together with arcs of two, three or seven days long, the relative geometry of the hours long arcs is very weak as compared to that implied by the days long arcs, thereby leading to high correlations among the components of initial state vectors of the hours long arcs. This inhomogeneity together with the potential to have many passes with weak geometry, when long baselines of about 4000 km are

estimated, results in an algorithmically singular normal equations matrix (see below).

Baseline 7110 - 7086, the steady state response of which is shown in Table 14, has a relatively large number of coobserved passes each having a substantially reduced number of observations as opposed to those recorded in the passes used in the estimation of the baselines described in Tables 9 through 13. Examination of the steady state response for this baseline will reveal the effect of the geometry, implied by the many passes, as opposed to the number of the available observations. The 41 cm a posteriori standard deviation obtained with the short arc solution, shown in the first row of this table, indicates that steady state has not yet been reached. Thus, six long arc solutions have been performed, the three of which use observations from 29 passes (Table 14, rows 2-4) while the other three use observations from 40 passes (rows 5-7) and arc lengths of up to three, five and seven days respectively. On the basis of 29 passes, processed in the long arc mode, steady state response has not been reached because changing the maximum arc length from five days to seven days the length of the estimated baseline changes as much as 18 cm (Table 14, rows 3-4). However, when 11 more passes with about 4,000 additional observations are included, the lengths of the estimated baseline change only at the centimeter level (rows 4-7) and their a posteriori standard deviations has dropped below the centimeter level, thereby suggesting that steady state response for this baseline has been reached. Since the a posteriori variance of unit weight is smaller than one, the estimated lengths are assumed not to have been influenced by any errors accumulated over these long periods and therefore, the length estimated with the smaller standard deviation is assumed to be the closest to that of the steady state (last row of this table).

In the short arc solution (1st row of Table 14), the correlations among the components of the adjusted parameter vector are almost all of them less than 0.90 with few just exceeding this value. These correlations (i.e., >0.90) exist among some components of the initial state vectors corresponding to arcs, the geometry of which is not favorable

Table 14 Steady State Response of Baseline 7110 - 7086, Passes Within ±20° - ±60°
All length units in meters.

No. of Passes	Integration Lengths (1)	No. of Observ.	σ_0^2 (2)	RMS of All Residuals	SRD Baseline 119829_.___
Short-Arc Mode					
40	40 (1 h)	16,752	0.76	0.078	1.110 ± 0.411
Long-Arc Mode					
29	8(1h), 1(4h) 3(1d), 2(2d) 3(3d)	12,395	0.81	0.081	0.814 ± 0.042
29	5(1h), 2(4h) 2(1d), 2(2d) 2(4d), 2(5d)	12,414	0.82	0.081	0.821 ± 0.036
29	4(1h), 1(1d) 1(2d), 2(4d) 2(5d), 2(7d)	12,400	0.84	0.083	0.998 ± 0.015
40	10(1h), 1(4h) 3(1d), 2(2d) 5(3d)	16,771	0.82	0.081	0.987 ± 0.009
40	7(1h), 1(4h) 3(1d), 3(2d) 1(3d), 2(4d) 2(5d)	16,790	0.80	0.080	1.024 ± 0.009
40	7(1h), 1(1d) 1(2d), 1(4d) 2(5d), 2(6d) 2(7d)	16,776	0.87	0.084	1.005 ± 0.008

(1) k (ℓ h) = k arcs of ℓ hours
k (ℓ d) = k arcs of ℓ days

(2) a posteriori variance of unit weight

with respect to the estimated baseline (Section 4.4.1), that is, when the passes are close to being perpendicular to the baseline and/or when their coobserved part is short and close the perpendicular bisector plane of the estimated baseline.

Increasing the maximum arc length results in arcs of different lengths ranging from one hour to either three, five, or seven days long, all of which are employed in the same long arc solution. This in turn

weakens the geometric strength of the short arcs because in those solutions the long arcs are the ones dominating the implied geometric strength. The weaker the geometry of those short arcs, in a short arc solution, the higher the correlations among their components adjusted in long arc solutions, in which these short arcs could not be matched with any other arcs. Furthermore, if only passes of weak geometry are matched together they result in a long arc also of weak geometry, thereby leading again to high correlations among the components of its adjusted initial state vector. These correlations become larger as the maximum arc length increases and the long arcs of weak geometry cannot be matched with any other ones of strong geometry. This pattern, which is present in the long arc solutions of Table 14, does not lead to an algorithmically singular normal equation matrix, simply because the length of the baseline is not long enough to result in a geometry so weak that could lead to near singularities, although passes parallel to this baseline do not exist (Fig. 18).

Table 15 contains the results for the steady state response of baseline 7110 - 7122, the geometry of which is such that passes parallel to this baseline do exist and in fact all of the passes employed in the solutions of Table 15 are parallel to this baseline. Since steady state response for this baseline was not possible through a short arc solution, long arc solutions have been performed on the basis of 15 passes (rows 1-2) and 22 passes (rows 3-5) with maximum arc lengths up to three, five and and seven days respectively. The temporal distribution of the observed passes is such that when 15 of them are used the solution allowing maximum length of three days coincides with that allowing maximum arc length of five days, and therefore only one of them is shown in Table 15 (1st row). These passes contain observations from station 7122 before and after it was upgraded (Table 2).

The 3 mm and 2 mm level of the a posteriori standard deviations associated with the baselines obtained through all of the long arc solutions, shown in Table 15, indicate that a steady state response for this baseline has been reached. This is also confirmed by the fact that the estimated baseline length changes at just the centimeter level when

Table 15 Steady State Response of Baseline 7110 - 7122, Long-Arc Mode, Parallel Passes (all length units in meters)

No. of Passes	Integration Lengths (1)	No. of Observ.	σ_0^2 (2)	RMS of All Residuals	SRD Baseline 1437139.__
15	1 (1 h) 5 (1 d) 1 (2 d)	42,328	0.65	0.044	.307 ± 0.003
15	1 (1 h) 4 (1 d) 1 (6 d)	42,329	0.66	0.045	.309 ± 0.002
22	2 (1 h) 4 (1 d) 3 (2 d) 1 (3 d)	69,803	0.52	0.035	.305 ± 0.002
22	1 (1 h) 5 (1 d) 2 (2 d) 1 (3 d)	69,804	0.54	0.037	.302 ± 0.002
22	2 (1 d) 1 (2 d) 1 (6 d) 2 (7 d)	69,807	0.81	0.055	.293 ± 0.002

(1) k (ℓ h) = k arcs of ℓ hours
k (ℓ d) = k arcs of ℓ days

(2) a posteriori variance of unit weight

on the basis of 22 passes the maximum arc lengths change from 3 to 7 days (Table 15, rows 4-5). The correlations follow the same pattern as that described for baseline 7110 - 7086 but since the passes are now parallel to the estimated baseline, weak geometry is implied only by those the coobserved part of which is extended only in between the baseline endpoints (Section 4.4.1). However, the geometry implied by those passes is not so weak to cause any algorithmic singularity in the normal equations matrix. Such weakness in the geometry causes problems when the lengths of the estimated baselines increases to 3500 km and 3700 km (Tables 16 and 17).

Table 16 Steady State Response of Baseline 7109 - 7105, Long-Arc Mode, Passes Within ±20° - ±30°
All length units in meters.

No. of Passes	Integration Lengths (1)	No. of Observ.	σ_0^2 (2)	RMS of All Residuals	SRD Baseline 3703351.___
Maximum Arc Length = 2 days					
42	10(1h), 5(4h) 2(7h), 6(1d)	78,801	0.54	0.032	.628 ± 0.003
54	12(1h), 5(4h) 2(7h), 8(1d)	106,770	0.52	0.032	.686 ± 0.003
62	14(1h), 5(4h) 2(7h), 9(1d)	129,147	0.50	0.031	.702 ± 0.002
72	18(1h), 5(4h) 2(7h),11(1d)	151,901	0.49	0.031	.693 ± 0.002
Maximum Arc Length = 3 days					
42	5(1h), 2(4h) 1(7h), 4(1d) 2(2d), 3(3d)	72,783	0.57	0.033	.677 ± 0.003
54	5(1h), 2(4h) 1(7h), 4(1d) 4(2d), 4(3d)	106,989	0.58	0.033	.689 ± 0.002
62	5(1h), 2(4h) 1(7h), 5(1d) 5(2d), 4(3d)	129,155	0.54	0.032	.699 ± 0.002
72	6(1h), 2(4h) 1(7h), 7(1d) 6(2d), 5(3d)	151,910	0.53	0.032	.695 ± 0.002

Table 16 (cont'd)

No. of Passes	Integration Lengths (1)	No. of Observ.	σ_0^2 (2)	RMS of All Residuals	SRD Baseline 3703351.___
Maximum Arc Length = 7 days					
42	4(1h), 1(4h) 1(7h), 1(1d) 1(2d), 1(3d) 1(5d), 4(6d) 1(7d)	78,809	1.11	0.046	.706 ± 0.004
54	4(1h), 1(4h) 1(7h), 1(1d) 1(2d), 1(3d) 1(5d), 5(6d) 2(7d)	106,780	3.33	0.081	.815 ± 0.005
62	4(1h), 1(4h) 1(7h), 1(1d) 1(2d), 1(3d) 1(5d), 6(6d) 2(7d)	129,159	2.78	0.073	.809 ± 0.005
72	4(1h), 1(4h) 1(7h), 2(1d) 1(2d), 1(3d) 1(4d), 1(5d) 7(6d), 2(7d)	151,916	2.45	0.069	.801 ± 0.004

(1) k (ℓ h) = k arcs of ℓ hours
k (ℓ d) = k arcs of ℓ days

(2) a posteriori variance of unit weight

For both of these baselines the pass-baseline geometry is weak and that of baseline 7110 - 7105 is even worse since passes intersecting this baseline at ±20 to ±60 degrees are only possible, and many of them are located close to the perpendicular bisector plane of this baseline.

For both of these baselines steady state response was not possible through a short arc solution, therefore, long arc solutions were performed on the basis of 42, 54, 62 and 72 passes and with maximum arc lengths up to two, three, and seven days respectively.

Examination of the results listed in rows 2-4 of Table 16 reveals that with maximum arc length up to two days steady state response has

been reached when 54 passes are available and the a posteriori standard deviation of the estimated baseline is 3 mm. Increasing the maximum arc length up to three days leads, as expected, to a faster steady state response since such a response is close to being reached with 42 rather than with 54 passes (Table 16, rows 2 and 5). When maximum arc length of 7 days is allowed, we see that steady state response has clearly been reached on the basis of 42 passes (Table 16 cont'd, row 1). However, the a posteriori standard deviation is greater than one, thereby suggesting that either accumulated orbital errors and/or possible ill-conditioning may be on their way up to corrupt the solution. Ill-conditioning, however, seems to be at work since many components of the recovered initial state vectors exhibit correlation at the .9999 level resulting mainly from the weak geometry and the inhomogeneity of the arc lengths employed in the solution shown in the 1st row of Table 16 cont'd. This is also confirmed, when on the basis of 54 passes (2nd row), the estimated baseline length jumps by 11 cm and the a posteriori standard deviation of unit weight jumps to 3.33. These behavior is caused by the high correlations existing among the components of the initial state vectors of those short or long arcs, the geometry of which became worse by the additional long arcs when 54 rather than 42 passes were employed (Table 16 cont'd, rows 1-2). Inclusion of additional observations, however, seems to lead the response of this solution to the right direction, as it is seen from the 2nd through 4th row of this table, but at a very slow pace, since the geometry is still too weak for a steady state response to take place.

The divergent response resulting from weak geometry manifests itself when baseline 7110 - 7105 is estimated on the basis of 56, 60 and 65 passes and with maximum arc lengths up to three, five and seven days respectively. For many of these passes the geometry with respect to baseline 7110 - 7105 is very weak (Section 4.4.1). This in turn leads to high correlations among the components of the corresponding initial state vectors. With arc lengths up to three days, steady state response seems to have been reached because with the incorporation of additional observations the length of the estimated baseline just changes at the

Table 17 Steady State Response of Baseline 7110 - 7105, Long-Arc Mode, Passes Within ±20° - ±60°
All length units in meters.

No. of Passes	Integration Lengths (1)	No. of Observ.	σ_o^2 (2)	RMS of All Residuals	SRD Baseline 3559743.___
Maximum Arc Length = 3 days					
56	12(1h), 1(5h) 1(8h), 5(1d) 3(2d), 4(3d)	120,111	0.58	0.036	.594 ± 0.003
60	12(1h), 1(5h) 1(8h), 4(1d) 3(2d), 5(3d)	136,356	0.56	0.036	.615 ± 0.003
65	15(1h), 1(5h) 1(8h), 5(1d) 3(2d), 5(3d)	146,956	0.55	0.035	.619 ± 0.003
Maximum Arc Length = 5 days					
56	11(1h), 1(5h) 1(8h), 3(1d) 2(2d), 1(3d) 3(4d), 1(5d)	120,114	0.64	0.038	.542 ± 0.003
60	11(1h), 1(5h) 1(8h), 2(1d) 2(2d), 2(3d) 3(4d), 1(5d)	136,359	0.63	0.038	.554 ± 0.003
Maximum Arc Length = 7 days					
56	8(1h), 1(1d) 1(2d), 2(4d) 5(6d), 2(7d)	120,118	1.25	0.053	.637 ± 0.004
60	8(1h), 1(1d) 2(2d), 2(4d) 5(6d), 2(7d)	136,362	1.14	0.051	.615 ± 0.004

(1) k (ℓ h) = k arcs of ℓ hours
k (ℓ d) = k arcs of ℓ days

(2) a posteriori variance of unit weight

centimeter level and the associated standard deviations assume 3 mm values (Table 17, rows 1-3). However, correlations at the 0.9999 level exist among the components of the initial state vectors of those arcs that are primarily composed of passes crossing this baseline close to its

perpendicular bisector plane. These correlations become larger when maximum arc lengths up five and up to seven days are allowed and when additional observations result in sharp inhomogeneity in regard to the arc lengths incorporated in the same solution (Table 17, rows 4-5, and 6-7). Thus, on the basis of 65 passes and when arcs up to five or seven days are allowed, the existence of high correlations leads to a singular normal equation matrix, thereby implying divergent response. Because of this, solutions were not possible with those arc lengths and therefore they are not shown in Table 17.

Thus, it is questionable whether for long baselines (>3500 km) steady state response through single SRD baseline solutions can be reached. For shorter baselines, however, steady state response can be reached even if passes parallel to the baseline do not exist.

The ill-conditioning affecting longer baselines could be prevented in a network solution if there exist observations from baselines that are parallel to the passes responsible for the ill-conditioning. Such solutions, however, for the reasons mentioned in the previous section could not be performed in the course of this study.

4.5 Baseline Comparison

The baseline lengths estimated with the geometric method are independent of any orbital errors and inconsistencies affecting the implementation of the terresrial reference frames; therefore, these lengths (Section 4.3.2) will constitute the standards of comparison when assessment is made about the accuracy of the baselines estimated via the SRD method. Both the geometric and the SRD baseline estimates will also be compared with those obtained via long arc range dynamic methods, on the basis of the MERIT data set, by the Central Institute for Physics of the Earth (ZIPE) in East Germany and by the Center for Space Research (CSR) at The University of Texas.

Both of these centers used in their solutions the gravitational constant proposed by MERIT standards (i.e., GM =3.98600448 * 10^{14} m^3s^{-2}) which is different from that employed in the single SRD baseline solutions (Section 2.2.5.1). A change in the gravitational constant will

not only affect the metric scale (the semimajor axis a) but also the dynamic scale (mean anomalistic motion n) according to Kepler's modified third law :

$$n^2a^3 = GM(1+\lambda) \qquad (4-9)$$

where λ is a small parameter depending on the satellite orbit. It is uncertain how the effect of this change will be divided between the metric and the dynamic scales. For regional baseline estimation however, the metric scale is primarily controlled by the velocity of light which is the same for all the SRD, ZIPE and (CSR)85L01 solutions. For this reason, changing the value of the gravitational constant (GM) in the SRD solutions presented in the previous section in accordance with MERIT Standards will affect at the centimeter level the lengths of only the two very long baselines (i.e., 7109-7105 and 7110-7105). The remaining baselines are affected either at the few millimeter or submillimeter level depending on the length of the estimated baseline and on the duration of the arcs employed in the corresponding solution. Nevertheless, for the sake of consistency the baseline differences shown in Table 18 have been adjusted to the same value of the gravitational constant by reestimating the SRD baselines on the basis of the (GM) value proposed by the MERIT Standards.

Table 18 lists the differences of those baselines only for which steady state response has been reached either through the SRD or the geometric solutions. The first column of this table lists the baseline ID's, the second one contains the length of the baseline rounded to the nearest meter, the third and fourth columns contain the differences of the baselines estimated through the SRD method and through the range dynamic method by both ZIPE and CSR, the fifth and sixth columns list the differences of the geometric and dynamic ZIPE and CSR baselines. The last column contains the differences of the baselines obtained through the SRD and the geometric methods. The baseline differences not listed in this table were not computed because steady state response for the SRD and/or the geometric method was not possible or because one of the stations constituting a baseline endpoint was not included in

Table 18 Baseline Differences

Baseline	Length (m) to nearest meter	ZIPE -SRD	(CSR)85L01 -SRD	ZIPE -GEOM	(CSR)85L01 -GEOM	SRD -GEOM
7109-7110	883602.	-0.03	-0.03	-0.03	-0.03	0.00
7109-7265	627044.	—	—	0.00	0.04	—
7109-7886	8.	-0.01	0.00	-0.02	-0.01	-0.01
7110-7122	1437139.	-0.03	-0.03	-0.02	-0.02	0.01
7110-7220	15.	—	-0.04	—	-0.01	0.03
7110-7265	274069.	-0.04	-0.07	-0.03	-0.06	0.01
7122-7265	1663983.	—	—	-0.02	-0.06	—
7122-7886	2280720.	—	—	0.01	0.02	—
7220-7265	274066.	—	—	—	0.00	—
7265-7886	627049.	—	—	0.01	0.06	—
7110-7886	883606.	-0.01	0.00	-0.01	0.00	0.00
7110-7086	1198291.	0.01	0.02	—	—	—
7109-7105	3703352.	0.06	0.05	—	—	—

the corresponding dynamic method. For instance, the difference (ZIPE - SRD) for baseline 7220-7265 could not be computed because steady state response for this baseline was not possible through a single SRD baseline solution; also for the same baseline the difference (ZIPE - GEOM) is not included in Table 18 because station 7220 was not listed in the reported ZIPE solutions (Montag et al., 1985).

The baseline differences between the SRD, ZIPE and CSR solutions shown in the third and fourth columns are negative for north-south baselines (rows 1-11) and positive for the east-west ones (rows 12-13) (Fig. 18). Since some of these differences are larger in magnitude for shorter baselines, scale difference between SRD and CSR or ZIPE solutions would account for part of these differences. The remaining differences, at the 2 cm or 3 cm level, must be caused by orbital errors affecting mostly the dynamic solutions, because the SRD solutions (column 7) are clearly closer to the geometric solution than both ZIPE and CSR solutions (Table 18, columns 5-6). The large differences of 6

cm between (CSR)85L01 and geometric solutions (column 6) are associated with station 7265 (MOHAVE). This station during the MERIT Main Campaign was equipped with a TLRS-1 laser instrument which experienced many problems, as was confirmed in the present study when editing the data with the data snooping procedure (Section 3.5). Therefore, it is very likely that erroneous observations from this station are still present in the (CSR)85L01 solution. This in turn would explain these relatively large baseline differences.

Although the geometric solution (Table 8, Type C3) used in Table 18 has been overconstrained to the (CSR)85L01 solution, SRD baseline estimates are on the average the "best" ones as compared to those of either the ZIPE or the (CSR)85L01 solutions. The term "best" indicates that a solution is the one closest to a geometric solution at its steady state. However, ZIPE baseline estimates when compared to those obtained in the (CSR)85L01 solution, are closer to the geometric solutions and therefore more accurate.

The root mean square of the differences between the geometric baseline estimates and those of the SRD, ZIPE and CSR are 1 cm, 2 cm, and 4 cm respectively.

Since these differences are based on baselines up to 1500 km, it is fair to state that SRD baseline estimates are at least as accurate as those obtained through the range dynamic mode methods.

4.6 RESPONSE OF THE SRD METHOD TO THE SIMPLIFICATIONS OF THE ORBITAL MODEL

It was mentioned in Section 2.2.5 that the aim of the present study is not to estimate Lageos' orbit with the highest degree of accuracy but rather to employ models as simple as possible and yet be able to recover baselines with an accuracy compatible to that of the observations.

Since the temporal variations of the baseline endpoints have been accounted for to the required degree of accuracy (Section 3.3), and since any inconsistencies in the implementation of the Terrestrial Reference Frame do not affect the SRD observables (Section 4.4.2), the

errors affecting the baselines estimated via the steady state response of the SRD method (Section 4.4.2) result only from those orbital errors accumulated over the integration periods and not cancelled out in the computation of the SRD observable. Thus, the question that should be addressed and investigated is twofold:

1) Is the sophistication of the orbital model, employed in the present study (Section 2.2.5) sufficient to result in baselines the accuracy of which is compatible to that of the observations?
2) If the answer is yes, how much could the sophistication of the orbital model be reduced without affecting the accuracy of the estimated baselines? If the answer is no, how much should the sophistication of the orbital model be enhanced so the estimated baselines have an accuracy compatible to that of the observations?

The errors affecting the estimated baselines are propagated from those affecting the corresponding Cartesian coordinates. These errors, which originated by the erroneous constraints imposed on a large number of estimable quantities entering in the computation of the SRD observable (eq. 2-60), tend to accumulate as the employed integration periods become longer.

For baselines of moderate length (<2000 km) accumulated radial errors are cancelled out almost totally in the computation of the SRD observable. These errors are propagated almost unaltered into the computed range observable (Pavlis, 1982). Depending, however, on the location of the observed satellite positions, accumulated latitudinal and longitudinal errors may affect the computed value of the SRD observable worse than they affect the range observable (ibid.) For shorter baselines (<200 km) the computed SRD observable is less affected by all these three errors (i.e., radial, latitudinal and longitudinal). Consequently, the answers to the questions posed in the beginning of this section depend on the length of the estimated baseline, on the magnitude of the accumulated orbital errors, and on whether these errors are radial, latitudinal or longitudinal. If these errors are primarily latitudinal and longitudinal, these answers depend also on the

relative orientation of the estimated baselines and its observed passes. This is the result of the anisotropy characterizing the latitudinal and longitudinal error surfaces. The orientation of the estimated baseline is not important for the propagation of the radial orbital errors because the radial error surfaces are isotropic. Since all of the baselines of Table 19 are extended in both north-south and east-west directions (Fig. 18), they will be affected by all three orbital errors (radial, latitudinal and longitudinal).

The estimable quantities, entering the satellite perturbations and being neglected in the simplification process, implicitly assume zero values in the resulting orbital model. If these constraints result in radial errors, then depending on the length of the estimated baselines, these errors should be relatively large in order to affect those baselines beyond the centimeter level. This in turn would allow longer lengths of continuous integration and, therefore, a reduced number of observations would be necessary to achieve steady state response of the SRD method (Section 4.4.2). However, if these constraints result, in addition to radial errors in both latitudinal and longitudinal errors, then even smaller lengths of continuous integration may affect baselines of moderate length (<2000 km) beyond the centimeter level. To set up the guidelines as to what simplifications of the orbital model can be applied without affecting the accuracy of the estimated baseline beyond the centimeter level, several tests have been performed the results of which are shown in Table 19.

Table 19 contains the baseline differences obtained as the orbital model was simplified from one containing a 12×12 gravity field, the direct point mass (PM) effects of Sun and Moon, the tidal(TD) effects due to Sun and Moon, the solar radiation (SR) pressure effects and the along-track (AT) acceleration effects, to that containing only a 2×2 gravity field and the direct (PM) effects of the Sun and the Moon. The first column of Table 19 lists the orbital models employed to estimate the baselines which subsequently were differenced from those estimated on the basis of orbital model shown on the title of this table (i.e., 12×12+(1)).

Table 19 Baseline Differences (in meters) With Respect to Those Computed Using an Orbital Model Including a 12×12 Gravity Field + (1)

Force Model Gravity Gravity Field + ( )	7110-7265 (274069.50)	7109-7110 (883602.25)	7110-7122 (1437139.30)
12×12 + (2)	0.01	0.00	0.00
12×12 + (3)	0.02	0.00	0.04
12×12 + (4)	-0.08	0.00	0.10
12×12	5.14	-0.02	-3.15
10×10 + (2)	0.01	0.00	0.01
10×10 + (4)	--	0.00	--
8×8 + (2)	0.03	0.00	0.01
8×8 + (4)	--	0.00	--
6×6 + (2)	1.02	0.00	2.02
6×6 + (4)	--	0.01	--
4×4 + (2)	0.90	0.00	3.37
4×4 + (4)	--	-0.01	--
3×3 + (4)	--	-0.02	--
2×2 + (4)	--	-0.07	--

(1) (PM) + (TD) + (SR) + (AT)
(2) (PM) + (TD) + (SR)
(3) (PM) + (TD)
(4) (PM)

PM = point mass effects of sun & moon
TD = tidal effects due to sun & moon
SR = solar radiation pressure effects
AT = along-track acceleration effects

The resulting differences are shown in the corresponding rows for only three baselines estimated on the basis of arcs up to seven days (Table 11, row 4), up to one hour (Table 12, row 4) and up to three days (Table 15, row 4).

Elimination of the AT acceleration, the SR pressure, the TD acceleration and the direct PM effects of the Sun and the Moon, introduces into the resulting orbital errors secular, long-period and short-period terms. Short-period terms directly related to Lageos' mean anomaly are common in all of these errors.

Since the eccentricity of Lageos' orbit is very small (~0.0039), elimination of the AT acceleration results primarily in latitudinal and longitudinal orbital errors (Obenson, 1970). The long periods of the resulting errors range from 66 days to 1100 days (Smith et al., 1985). Elimination of the SR pressure acceleration results also in radial, latitudinal and longitudinal orbital errors. Besides the additional

short-period terms related to the "ramp-like" behavior of the solar radiation pressure, the long periods of the resulting orbital errors are directly related to the motion of the Earth around the Sun and to the motion of the ecliptic in space (Musen, 1960; Kozai, 1961; El'Yasberg, 1967; Blitzer, 1970). In addition to the short-period perturbations related to the daily motion of the Earth, the nonstationary disturbances of the Earth's potential due to the attraction of the Sun and the Moon perturb the satellite periods with periods greater than a week (Kozai, 1973; Goad, 1977). As a result radial, latitudinal and longitudinal orbital errors, having those periods will be introduced from the elimination of the TD acceleration. Finally, elimination of the direct PM effects of the Sun and the Moon introduces again the three types of orbital errors having, besides the short periods associated with Lageos' mean anomaly, intermediate periods associated with the motion of the Earth around the Sun(~ multiple of 180 days) and the motion of the Moon around the Earth(~ multiple of 14 days), and long periods associated with the space motions of the ecliptic and the orbital plane of the Moon (Kozai, 1959; El'Yasberg, 1967; Fisher, 1971; Blitzer, 1970).

Therefore, elimination of each of the mentioned accelerations introduces radial, latitudinal and longitudinal orbital errors. Since periods longer than a week are present, these errors will accumulate as the integration periods increase from one hour to seven days. The effects of these errors on the estimated baselines are shown in Table 19 (rows 1-4).

The perturbations caused in the motion of the satellites by the ocean tides can reach as much as 20% of the perturbations caused by the tides of solid Earth (Musen, 1973). Inspection of Table 19, row 3, reveals that elimination of ocean tidal effects from the orbital model, as is the case in this study (Section 2.2.5), will hardly affect the estimated baselines at the centimeter level.

Therefore, centimeter level accuracy for baselines up to 1500 km, estimated via long-arc solutions, can be achieved if in addition to gravitational effects of the Earth, the SR pressure, the TD and the direct PM effects of Sun and Moon are included in the orbital model.

However, if steady state response is possible via a short arc solution, centimeter level accuracy for baselines up to 1000 km can be achieved if in addition to the gravitational effects of the Earth only the direct PM effects of the Sun and the Moon are included (Table 19, column 3).

The question as to how much the gravity field of the Earth can be reduced without affecting at the centimeter level the estimated baselines is investigated by performing several solutions, the results of which are shown Table 19 (rows 5-14). In these solutions the gravity field is being reduced by two degrees at a time while the SR pressure, the TD and the direct PM effects of the Sun and the Moon are included in the orbital model (Table 19, rows 5, 7, 9 and 11). For baseline 7109-7110, estimated via short-arc solutions, an additional solution has been performed with each reduced gravity field and with only the direct PM effects of the Sun and the Moon (Table 19, column 3, rows 6, 8, 10, 12, 13 and 14). Eliminating two degrees at the time introduces secular orbital errors due to elimination of the even zonal harmonics, long-period errors due to the elimination of the zonals, and short periods due to the elimination of all of the harmonics included in those degrees. Thus, as the length of continuous integration increases radial, latitudinal and longitudinal orbital errors tend to increase to the extent that the estimated baselines will be affected beyond the centimeter level.

Careful study of the results shown in Table 19 reveals that baselines of up to 1500 km estimated via the SRD method will be affected at just the centimeter level if the orbital model includes :

1) in short arc solutions:
   gravity field 4×4, and
   the direct point mass effects of the Sun and the Moon.
2) in long arc solutions with arcs up to three days:
   gravity field (8×8),
   the PM effects of the Sun and Moon,
   TD effects, and
   SR pressure effects.

3) in long-arc solutions with arcs up to seven days:

gravity field (10×10),

the PM effects of the Sun and Moon,

TD effects, and

SR pressure effects.

Therefore, the sophistication of the orbital model employed in the present study results in baselines having centimeter-level accuracy. This accuracy is compatible with the accuracy of the laser observations employed in this study (Section, 4.2). This constitutes the answer to question (1); question (2) has already been answered by the conclusions stated above.

Chapter 5

CONCLUSIONS AND RECOMMENDATIONS

5.1 CONCLUSIONS

The severe requirements of the geometric solutions to have simultaneous observations from four or more stations (Section 2.1.3), results in rejection of a large number of nonsimultaneous observations. The rejection is even greater with weather dependent satellite observations not specifically designed for simultaneous tracking as happens with the laser range observations.

Although during the MERIT Main Campaign many stations committed themselves to collecting simultaneous observations (Section 3.4), these observations were not enough to yield strong geometric solutions because of their sensitivity to configurations being close to those leading to singularities B and C (Sections 2.1.3 and 4.3.1). Because of these configurations, a steady state response in minimum constraint geometric solutions was possible only for two very short baselines. However, stronger implementation of the scale through an overconstraint solution (Table 8, solution C3) resulted in a steady state response for baselines of up to 2280 km (Section 4.3.2). These baselines formed the standards of comparison in assessing the accuracy of those obtained via both the SRD semidynamic and range dynamic mode methods (Section 4.5). Although the scale in this overconstraint solution was partly implied by that of the (CSR)85L01 (Section 4.3.2), it is feasible in the forseable future to incorporate the VLBI scale on the basis of only one or two baselines. This in turn could lead through a geometric solution to the estimation of a large number of baselines of compatible accuracy. These baselines could be effectively used to assess the accuracy of those obtained via the range dynamic methods. This practice might be of

great importance with the upcoming millimeter accuracy laser range systems.

As a result, regular baseline estimation through geometric solutions using laser range observations is impossible and therefore, since geometric solutions are free of errors affecting the orbit and the TRF frame they should be used, whenever possible, as standards of comparison.

In contrast to the geometric method, the SRD semidynamic mode method can be effectively used for regional baseline estimation, especially with laser range observations to Lageos, since the altitude of its orbit makes it possible for stations as far as 3703 km apart to collect enough simultaneous observations to result in a steady state response of the SRD method. The number of observations required for such a response to take place is a function of

- the baseline length,
- the geometry and the length of the arcs employed,
- and the accuracy of the available observations.

Table 20 shows the number of passes used in the present study to achieve steady state response for different baseline lengths. In general, as the length of the estimated baseline increases, more arcs, stronger geometry, and more observations are required for a steady state response to take place. The speed of the steady state response will primarily depend on the number, distribution and accuracy of the available observations, and on the length of the arcs employed in the SRD solutions.

For instance, when the geometry is favorable (i.e., parallel passes are available) and the observations of the baseline end stations have an accuracy of about 3 cm, baselines of 883 km can be estimated via both short arc and long arc solutions (Table 12). This is possible on the basis of only 12 passes collected within a period of a week. However, as the accuracy of the observations decreases, even in the light of favorable geometry, the steady state response of a baseline having

Table 20 Steady State Response of the SRD Method

No. of Passes Needed	Approx. Occupation Time in This Dataset	Steady State Up to ___ km
10 - 15	1 week	1000
20 - 25	3 months	1500
25 - 30	3 months	2500
50 - 55	8 months	3500

about the same length as that in Table 12 (see Table 13) was not possible on the basis of approximately the same number of observations and through a short arc solution because the accuracy of its end stations was worse than that of Table 12 (see Table 2). Nevertheless, a steady state response for this baseline was possible through a solution employing arcs of up to two days long. For longer baselines of up to 1437 km, the end stations of which recorded observations of 3 cm and 9 cm accuracy respectively, a steady state response in the light of favorable geometry was possible on the basis of 22 passes and only through a long arc solution employing arcs up to three days long (Table 15).

When the baseline-pass geometry is not favorable, (i.e., passes ±30° to ±50°) and the accuracy of the observations of the baseline end stations is approximately 3 cm and 8 cm respectively, a steady state response for a 274 km baseline was possible on the basis of 17 passes and only through a long arc solution employing arcs up to four days long (Table 11). For another baseline of about 1198 km having unfavorable pass-baseline geometry, a steady state response was possible on the basis of 40 passes and through a solution employing arcs up to seven days long (Table 14). The number of observations required for the steady state response of this baseline is substantially reduced as compared to those required for all the other baselines shown in Tables 9 through 17. This is not surprising because the stronger geometry implied by the 40 passes compensated for the reduced number of observations. However, if more observations could have been collected during each pass, fewer passes would be required for a steady

state response.

For very long baselines of about 3703 km, although passes of favorable geometry are not available, a steady state response was still possible on the basis of 54 passes and through a solution employing arcs up to one day long (Table 16). This response, however, started diverging when for the determination of this baseline arcs up to seven days long were employed (Table 16). Furthermore, for a baseline of about 3559 km, the pass-baseline geometry of which is very weak (i.e., passes within ±20° to ±60°), a steady state response was possible only with arcs up to three days (Table 17). Therefore, for so long baselines and when the geometry is fairly weak care should be exercised as to whether or not a steady state response is possible.

From the above discussion it is evident that for baselines up to 1500 km, steady state response can be reached without any problems even if the geometry is not favorable. However, tracking passes of favorable geometry with accurate (i.e., 3 cm) and high repeatability laser instruments increases the resolution of baseline recovery to weekly estimates. Although this was shown only for baselines of up to 883 km, baselines of up to 1437 km can also be recovered on a weekly basis, because steady state response for these baselines was reached on the basis of about 69,000 observations (Table 15).

In addition to the increased temporal resolution the comparison of the SRD method with the geometric solution (Table 8, solution C3) evidently demonstrated an accuracy of 1cm (Table 18), accomplished on the basis of a simple modeling and a limited orbit adjustment (Section 4.6). This demonstrates the potential of the SRD method for accurate differential positioning, and the insensitivity of the SRD observable not only to the errors affecting the orbit but also to those affecting the implementation of the TRF frame. The simple modeling of the orbit and its limited adjustment result in relaxing requirements in regard to availability of sophisticated software and extensive computer facilities which in turn makes it feasible to implement this method in the PC environment.

The stability characteristics of the SRD single baseline semidynamic solutions make it possible to estimate baselines of up to 1437 km without any need for a local support tracking network which is required in regional baseline estimation via the range semidynamic mode method (Christodoulidis et al., 1981).

The steady state response of baseline 7109-7105 (Table 16), reached on the basis of weak pass-baseline geometry strongly suggests that with parallel passes single SRD baseline solutions may very well lead to accuracy at the 2 to 3 cm level for baselines of up to 3500 km or 4000 km.

The stability characteristics and the high accuracy of the SRD method make it ideal for regional baseline estimation. This in turn makes it possible to obtain baselines up to 1500 km on a weekly basis free of the fluctuations usually affecting the monthly estimates of the range dynamic method. The stability characteristics could be greatly enhanced with a network solution which on the basis of SRD normal points would also substantially reduce the bulk of the computations without affecting the speed of the steady state response since the almost noise free SRD normal points will lead to a faster steady state (Section 4.4). However, with a network solution there might exist baselines for which simultaneous observations will not be available or the SRD observables will contain very little information for those baselines. This happens when the intersection of the visibility regions of the baseline end points is either an empty set or one having very few points. If a steady state response for those baselines has been reached it will entirely depend on the strength of the network which in the semidynamic environment tends to depend on the geometric strength of the observations which may not lead to a steady state response for longer baselines as it was the case with the geometric solutions. Steady state response of those baselines would require increasing the integration period. If this increase leads to a steady state, the estimated lengths for those baselines would primarily depend on the orbital strength, and therefore they would be susceptible not only to accumulated orbital errors but also to any inconsistencies affecting the

implementation of the TRF frame. However, employing the same orbital model as in the range dynamic solutions, the SRD baseline estimates will be less affected by the accumulated orbital errors.

In a network solution care should be exercised to account for the correlations resulting from the redundancy of having pairs of stations with common observations.

In the implementation of the SRD method a great deal of effort was spent to edit the data and create the SRD observables. Editing the observed laser ranges before generating those observables is crucial because generating them on the basis of erroneous laser ranges leads to the distribution of these errors among all of the generated SRD observables and therefore it will be difficult, if not impossible, to effectively edit the SRD observables in the final orbit adjustment.

The effects of gaps should also be well controlled and should be kept below the noise level of the observations. This was the reason why so much care was taken in the generation of SRD observables (Chapter 3). This in turn increased considerably the bulk of the computations required for the implementation of the SRD method.

These two factors do not by any means limit the potential of the SRD method because through proper arrangements either full rate SRD observables or preferably SRD normal points could be very easily generated with some slight modifications of the software employed by the computational centers responsible for the generation of the range normal points. With SRD normal points at our disposal a network SRD solution could be performed even in a PC environment, and since normal points are almost noise free they would lead to a faster steady state response of the SRD method.

5.2 RECOMMENDATIONS

Since the SRD method, based on a relatively simple orbital modeling and a limited orbit adjustment, is for regional baseline estimations at least as accurate as the dynamic mode methods, it is recommended that for such applications serious consideration should be given to regularly implement

this method for accurate differential positioning. If such a step is to be taken it is also suggested that:

- Further effort should be made by the observing stations to achieve simultaneous tracking.
- The direction of the baselines being estimated should be chosen, if this is feasible, to closely resemble the two main Lageos groundtrack directions.

- SRD normal points should be generated by the computational center responsible for the generation of range normal points.
- Research the response of the method, on the basis of normal points, when different network configurations are employed.

Projects specifically designed for studies of regional plate tectonic motions, determined on the basis of laser range observations to Lageos, are ideal for implementation of the SRD method. Such a project is currently under way in the area around the Mediterranean Sea (MEDLAS/WEGENER project), and therefore for this project the SRD method could offer an accurate and inexpensive alternative to study regional plate tectonic motions.

Appendix A

PARTIAL DERIVATIVES OF THE SRD OBSERVABLE

Expressing the SRD observable relative to an earth-fixed frame takes the following form:

$$\delta\rho_j = (\bar{E}_{j2}^T \cdot \bar{E}_{j2})^{1/2} - (\bar{E}_{j1}^T \cdot \bar{E}_{j1})^{1/2} \qquad \text{(A-1)}$$

with

$$\bar{E}_{j2} = \bar{X}_j - \bar{Y}_2 \quad \text{and} \quad \bar{E}_{j1} = \bar{X}_j - \bar{Y}_1 \qquad \text{(A-2)}$$

where $\bar{X}_j$, $\bar{Y}_2$ and $\bar{Y}_1$ are the earth-fixed position vectors of the satellite at the epoch j and stations (2) and (1) respectively.

Differentiating $\delta\rho_j$ with respect to $\bar{Y}_2$ one obtains:

$$\frac{\partial\delta\rho_j}{\partial\bar{Y}_2} = \frac{\partial\delta\rho_j}{\partial\bar{E}_{j2}} \cdot \frac{\partial\bar{E}_{j2}}{\partial\bar{Y}_2} = \frac{1}{\rho_{j2}} \bar{E}_{j2}^T \cdot (-I) = -\frac{\bar{E}_{j2}^T}{\rho_{j2}}$$

Thus

$$\frac{\partial\delta\rho_j}{\partial\bar{Y}_2} = -\frac{(\bar{X}_j - \bar{Y}_2)^T}{\rho_{j2}} \qquad \text{(A-3)}$$

where ρ_{j2} is the distance from station (2) to satellite position J.

Suppose that

$$\bar{R}_o = (X_o, Y_o, Z_o) \qquad \text{(A-4)}$$

and

$$\dot{\bar{R}}_o = (\dot{X}_o, \dot{Y}_o, \dot{Z}_o)^T \qquad \text{(A-5)}$$

are the initial position and velocity vectors with respect to an inertial frame. Differentiating equation (A-1) with respect to the initial state vector $(\bar{R}_o, \dot{\bar{R}}_o)$ one obtains:

$$\frac{\partial \delta\rho_j}{\partial(\bar{R}_o,\dot{\bar{R}}_o)} = \frac{\partial \delta\rho_j}{\partial \bar{E}_{j2}} \cdot \frac{\partial \bar{E}_{j2}}{\partial \bar{X}_j} \cdot \frac{\partial \bar{X}_j}{\partial(\bar{R}_o,\dot{\bar{R}}_o)} + \frac{\partial \delta\rho_j}{\partial E_{j1}} \cdot \frac{\partial E_{j1}}{\partial \bar{X}_j} \cdot \frac{\partial \bar{X}_j}{\partial(\bar{R}_o,\dot{\bar{R}}_o)} \qquad (A\text{-}6)$$

From equ. (A-1) and (A-2) it follows that:

$$\frac{\partial \delta\rho_j}{\partial \bar{E}_{j2}} = \frac{1}{\rho_{j2}} \bar{E}_{j2}{}^T = \frac{\bar{X}_j{}^T - \bar{Y}_2{}^T}{\rho_{j2}} \qquad (A\text{-}7)$$

$$\frac{\partial \bar{E}_{j2}}{\partial \bar{X}_j} = I \qquad (A\text{-}8)$$

$$\frac{\partial \bar{X}_j}{\partial(\bar{R}_o,\dot{\bar{R}}_o)} = \left[\frac{\partial \bar{X}_j}{\partial X_o}, \ \ldots, \ \frac{\partial \bar{X}_j}{\partial \dot{Z}_o}\right] = \left[\frac{\partial (SNP)\bar{R}_j}{\partial X_o}, \ \ldots, \ \frac{\partial (SNP)\bar{R}_j}{\partial \dot{Z}_o}\right] \qquad (A\text{-}9)$$

where ρ_{j2} is the distance from the station (2) to the satellite position j; $\bar{R}_j$ is the inertial position vector of the satellite at the epoch j; and S, N, P are the earth rotation, nutation and precession matrices respectively. Similarly to eq. (A-7), the partial $\partial \delta\rho_j / \partial E_{j1}$ takes the following form:

$$\frac{\partial \delta\rho_j}{\partial \bar{E}_{j1}} = \frac{\bar{X}_j{}^T - \bar{Y}_1{}^T}{\rho_{j1}} \qquad (A\text{-}10)$$

where ρ_{j1} is the distance from station (1) to satellite position j.

Substituting eq. (A-7) - (A-10) into eq. (A-6) the following formula results:

$$\frac{\partial \delta\rho_j}{\partial(\bar{R}_o,\dot{\bar{R}}_o)} = \left\{\frac{(\bar{X}_j - \bar{Y}_2)^T}{\rho_{j2}} - \frac{(\bar{X}_j - \bar{Y}_1)^T}{\rho_{j1}}\right\} \cdot \left[\frac{\partial \bar{X}_j}{\partial X_o}, \ \ldots, \ \frac{\partial \bar{X}_j}{\partial \dot{Z}_o}\right] \qquad (A\text{-}11)$$

or

$$\frac{\partial \delta\rho_j}{\partial(\bar{R}_o,\dot{\bar{R}}_o)} = \left\{\frac{(\bar{X}_j - \bar{Y}_2)^T}{\rho_{j2}} - \frac{(\bar{X}_j - \bar{Y}_1)^T}{\rho_{j1}}\right\} \cdot \left\{(SNP)\frac{\partial \bar{R}_j}{\partial X_o}, \ \ldots, \ (SNP)\frac{\partial \bar{R}_j}{\partial \dot{Z}_o}\right\} \qquad (A\text{-}12)$$

Thus, from eq. (A-11) and (A-12) it is easily deduced that the partial derivative of the SRD observable with respect to the first coordinate (i.e., X_o) of the initial state vector $(\bar{R}_o,\dot{\bar{R}}_o)$ takes the following form:

$$\frac{\partial \delta \rho_j}{\partial X_o} = \left[\frac{\bar{X}_j - \bar{Y}_2}{\rho_{j2}} - \frac{\bar{X}_j - \bar{Y}_1}{\rho_{j1}}\right]^T \cdot (SNP)\frac{\partial \bar{R}_j}{\partial X_o} \qquad \text{(A-13)}$$

$$\frac{\partial \delta \rho_j}{\partial X_o} = \left[\frac{\bar{X}_j - \bar{Y}_2}{\rho_{j2}} - \frac{\bar{X}_j - \bar{Y}_1}{\rho_{j1}}\right]^T \frac{\partial \bar{X}_j}{\partial X_o} \qquad \text{(A-14)}$$

Similarly one can obtain the partial derivative of the SRD observable with respect to all of the remaining componenets of the inertial initial state vector.

Appendix B

SENSITIVITY OF THE PARTIAL DERIVATIVES WITH RESPECT TO THE INITIAL STATE VECTORS

With the tendency of the observed ranges ρ_{j2} and ρ_{j1} from stations (1) and (2) to become equal (Section 4.4.1).

$$\rho_{j2} \cong \rho_{j1} = \rho_j \tag{B-1}$$

equation (A-11) becomes

$$\frac{\partial \delta \rho_j}{\partial(\bar{R}_o, \dot{\bar{R}}_o)} = \frac{(\bar{Y}_1 - \bar{Y}_2)^T}{\rho_j} \left[\frac{\partial \bar{X}_j}{\partial X_o}, \ \ldots, \ \frac{\partial \dot{\bar{X}}_j}{\partial \dot{Z}_o}\right] \tag{B-2}$$

This equation can also be expressed as follows

$$\frac{\partial \delta \rho_j}{\partial(\bar{R}_o, \dot{\bar{R}}_o)} = \frac{1}{\rho_j} (\bar{Y}_1 - \bar{Y}_2) \cdot (\bar{D}^j_{X_o}, \ \ldots, \ \bar{D}^j_{\dot{Z}_o})$$

where $(\cdot)$ and $(\bar{D}^j_{X_o}, \ \ldots, \ \bar{D}^j_{\dot{Z}_o})$ denote the dot product and the partial derivative vectors $\left[\frac{\partial \bar{X}_j}{\partial X_o}, \ \ldots, \ \frac{\partial \dot{\bar{X}}_j}{\partial \dot{Z}_o}\right]$ at the epoch j respectively.

If $\omega^j_{X_o}, \ \ldots, \ \omega^j_{\dot{Z}_o}$ designate the angles between the baseline vector and the partial derivative vectors respectively, equation (B-3) takes the following form

$$\frac{\partial \delta \rho_j}{\partial(\bar{R}_o, \dot{\bar{R}}_o)} = \frac{1}{\rho_j} |\bar{Y}_1 - \bar{Y}_2| (|\bar{D}^j_{X_o}| \cdot \cos(\omega^j_{X_o}), \ \ldots, \ |\bar{D}^j_{\dot{Z}_o}| \cos\omega^j_{\dot{Z}_o}) \tag{B-4}$$

Therefore, from epoch to epoch the variations among the entries of the columns, corresponding to the components of an initial state vector, are controlled by the variations of the projection of the partial derivative vectors $\bar{D}^j_{X_o}, \ \ldots, \ \bar{D}^j_{\dot{Z}_o}$ in the direction of the estimated baseline. These variations tend to be reduced as the observed part of the pass

becomes short and/or perpendicular to the estimated baseline. This geometry is closer to reality for longer baselines because as the baseline length increases the intersection of the visibility regions of the baseline endpoints tends to become smaller and closer to the perpendicular bisector plane of the baseline, thereby leading to a geometry close to also fulfilling assumption (B-1).

REFERENCES

Abshire, J.B., C.S. Gardner (1985), "Atmospheric Refractivity Corrections in Satellite Laser Ranging," ***IEEE Transactions on Geoscience and Remote Sensing***, Vol. GE-23, No. 4.

Abshire, J.B., T.W. Zagwodzki, J.F. McGarry, J.J. Degnan (1984), "An Experimental Large Aperture Satellite Laser Ranging Station at GSFC," Proc. of Fifth International Workshop on Laser Ranging Instrumentation, Herstmonceux Castle, U.K., Sept. 10-14; J. Gaignebet, ed., Groupe de Recherches de Geodesie Spatiale.

Afonso, G., F. Barlier, C. Berger, F. Mignard, J.J. Walch (1985), "Reassessment of the Charge and Neutral Drag of Lageos and Its Geophysical Implications," ***J. of Geophys. Res.***, Vol. 90, No. B11, 9381-9398.

"Analysis of Lageos Laser Range Data, Sept. 1983 - Oct. 1984," Center for Space Research, Univ. of Texas at Austin.

"Analysis of Lageos Laser Range Data, Aug. 1985," Center for Space Research, Univ. of Texas at Austin.

The Astronomical Almanac, 1984, U.S. Govt. Printing Office, Washington, D.C.

Baarda, W. (1968), "A Testing Procedure for Use in Geodetic Networks," Publications on Geodesy, New Series, Vol. 2, No. 5, Netherlands Geodetic Commission, Delft.

Bjerhammar, A. (1985), "On a Relativistic Geodesy," ***Bull. Geodesique***, Vol. 59, No. 3, 207-220.

Blaha, G. (1971), "Investigations of Critical Configurations for Fundamental Range Networks," Dept. of Geodetic Science Rep. 150, Ohio State Univ., Columbus.

Blitzer, L. (1970), ***Handbook of Orbital Perturbations, TRW Systems Group***, Redondo Beach, Calif.

Boucher, C., M. Feissel (1984), "Realization of the BIH Terrestrial System," Proc. of the International Symp. on Space Techniques for Geodynamics, Research Inst. of the Hungarian Academy of Sciences, Sopron, Hungary.

Boucher, C., Z. Altamimi (1985), "Towards an Improved Realization of the BIH Terrestrial Frame," Proc. of the International Conf. on Earth Rotation and the Terrestrial Reference Frame, Vol. 2, Dept. of Geodetic Science and Surveying, Ohio State Univ., Columbus.

Boucher, C., Z. Altamimi (1986), "Status of the Realization of the BIH Terrestrial System," Proc. of IAU Symp. 128, ***The Earth's Rotation and Reference Frames for Geodesy and Geodynamics***, Reidel Publ.

Bureau International de l'Heure, Annual Reports, 1983, 1984.

Cappellari, J.O., C.E. Velez, A.J. Fuchs, eds. (1976), "Mathematical Theory of the Goddard Trajectory Determination System," NASA/Goddard Space Flight Center, NASA X-582-76-77, NTIS N76-24291 - N76-24302.

Carnahan, B., H.A. Luther, J.O. Wilkes (1969), ***Applied Numerical Methods***, Wiley and Sons, New York.

Christodoulidis, D.C., D.E. Smith (1981), "Prospects for TLRS Baseline Accuracies in the Western USA Using Lageos," NASA Technical Memorandum 82133, Goddard Space Flight Center, Greenbelt, Maryland.

Christodoulidis, D.C., D.E. Smith, S.M. Klosko, M.H. Torrence, P.J. Dunn (1985), "A GSFC Alternative to the SLR MERIT Standards," Proc. of the International Conf. on Earth Rotation and the Terrestrial Reference Frame, Vol. 2, Dept. of Geodetic Science and Surveying, Ohio State Univ., Columbus.

Coates, R.J., H. Frey, G.D. Mead, J.M. Bosworth (1985), "Space-Age Geodesy, The NASA Crustal Dynamics Project," ***IEEE Transactions on Geoscience and Remote Sensing***, Vol. GE-23, No. 4, 360-367.

Cohen, S.C., D.E. Smith (1985), "Lageos Scientific Results: Introduction," ***J. of Geophys. Res.***, Vol. 90, No. B11.

Davis, P.J. (1975), ***Interpolation and Approximation***, Dover Publications, New York.

Degnan, J.J. (1985), "Satellite Laser Ranging: Current Status and Future Prospects," ***IEEE Transactions on Geoscience and Remote Sensing***, Vol. GE-23, No. 4, 398-413.

DeGroot, M.H. (1975), ***Probability and Statistics***, Addison-Wesley Publ., Reading, Massachusetts.

Diamante, J., R. Williamson (1972), "Error Models for Solid Earth and Ocean Tidal Effects in Satellite Systems Analysis," Wolf Research and Development Corp., Greenbelt, Maryland

Drain, L.E. (1980), ***The Laser Doppler Technique***, Wiley and Sons, New York.

Eanes R.J., B. Schutz, B. Tapley (1983), "Earth and Ocean Tide Effects on Lageos and Starlette," Proc. of the Ninth International Symp. on Earth Tides, E. Schweizerbart'sche Verlagsbuchhandlung, Stuttgart, FRG.

El'Yasberg, P.E. (1967), "Introduction to the Theory of Flight of Artificial Earth Satellites," translated from Russian by Z. Lerman, Israel Program for Scientific Translations, Jerusalem. Avail. Clearinghouse for Federal Scientific and Technical Information, Springfield, VA 22151.

Fisher, D. (1971), "Lunisolar Perturbations of the Motion of Artificial Satellites," Mission Trajectory Determination Branch, Goddard Space Flight Center, Greenbelt, MD, Preprint X-552-71-60.

Fitzmaurice, M.W., P.O. Minott, J.B. Abshire, H.E. Rowe (1977), "Prelaunch Testing of the Laser Geodynamic Satellite (LAGEOS)," NASA Tech. Paper 1062, NASA/Goddard Space Flight Center, Greenbelt, Maryland.

Forsythe, G., C.B. Moler (1967), ***Computer Solution of Linear Algebraic Systems***, Prentice-Hall, Englewood Cliffs, New Jersey.

Fukushima, T. (1986), "Coordinate System in General Relativity," Proc. of IAU Symp. 128, ***The Earth's Rotation and Reference Frames for Geodesy and Geodynamics***, Reidel Publ.

Goad C.C. (1977), "Application of Digital Filtering to Satellite Geodesy," NOAA Technical Rept. NOS 71 NGS 6, Rockville, Maryland.

Grafarend, E., B. Schaffrin (1974), "Unbiased Free Net Adjustment," ***Survey Review***, Vol. XXII, No. 171, 200-218.

Gruen, A. (1979), "Gross Error Detection in Bundle Adjustment," pres. at International Symp. on Current Trends in the Development, Execution and Use of Aerial Triangulation, Brisbane, Australia, Oct. 15-17.

Halliday, D., R. Resnick (1962), ***Physics, Part II***, Wiley and Sons, New York.

Hamilton, W.C. (1964), ***Statistics in Physical Science***, Ronald Press, New York.

Heck, B. (1982), "Report of the FIG Working Group on the Analysis of Deformation Measurements," FIG Symp., Budapest.

Heiskanen, W.A., H. Moritz (1967), ***Physical Geodesy***, W.H. Freeman, San Francisco.

Himwich, W.E., E.J. Harder (1986), "Direct Estimation of Nutation Coefficients from VLBI Data," Proc. of IAU Symp. 128, ***The Earth's Rotation and Reference Frames for Geodesy and Geodynamics***, Reidel Publ.

Johnson, T.S., J.J. Degnan, T.E. McGunigal (1978), "200 Picosecond Laser Development. A Status Report," Workshop on Laser Ranging Instrumentation, III, NASA TM-79643, NASA/Goddard Space Flight Center, Greenbelt, MD.

Kaula, W.M. (1961), "Analysis of Gravitational and Geometric Aspects of Geodetic Utilization of Satellites," ***Geophysical J. of R. Astron. Soc.***, Vol. 5, No. 2.

Kaula, W.M. (1966), ***Theory of Satellite Geodesy, Applications of Satellites to Geodesy***, Blaisdell Publ., Waltham, Massachusetts.

Kovalevsky, J., I.I. Mueller (1981), "Comments on Conventional Terrestrial and Quasi-Inertial Reference Systems," ***Reference Coordinate Systems for Earth Dynamics***, E.M. Gaposchkin and B. Kolaczek, eds., Reidel Publ.

Kozai, Y. (1959), "On the Effects of the Sun and the Moon Upon the Motion of a Close Earth Satellite," Smithsonian Institution Astrophysical Observ., Research in Space Science Special Rep. 22.

Kozai, Y. (1961), "Effects of Solar Radiation Pressure on the Motion of an Artificial Satellite," Smithsonian Institution Astrophysical Observ., Research in Space Science Special Rep. 56.

Kozai, Y. (1973), "A New Method to Compute Lunisolar Perturbations in Satellite Motions," Smithsonian Astrophysical Observ., Special Rep. 349.

Krakiwsky, E.J., A.J. Pope (1967), "Least Squares Adjustment of Satellite Observations for Simultaneous Directions or Ranges," Dept. of Geodetic Science Rep. 86, Ohio State Univ., Columbus.

Krakiwsky, E.J., B. Wanless, B. Buffett, K.P. Schwarz, M. Nakiboglu (1985), "GPS Orbit Improvement and Precise Positioning," Proc. of the First International Symp. on Precise Positioning with the Global Positioning System, Rockville, Maryland.

Krogh, F.T. (1969a), "A Variable Step Variable Order Multistep Method for the Numerical Solution of Ordinary Differential Equations," ***Information Processing***, 68, North-Holland Publ., Co., Amsterdam.

Krogh, F.T. (1969b), "VODQ/SVDQ/DVDQ, Variable Order Integrators for the Numerical Solutions of Ordinary Differential Equations," Technology Utilization Document No. CP-2308, Jet Propulsion Laboratory, Pasadena, California.

Krogh, F.T. (1973a), "On Testing a Subroutine for the Numerical Integration of Ordinary Differential Equations," ***J. of the Assoc. for Computing Machinery***, Vol. 20, No. 4, 545-562.

Krogh, F.T. (1973b), "Algorithms for Changing the Step Size," ***SIAM J. Numer. Anal.***, Vol. 10, No. 5, 949-965.

Krogh, F.T. (1974), "Changing Stepsize in the Integration of Differential Equations Using Modified Divided Differences," Proc. of the Conf. on the Numerical Solution of Ordinary Differential Equations, ***Lecture Notes in Mathematics***, Vol. 362, Springer-Verlag, New York, 22-71.

Landau, L.D., E.M. Lifshitz (1960), ***Mechanics***, transl. from Russian by J.B. Sykes and J.S. Bell, Pergamon Press.

Latimer, J.H., E.M. Gaposchkin (1977), "Scalar Translocation Using Laser Range Data," Smithsonian Astrophysical Observ., Center for Astrophysics Preprint Series No. 750, Cambridge, Massachusetts.

Lerch, F.J., S.M. Klosko, G.B. Patel, C.A. Wagner (1985), "A Gravity Model for Crustal Dynamics (GEM-L2)," ***J. of Geophys. Res.***, Vol. 90, No. B11, 9301-9311.

Lieske, J.H. (1979), "Precession Matrix Based on IAU (1976) System of Astronomical Constants," ***Astronomy and Astrophysics***, 73, 282-284.

Marini, J.W., C.W. Murray, Jr. (1973), "Correction of Laser Range Tracking Data for Atmospheric Refraction at Elevation Angles Above 10 Degrees," NASA Technical Rep. X-591-73-351, NASA/Goddard Space Flight Center, Greenbelt, Maryland.

Melbourne W., R. Anderle, M. Feissel, R. King, D. McCarthy, D. Smith, B. Tapley, R. Vicente (1983), "Project MERIT Standards," U.S. Naval Observatory Circular No. 167, Washington, D.C. 20390.

Montag, H., G. Gendt, R. Dietrich, K. Kurth (1985), "Investigation of Polar Motion and the Length of Day by Means of SLR Data of the MERIT Campaign," Proc. of the International Conf. on Earth Rotation and the Terrestrial Reference Frame, Dept. of Geodetic Science and Surveying, Ohio State Univ., Columbus.

Moritz, H. (1979), "Concepts in Geodetic Reference Frames," Dept. of Geodetic Science Rep. 294, Ohio State Univ., Columbus.

Moritz, H., I.I. Mueller (1987), ***Earth Rotation, Theory and Observation***, Ungar Publ., New York.

Moyer, T.D. (1971), "Mathematical Formulation of the Double-Precision Orbit Determination Program (DPODP)," TR-32-1527, Jet Propusion Laboratory, Pasadena, California.

Mueller, I.I. (1964a), "The Geodetic Applications of Satellites," Institute of Geodesy, Photogrammetry and Cartography Rep. 34, Ohio State Univ., Columbus.

Mueller, I.I. (1964b), ***Introduction to Satellite Geodesy***, Ungar Publ., New York.

Mueller, I.I. (1969), ***Spherical and Practical Astronomy As Applied to Geodesy***, Ungar Publ., New York.

Mueller, I.I., B.H.W. van Gelder, M. Kumar (1975), "Error Analysis for the Proposed Close Grid Geodynamic Satellite Measurement System (CLOGEOS)," Dept. of Geodetic Science Rep. 230, Ohio State Univ., Columbus.

Mueller, I.I. (1981), "Reference Coordinate Systems for Earth Dynamics, A Preview," ***Reference Coordinate Systems for Earth Dynamics***, E.M. Gaposchkin and B. Kolaczek, eds., Reidel Publ.

Mueller, I.I. (1985), "Reference Coordinate Systems and Frames: Concepts and Realization," ***Bull. Geodesique***, Vol. 59, No. 2, 181-188.

Mueller, I.I., G.A. Wilkins (1986), "Earth Rotation and the Terrestrial Reference Frame, ***Adv. Space Res.***, Vol. 6, No. 9, 5-11.

Obenson, G. (1970), "Direct Evaluation of the Earth's Gravity Anomaly Field from Orbital Analysis of Artificial Satellites," Dept. of Geodetic Science Rep. 129, Ohio State Univ., Columbus.

Musen, P. (1960), "The Influence of the Solar Radiation Pressure on the Motion of an Artificial Satellite," ***J. of Geophys. Res.***, Vol. 65, No. 5, 1391-1400.

Musen, P. (1973), "A Semi-Analytical Method of Computation of Oceanic Tidal Perturbations in the Motion of Artificial Satellites, X-590-73-190, NASA/Goddard Space Flight Center, Greenbelt, MD.

Pavlis, E.C. (1982), "On the Geodetic Applications of Simultaneous Range-Differencing to LAGEOS," Dept. of Geodetic Science and Surveying Rep. 338, Ohio State Univ., Columbus.

Pavlis, E.C., I.I. Mueller (1983), "The Effect of Earth Orientation Errors in Baseline Determination," ***Bull. Geodesique***, Vol. 57, No. 3, 273-282.

Pope, A.J. (1976), "The Statistics of Residuals and the Detection of Outliers," NOAA Technical Rep. NOS 65 NGS1, National Geodetic Survey, Rockville, Maryland.

Rao, C.R. (1973), ***Linear Statistical Inference and Its Applications***, 2nd ed., Wiley and Sons, New York.

Rinner, K. (1966), "Systematic Investigations of Geodetic Networks in Space," U.S. Army Research and Development Group (Europe), May.

Rizos, C., A. Stolz (1985), "Force Modeling for GPS Satellite Orbits," Proc. of First International Symp. on Precise Positioning with the Global Positioning System, Rockville, Maryland.

Rubincam, D.P. (1980), "Atmospheric Drag As the Cause of the Secular Decrease in the Semimajor Axis of LAGEOS' Orbit," ***Geophys. Res. Lett.***, 7, 468-470.

Rubincam, D.P., N.R. Weiss (1985), "The Orbit of LAGEOS and Solar Eclipses," ***J. of Geophys. Res.***, Vol. 90, No. B11, 9399-9402.

Schutz, B.E. (1983a), "Satellite Laser Ranging Participants During Project MERIT," Center for Space Research, Univ. of Texas at Austin.

Schutz, B.E. (1983b), "Satellite Laser Ranging Procedures Guide for Project MERIT," Center for Space Research, Univ. of Texas at Austin.

Schutz, B.E. (1985), "Report of the Satellite Laser Ranging Coordinator," Report on the MERIT-COTES Campaign on Earth Rotation and Reference Systems, Part I, G.A. Wilkins, ed., Royal Greenwich Observ., Herstmonceux, U.K.

Schwarz, C.R. (1969), "The Use of Short Arc Orbital Constraints in the Adjustment of Geodetic Satellite Data," Dept. of Geodetic Science Rep. 118, Ohio State Univ., Columbus.

Shawe, M.E., A.G. Adelman (1985), "Precision Laser Tracking for Global and Polar Motion," ***IEEE Transactions on Geoscience and Remote Sensing***, Vol. GE-23, No. 4.

Shelus, P.J. (1983) "Transportable Laser Ranging Station TLRS-1," International Coordination of Space Techniques for Geodesy and Geodynamics," ***CSTG Bulletin No. 5***, 112-116, Dept. of Geodetic Science and Surveying, Ohio State Univ., Columbus.

Silverberg, E.C. (1982), "The Feedback Calibration of the TLRS Ranging System," Proc. of the 4th International Workshop on Laser Ranging Instrumentation, Geodetic Inst., Univ. of Bonn.

Smith, D.E., D.C. Christodoulidis, R. Kolenkiewicz, P.J. Dunn, S.M. Klosko, M.H. Torrence, S. Fricke, S. Blackwell (1985), "A Global Geodetic Reference Frame from Lageos Ranging (SL5.1AP)," ***J. of Geophys. Res.***, Vol. 90, No. B11, 9221-9233.

Spath, H. (1974), ***Splines Algorithms for Curves and Surfaces***, transl. from German by W.D. Hoskins and H.W. Sager, Utilitas Mathematica Publ., Winnipeg, Canada.

Standish, E.M. (1981), "Letters," ***Astron. Astrophys.***, 101, L17.

Tapley, B.D., B.E. Schutz, R.J. Eanes (1985a), "Station Coordinates, Baselines, and Earth Rotation from LAGEOS Laser Ranging: 1976-1984," ***J. of Geophys. Res.***, Vol. 90, No. B11.

Tapley, B.D., R.J. Eanes. B.E. Schutz (1985b), "UT/CSR Analysis of Earth Rotation from Lageos SLR Data," Proc. of the International Conf. on Earth Rotation and the Terrestrial Reference Frame, Vol. 1, Dept. of Geodetic Science and Surveying, Ohio State Univ., Columbus.

"Transportable Laser Ranging System No. 2 (TLRS-2), Tech. Manual," NASA/GSFC Publ. MS-428-10, Goddard Space Flight Center, Greenbelt, Maryland.

Tsimis, E. (1972), "On the Geometric Analysis and Adjustment of Optical Satellite Observations," Dept. of Geodetic Science Rep. 185, Ohio State Univ., Columbus.

Tsimis, E. (1973), "Critical Configurations (Determinantal Loci) for Range and Range-Difference Satellite Networks," Dept. of Geodetic Science Rep. 191, Ohio State Univ., Columbus.

Uotila, U.A. (1967), "Introduction to Adjustment Computations with Matrices," lecture notes, Dept. of Geodetic Science, Ohio State Univ., Columbus.

Uotila, U.A. (1986), "Notes on Adjustment Computations, Part I," Dept. of Geodetic Science and Surveying, Ohio State Univ., Columbus.

Van Gelder, B.H.W. (1978), "Estimability and Simple Dynamical Analysis of Range (Range-Rate and Range-Difference) Observations to Artificial Satellites," Dept. of Geodetic Science Rep. 284, Ohio State Univ., Columbus.

Veis, G. (1960), "Geodetic Uses of Artificial Satellites," ***Smithsonian Contrib. to Astrophys.***, Vol. 3, No. 9.

Wahr, J.M. (1981a), "The Forced Nutations of an Elliptical, Rotating, Elastic and Oceanless Earth," ***Geophys. J. R. astr. Soc., 64***, 705-727.

Wahr, J.M. (1981b), "Body Tides on an Elliptical, Rotating, Elastic Oceanless Earth," ***Geophys. J.R. astr. Soc., 64***, 677-703.

Wilkins, G.A., ed. (1980), "A Review of the Techniques to Be Used During Project MERIT to Monitor the Rotation of the Earth," publ. jointly by Royal Greenwich Obs., Herstmonceux, U.K., and Inst. f. Angewandte Geodäsie, Frankfurt, FRG.

Wilkins, G.A., I.I. Mueller (1986), "On the Rotation of the Earth and the Terrestrial Reference System," ***Bull. Geodesique***, Vol. 60, No. 1.